BNL-81623-2008

Covariance Evaluation Methodology for Neutron Cross sections

M.Herman, R.Arcilla, C.M.Mattoon, S.F.Mughabghab, P.Oblozinsky, M.Pigni, B.Pritychenko, A.A.Songzoni

1 *National Nuclear Data Center, Brookhaven National Laboratory, Upton, NY 11973, USA*

M3 Report prepared for GNEP, U.S. DOE Reactors Campaign
September 2008

National Nuclear Data Center
Energy Sciences & Technology Department
Brookhaven National Laboratory
P.O. Box 5000
Upton, NY 11973-5000
www.bnl.gov

DISCLAIMER

Covariance Evaluation Methodology

***

M3 Report prepared for GNEP, U.S. DOE Reactors Campaign

M.Herman, R.Arcilla, C.M.Mattoon, S.F.Mughabghab,
P.Obložinský, M.Pigni, B.Pritychenko, A.A.Songzoni

National Nuclear Data Center, BNL, Upton, NY 19973, USA

September 2008

Abstract

We present the NNDC-BNL methodology for estimating neutron cross section covariances in thermal, resolved resonance, unresolved resonance and fast neutron regions. The three key elements of the methodology are Atlas of Neutron Resonances, nuclear reaction code EMPIRE, and the Bayesian code implementing Kalman filter concept. The covariance data processing, visualization and distribution capabilities are integral components of the NNDC methodology. We illustrate its application on examples including relatively detailed evaluation of covariances for two individual nuclei and massive production of simple covariance estimates for 307 materials. Certain peculiarities regarding evaluation of covariances for resolved resonances and the consistency between resonance parameter uncertainties and thermal cross section uncertainties are also discussed.

Summary

Covariances play important role in GNEP data adjustment project aiming to produce nuclear data library that should be used for all future neutronics simulations needed to develop fast, Advanced Burner Reactor. The present document is a FY2008 milestone level 3 report prepared by Brookhaven National Laboratory that leads GNEP covariance effort.

We provide summary of the National Nuclear Data Center (NNDC) methodology for generating neutron cross section covariances. Extensive activities regarding various aspects of covariances have been carried out at the NNDC during the last year. Comprehensive approach adopted at the NNDC covers all essential steps that have to be performed in order to provide reliable covariances to end users. These steps include: (i) estimation of covariances using experimental data and nuclear reaction theory, (ii) storing covariances in the ENDF-6 format and processing them into the desired group structure, (iii) visualization of uncertainties and correlations for verification and eventual comparison with other available estimates, (iv) distribution through the NNDC web portal. This report provides a detailed description of the NNDC covariance methodology as reported in seven papers/reports published in 2008 and attached here as Appendices.

Below we summarize salient points of these seven FY 2008 papers and reports:

EMPIRE code system - the NNDC has extended the EMPIRE code system to enable estimating covariances in the thermal, resonance and fast neutron ranges, as described in **Appendix A**. The Atlas of Neutron Resonances by Mughabghab is used as a primary source of information on uncertainties at low energies. The resulting resonance parameter covariances are formatted in the ENDF-6 File 32, which allows to generate cross sections covariances on any energy grid. In the fast neutron range our methodology is based on sensitivity calculations in the frame of various reaction models that are contained in the EMPIRE code. These sensitivity matrices are used in the deterministic Kalman filter approach, which also allows to combine theory constraints with experimental data. We compare this approach with the stochastic Monte Carlo method, also available in the EMPIRE code system, and find that the two procedures yield comparable results. In the same paper, we discuss a long-standing issue of unreasonably low uncertainties that result from certain Bayesian analyzes and we point to the rigidity of a reaction model as one of the reasons. These finding, together with the better understanding of cross correlations between different experiments, should ensure reasonable magnitude of uncertainties in all cases.

Consistency between thermal and resonance region - particular attention has been dedicated to the consistency of uncertainties for resonance parameters with the uncertainty of the thermal cross sections. Often, the latter ones are very accurately measured and propagating uncertainties of resonance parameters to the thermal region results in a severe overestimation of the thermal cross section uncertainties. The opposite cases are rare but do happen. To address this problem, a study presented in **Appendix B** was initiated to achieve consistency for 15 actinides and 21 structural and coolant moderator materials. This was realized by assigning uncertainties to the parameters of

the negative-energy resonances and changing, if necessary, significantly the uncertainties of the low-lying positive-energy resonances. The influence of correlations between parameters on the derived uncertainties is examined and discussed in **Appendix A**.

Analysis of cross section covariances in the resolved resonance region - is presented in **Appendix C**. In this work we studied how cross section uncertainties are affected by the uncertainties of specific resonance parameters and their correlations. It turns out that uncertainties of neutron-, radiative- and fission-widths are important, while the uncertainties of resonance energies can be effectively neglected. We conclude that, whenever possible, the correlations between neutron and radiative (fission) widths should be taken into account. In general, however, there is no unambiguous way of deducing these correlations from the Atlas of Neutron Resonances.

Examples of covariance estimates - examples of the practical application of the developed covariance methodology are given in **Appendices D** and **E**. In the former, we describe estimates of neutron cross section covariances for ^{55}Mn and ^{90}Zr, in the full energy range, considering the most important reaction channels, total, elastic, inelastic, capture, and (n,2n). The experimental data were analyzed and both statistical and systematic uncertainties were extracted from almost 30 selected experiments. The sensitivity to model parameters was calculated by perturbation of parameters that define the optical model potential, nuclear level densities and strength of the pre-equilibrium emission. Then, the Bayesian code KALMAN was used to combine the sensitivity analysis and the experiments.

In another work, described in **Appendix E**, we generated, for the first time, a very comprehensive set of model based estimates of cross section covariance data in the neutron energy range of 5 keV - 20 MeV. The covariance matrices were obtained for 307 materials, from ^{19}F to ^{209}Bi. Taking into account the large number of materials studied, all of them were calculated using the same reaction models, default model parameters and the same model parameters were varied to obtain sensitivity matrices. Experimental data were consulted occasionally, only to guide the selection of global uncertainties of model parameters.

Processing covariances - our efforts related to processing covariance data in the ENDF-6 format are described in **Appendix F**. The NNDC is using both available processing codes, PUFF-IV (ORNL) and NJOY-99.259 (LANL), to process all new covariance data. This step is considered to be a part of the Quality Assurance procedure, which ensures that the new evaluations can be used in transport calculations. It allows also for a visual inspection of uncertainties and correlation matrices that, otherwise, could not easily be checked neither by the evaluators nor by the users.

Visualization of covariances - the NNDC is striving to provide users with an easy access to the covariances in the evaluated nuclear data files through the NNDC web services. To this end we are developing a new retrieval system called SIGMA. The most recent version of SIGMA is capable of plotting cross section covariances in addition to their retrieval. The details are reported in **Appendix G**.

Appendix A

Covariance Capabilities in EMPIRE

Development of covariance capabilities in EMPIRE code

M. Herman[1], M.T. Pigni[1], P. Obložinský[1], S.F. Mughabghab[1], C.M. Mattoon[1],
R. Capote[2], Young-Sik Cho[3], A. Trkov[4]
[1] *National Nuclear Data Center, Brookhaven National Laboratory, Upton, NY 11973, USA*
[2] *Nuclear Data Section, IAEA, Vienna, Austria*
[3] *KAERI, Daejeon, S. Korea and*
[4] *Jozef Stefan Institute, Ljubljana, Slovenia*
(Dated: September 2, 2008)

The nuclear reaction code EMPIRE has been extended to provide evaluation capabilities for neutron cross section covariances in the thermal, resolved resonance, unresolved resonance and fast neutron regions. The Atlas of Neutron Resonances by Mughabghab is used as a primary source of information on uncertainties at low energies. Care is taken to ensure consistency among the resonance parameter uncertainties and those for thermal cross sections. The resulting resonance parameter covariances are formatted in the ENDF-6 File 32.

In the fast neutron range our methodology is based on model calculations with the code EMPIRE combined with experimental data through several available approaches. The model-based covariances can be obtained using deterministic (Kalman) or stochastic (Monte Carlo) propagation of model parameter uncertainties. We show that these two procedures yield comparable results. The Kalman filter and/or the generalized least square fitting procedures are employed to incorporate experimental information. We compare the two approaches analyzing results for the major reaction channels on ^{89}Y. We also discuss a long-standing issue of unreasonably low uncertainties and link it to the rigidity of the model.

I. INTRODUCTION

In recent years there has been an increasing demand from nuclear research, industry, safety and regulatory bodies for best estimate predictions of system performance, such as the design and operational parameters of nuclear reactors, to be provided with their confidence bounds. Estimates of the accuracy of predictions of such integral quantities can be obtained through the propagation of uncertainties in microscopic evaluated neutron cross section data.

A methodology for evaluating cross section covariance data has therefore been developed within the EMPIRE code system. The methodology covers the thermal energy, resolved resonance, unresolved resonance and fast neutron regions and builds on the following major components:

- Nuclear reaction model code EMPIRE [1]
- Atlas of Neutron Resonances [2]
- Kalman filter code [3] and Monte Carlo sampling [4].

The EMPIRE code is a key element in a broader effort pursued by the NNDC in developing covariance capabilities. This effort, that started with covariances in the fast neutron region, currently covers also the resonance region and extends to covariance visualization [5] and processing [6].

EMPIRE provides a natural environment for implementing the covariance evaluation capabilities. It is built around a physics core designed for modeling low- to-intermediate-energy nuclear reactions. It incorporates an extensive set of nuclear reaction models able to describe all relevant reaction mechanisms, each of them conveniently coupled to the up-to-date library of input model parameters [7]. The code is also suitable for massive calculations, is easy to use, has readily available default input values for all parameters, and is applicable to a wide range of target nuclei and incident neutron energies from about 1 keV to 150 MeV. Results may be stored in ENDF-6 format and subsequently plotted against experimental data for verification.

EMPIRE now includes a newly-developed resonance module that extends its covariance capability to the thermal and resonance ranges. The module utilizes the recently published Atlas of Neutron Resonances [2], a monumental work by S.F. Mughabghab containing the resonance parameters frequently adopted by many evaluations in major evaluated data libraries. The resonance module contains an electronic version of these resonance parameters along with modernized versions of the legacy codes used to develop and maintain the Atlas. In addition, the Atlas contains parameter uncertainties and the resonance module was extended to utilize this information for producing covariances in the thermal and epithermal regions.

The generation of covariances at the NNDC is based on the deterministic Kalman filter technique, which is used in the thermal and resonance range as well as in the fast neutron range. The IAEA developers, who work only in the fast region, opted for the stochastic Monte Carlo (MC) procedure to generate the model-prior, coupled to the generalized least-squares code GANDR [8] to include the experimental data. There are several fundamental and operational differences between the two methods. MC propagates uncertainties of model parameters by means of random sampling while deterministic propagation of uncertainties, using the first-order Taylor expansion, is used in the Kalman approach. Accordingly, higher-order effects are included in MC but not in Kalman. The two approaches currently also differ regarding treatment of experimental data; it is naturally included in Kalman whereas a generalized least squares code GANDR must be run with the MC generated model-based prior as input.

The paper is organized as follows. In Chapter II we describe covariance methodology. Then, in Chapter III we discuss the resonance region, followed by Chapter IV devoted to fast neutrons. In Chapter V we summarize our covariance evaluations.

Conclusions are given in Chapter VI.

II. COVARIANCE METHODOLOGY IN EMPIRE

A. EMPIRE-KALMAN approach

The Kalman filter technique is used both in the resonance and in the fast neutron region. It is based on minimum variance estimation and naturally combines covariances of model parameters, of experimental data and of cross sections. This universality is a major advantage of the method. KALMAN uses measurements along with their uncertainties to constrain covariances of the model parameters via the sensitivity matrix. Then, the final cross section covariances are calculated from the updated covariances for model parameters. This procedure consistently accounts for the experimental uncertainties and the uncertainties of the model parameters ensuring that the final cross section uncertainties are at least as good as the smaller of the two. We emphasize that under the term 'reaction model' we mean also the resonance region described by models such as the Multi-Level Breit-Wigner formalism.

The key ingredient of the method is the sensitivity matrix, which represents complex nuclear reaction calculations. If we denote the combination of nuclear reaction models as an operator $\hat{\mathbf{M}}$ that transforms the vector of model parameters $\mathbf{p}$ into a vector of cross sections $\boldsymbol{\sigma}(\mathbf{p})$ for a specific reaction channel, then the sensitivity matrix $\mathbf{S}$ can be interpreted as the linear term in the expansion of the operator $\hat{\mathbf{M}}$,

$$\begin{aligned} \hat{\mathbf{M}}\mathbf{p} &= \boldsymbol{\sigma}(\mathbf{p}) \\ \hat{\mathbf{M}}(\mathbf{p}+\delta\mathbf{p}) &= \boldsymbol{\sigma}(\mathbf{p}) + \mathbf{S}\delta\mathbf{p} + \dots \end{aligned} \tag{1}$$

We use 'hat' to stress that $\hat{\mathbf{M}}$ is the operator rather than a matrix. In practice, the elements $s_{i,j}$ of the sensitivity matrix are calculated numerically as partial derivatives of the cross sections σ at the energy E_i with respect to the parameter p_j,

$$s_{i,j} = \frac{\partial\sigma(E_i,\mathbf{p})}{\partial p_j}\,. \tag{2}$$

In case of covariance determination, the initial values of the parameters, $\mathbf{p}_1$, are already optimized, *i.e.*, when used in the model calculations they provide the evaluated cross sections. Their covariance matrix $\mathbf{P}_1$ is assumed to be diagonal while the uncertainties of the parameters are estimated using systematics, independent measurements or educated guesses. The model-based covariance matrix (prior) for the cross sections, $\mathbf{C}_1$, can be obtained through a simple error propagation formula,

$$\mathbf{C}_1 = \mathbf{S}\mathbf{P}_1\mathbf{S}^{\mathrm{T}}\,, \tag{3}$$

where superscript T indicates a transposed matrix.

The experimental data, if available, are included through a sequential update of the parameter vector $\mathbf{p}$ and the related covariance matrix $\mathbf{P}$ as

$$\begin{aligned} \mathbf{p}_{n+1} &= \mathbf{p}_n + \mathbf{P}_n\mathbf{S}^{\mathrm{T}}\mathbf{Q}_n(\boldsymbol{\sigma}_n^{\mathrm{exp}} - \boldsymbol{\sigma}(\mathbf{p}_n)) \\ \mathbf{P}_{n+1} &= \mathbf{P}_n - \mathbf{P}_n\mathbf{S}^{\mathrm{T}}\mathbf{Q}_n\mathbf{S}\mathbf{P}_n\,. \end{aligned} \tag{4}$$

Here,

$$\mathbf{Q}_n = (\mathbf{C}_n + \mathbf{C}_n^{\mathrm{exp}})^{-1}\,, \tag{5}$$

n denotes the n^{th} step in the evaluation process related to the sequential inclusion of the n^{th} experimental data set, vector $\mathbf{p}_{n+1}$ contains the improved values of the parameters starting from the vector $\mathbf{p}_n$, and $\mathbf{P}_{n+1}$ is the updated covariance matrix of the parameters $\mathbf{p}_{n+1}$. The $\mathbf{C}_n^{\mathrm{exp}}$ is the cross section covariance matrix for the n^{th} experiment. The updated (posterior) covariance matrix for the cross sections is obtained by replacing $\mathbf{P}_1$ with $\mathbf{P}_{n+1}$ in Eq. (3),

$$\mathbf{C}_{n+1} = \mathbf{S}\mathbf{P}_{n+1}\mathbf{S}^{\mathrm{T}}\,. \tag{6}$$

The updating procedure described above is often called Bayesian, although Eqs. (4-6) can be derived without any reference to the Bayes theorem as shown in Ref. [9].

The experimental covariance matrix, $\mathbf{C}_n^{\mathrm{exp}}$, is usually non-diagonal, due to the correlations among various energy points E_i. Assuming that systematic experimental uncertainties are fully correlated, the matrix elements are expressed through the statistical, $\Delta^{\mathrm{sta}}\sigma_n^{\mathrm{exp}}$, and systematic, $\Delta^{\mathrm{sys}}\sigma_n^{\mathrm{exp}}$, experimental uncertainties. This yields

$${}_nc_{i,i}^{\mathrm{exp}} = (\Delta^{\mathrm{sta}}\sigma_n^{\mathrm{exp}}(E_i))^2 + (\Delta^{\mathrm{sta}}\sigma_n^{\mathrm{exp}}(E_i))^2 \tag{7}$$

and, for $i \neq k$,

$${}_nc_{i,k}^{\mathrm{exp}} = \Delta^{\mathrm{sys}}\sigma_n^{\mathrm{exp}}(E_i) \times \Delta^{\mathrm{sys}}\sigma_n^{\mathrm{exp}}(E_k)\,. \tag{8}$$

An important technical issue, which has to be addressed in most of the covariance methods, is ensuring that the energy grid, E_i, for the model calculations and experimental data is the same to enable matrix operations in Eqs. (4-6). In the KALMAN code this is achieved by bi-spline interpolation of model cross sections and sensitivity matrices.

The above description can easily be generalized to account for correlations among different experiments. To this end one should construct a single vector containing all experimental points and the related covariance matrix, which now may contain blocks correlating different experiments. Only one update is needed in such a case but the covariance matrices are much bigger (in the current implementation of the Kalman filter the model-based covariance matrix is expanded to match the experimental one).

The quality and consistency of the evaluated cross sections can be assessed by scalar quantity

$$\chi^2 = \sum_n (\boldsymbol{\sigma}_n^{\mathrm{exp}} - \boldsymbol{\sigma}(\mathbf{p}_{\mathrm{fin}}))^{\mathrm{T}}(\mathbf{C}_n^{\mathrm{exp}})^{-1}(\boldsymbol{\sigma}_n^{\mathrm{exp}} - \boldsymbol{\sigma}(\mathbf{p}_{\mathrm{fin}}))\,, \tag{9}$$

where $\mathbf{p}_{\mathrm{fin}}$ is the final set of model parameters. A value of χ^2 per degree of freedom exceeding unity indicates underestimation of the evaluated uncertainties. It is a fairly common

practice to multiply such uncertainties by a square root of χ^2 per degree of freedom to address this issue.

The evaluator may choose to perform a sequential update using experimental data for several/all reactions or just for a single one. In the former case, all considered reactions are correlated and unique set of parameters along with the related covariance matrix are produced. On the other hand, poor experimental data in one reaction channel can negatively influence predictions for other channels.

We note that EMPIRE-KALMAN system is a general and powerful tool for evaluation of nuclear reactions. In addition to covariance calculations it may also be used to adjust model parameters to reproduce experimental cross sections and other observables within the selected reaction models and initial uncertainties of model parameters. Therefore, the Kalman filter can be used throughout the whole evaluation procedure to ensure consistency between cross sections, model parameters, and related covariance matrices.

B. EMPIRE-MC approach

The Monte-Carlo (MC) method is used in EMPIRE only in the fast neutron region. Its application to determination of covariances for the nuclear reaction observables is very transparent [4]. First, model input parameters that play a significant role in defining reaction observables of interest are identified. Then, the EMPIRE code is run a number of times with relevant input parameters being drawn randomly within the assumed limits around the central (optimal) values of the parameters. Typically, a flat distribution is used for drawing but there is also a provision for the Gaussian one. Each such calculation covers the desired incident energy range and produces full set of cross sections, spectra, angular distributions and other observables. Standard statistical methods are used to obtain covariances for the calculated quantities automatically including cross-reactions correlations. The same approach can also be used for estimating cross-correlations between any two quantities.

The MC calculations are conceptually straightforward and free of certain simplifying assumptions, *e.g.*, the assumption of a linear response of the observables to the variation of parameters, which is inherent in the KALMAN method. There is no need for a preliminary sensitivity calculation and the computing time is independent of the employed number of model parameters. These advantages come at a price - the number of required calculations is in the range of hundreds and the convergence of the results has to be demonstrated.

The standard implementation of the MC method has no provision for incorporating experimental data; the uncertainties and correlations depend only on the assumed uncertainties of the model parameters. However, the so-obtained covariance matrix can be used as a prior in a full analysis by the generalized least-squares method, taking experimental data and their uncertainties rigorously into account, *e.g.*, the GANDR system had been used in recent IAEA evaluations. Furthermore, the model-based covariances obtained with the MC method constitute a reliable benchmark for validating the faster but linear-model calculations with KALMAN code.

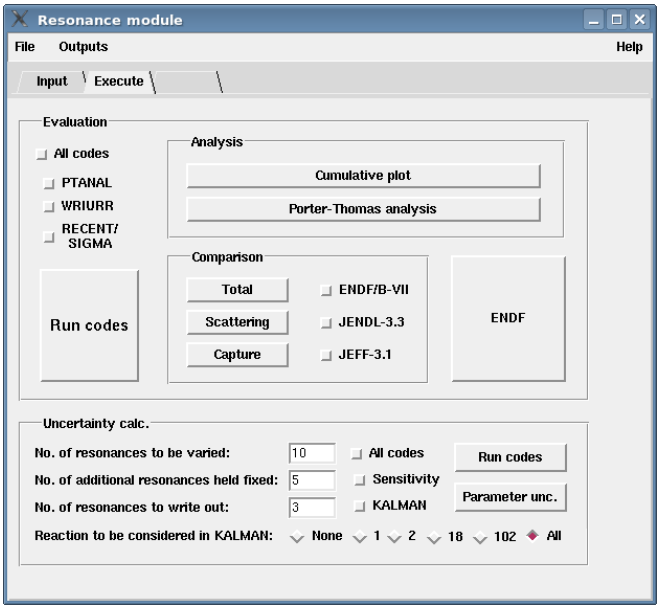

FIG. 1: Graphic user interface (GUI) of the EMPIRE resonance module. The buttons for covariance calculations are in the lower part.

III. RESONANCE REGION

A. EMPIRE resonance module

A new module for evaluating neutron cross sections in the resonance region automates most of the evaluation procedures and can be executed within EMPIRE or as a stand-alone program. It includes a graphic user interface (see Fig. 1) and a number of codes and scripts that read individual, as well as average, resonance parameters from the Atlas of Neutron Resonances [2] and other physical constants from RIPL-2 [7]. This allows performing a statistical analysis of the available resonances and computing cross sections in the resolved and unresolved resonance regions which are then compared with experimental data. The module also provides an ENDF-6 formatted file for a resonance region and various plots for verifying the procedure.

The PTANAL and WRIURR codes [10] constitute the computational core of the module. PTANAL assigns missing angular momentum and spin values to resonances using the Bayesian method and a random assignment method, respectively. It also assigns the mean radiative width to resonances with unknown Γ_γ. In addition, the reduced resonance widths are analyzed and fit with the Porter-Thomas distribution. The WRIURR code, starting from the Atlas values, constructs energy dependent average resonance parameters for the unresolved region and stores them in ENDF-6 format. All these tasks are executed with simple mouse clicks.

The reader is referred to Ref. [2] for more detailed explanation of the physics and mathematical formalism involved. The

fundamental roles of this new module are to preserve know-how accumulated over several decades by S. Mughabghab and to make it available in a modern computer environment. This will allow us to continue with the maintenance of the Atlas of Neutron Resonances in future.

B. EMPIRE resonance covariance module

Initially, we took advantage of the fact that resonances are well described by a model such as Multilevel-Breit-Wigner (MLBW) with parameters fully deduced from experiments. Considering that often also their uncertainties were known, we extended the approach already developed for the fast region that was based on the propagation of parameter uncertainties into MF33 cross section uncertainties and correlations. This approach was used for producing covariances for ^{89}Y, ^{99}Tc and ^{191,193}Ir included in ENDF/B-VII.0 [11].

More recently, we realized that more straightforward approach would be to utilize MF32 representation of resonance parameter covariances and leave production of cross section covariances to the processing codes such as NJOY-99 and PUFF-IV. An initial study along these lines is available [12].

Following the above idea the resonance module has been extended to permit generation of MF32 covariances (see lower part of the Fig. 1). This is achieved in several steps:

- Uncertainties for resonance parameters and thermal values are retrieved from the electronic version of the Atlas. The missing information is supplied by making use of systematics or estimates. These uncertainties are put into an MF=32 file of resonance parameter covariances in the compact representation. This initial matrix is diagonal since no correlations are provided in the Atlas.

- The correlations between various parameters are estimated. In general, these are correlations for the same resonance, discussed in more detail by Mughabghab [13].

- The resonance parameter uncertainties are adjusted so that the uncertainties of thermal values are reproduced, as discussed below.

The resonance module has been designed to ensure consistency among thermal cross section uncertainties and uncertainties of the resonance parameters, a feature that was not addressed during the development of the Atlas database. Thermal cross sections are usually measured with higher accuracy than resonance parameters. In order to take advantage of their superior precision while still ensuring internal consistency of the estimated covariances, we have coupled the resonance module with the Kalman filter code, which allows for an objective adjustment of the original uncertainties. We illustrate such adjustment on the two extreme cases of neutron capture on ^{55}Mn and ^{90}Zr. In the case of ^{55}Mn the thermal capture cross section is known with the accuracy of 0.37%, which is far better than the precision of the resonance parameters. ^{90}Zr is a rare exception, in which the uncertainties in the resonance region are about three times smaller than for the thermal capture (20%).

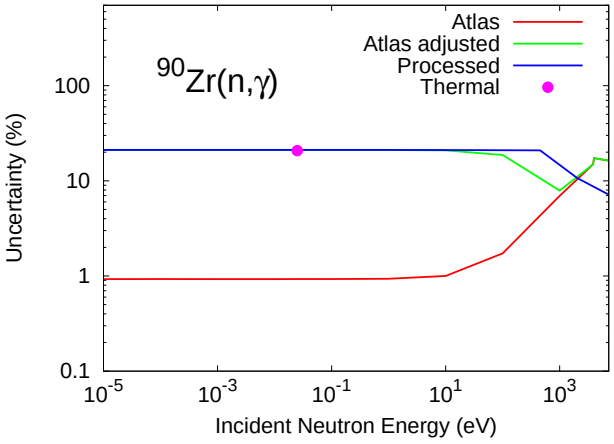

FIG. 2: Uncertainties of $^{90}\mathrm{Zr}(n,\gamma)$ cross sections. Compared is the direct propagation of the uncertainties of the resonance parameters reported in the Atlas (red), adjustment in which non-zero uncertainties were assigned to widths of the bound resonance (green) and the group-wise representation obtained with PUFF-IV (blue). The recommended uncertainty of the thermal value is also shown.

The case of ^{90}Zr is relatively straightforward - since propagation of the uncertainties of positive resonances to the thermal region falls short of the experimental capture uncertainty (see Fig. 2), we impose uncertainties of the neutron and radiative widths of the bound resonance. The original Atlas uncertainties of the positive resonances are preserved and there is no need for any correlations among parameters. The resulting uncertainties shown in Fig. 2 are in point-wise form. The same data in group form were taken from the contribution by Arcilla *et al.* [6]. The agreement is perfect in the thermal region, in which the cross sections are strongly correlated. In the region of resolved resonances the point-wise data are higher than the group uncertainties due to statistical averaging over uncorrelated resonances.

To address an inconsistency observed in the case of ^{55}Mn we considered three scenarios:

1. Adjustment of the resonance parameter uncertainties without invoking correlations among the parameters.

2. Adjustment of the positive-energy resonances using Kalman filter technique, which implies considering a full covariance matrix of the parameters.

3. The same as in point 2 but including also bound (negative-energy) resonances in the analysis.

Detailed discussion of the first scenario, along with its application to the neutron radiative capture on ^{55}Mn, was done by Mughabghab and Obložinský [13]. Restricting adjustment to the parameter uncertainties led to a considerable modification of the Atlas data.

In the second scenario we extend the above analysis by allowing correlations among resonance parameters, but restrict

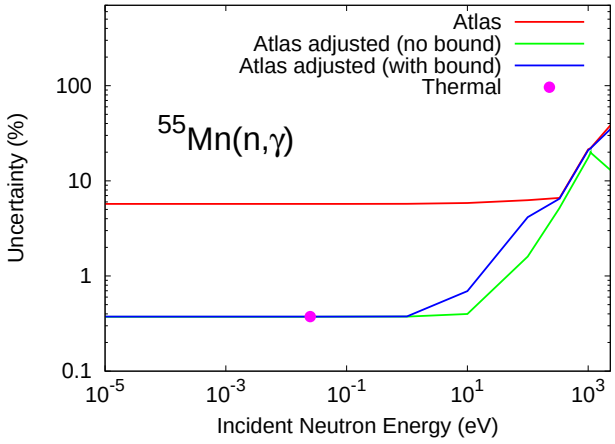

FIG. 3: Uncertainties of ^{55}Mn(n,γ) cross sections. Direct propagation of the uncertainties of the resonance parameters reported in the Atlas (red) is compared with the results of the adjustment procedure with bound resonances excluded (green) and included (blue) in the analysis. The recommended uncertainty of the thermal value is also shown.

the analysis to the positive resonances. Fig. 3 shows that the adjustment brings uncertainties at the thermal energy into a perfect agreement with the experimental uncertainty. Inspection of the adjusted uncertainties in Table I (A1 column) indicates very small changes compared to the initial uncertainties (Atlas column). Only the radiative width uncertainty for the third resonance was changed significantly, by a factor of 0.3. The reduction of the capture cross section uncertainty at the thermal energy was obtained by introducing strong anti-correlations between the radiative widths of the three considered resonances.

The third scenario brings bound resonance(s) into the play, and treats them on the same footing as the positive-energy resonances. The generous initial uncertainties of the parameters for the two bound resonances (50% for the widths and 5% for the energies) are assumed to redirect the Kalman filter emphasis from the real resonances to the bound ones. Actually, the first bound and the first positive resonances are the major players contributing 27% and 59% of the thermal capture cross section, respectively. The results are plotted in Fig. 3, while the respective relative resonance parameters and their uncertainties are listed in columns A2 of Table I.

As in the second scenario, the Kalman filter makes use of the additional degrees of freedom and ensures low uncertainty in the thermal region by introducing anti-correlation among widths of bound resonances and widths of positive resonances, while correlations between radiative widths for the positive resonances are negligible. This treatment is consistent with the actual motivation for invoking negative resonances.

Fig. 4 shows the cross section correlation matrix obtained within this approach. The thermal region appears to be fully correlated, while the resolved resonances tend to be uncorrelated. Apart from the transitional region around 10 eV there are no correlations between the thermal and resolved resonance regions.

TABLE I: Relative values and uncertainties of ^{55}Mn resonance parameters for the two bound and the first three positive-energy resonances. A1 refers to values obtained when only the first three positive resonances were allowed to be varied, while A2 values were obtained when also the two bound resonances were included in the adjustment. The uncertainties of Ref. [2] are labeled as Atlas. The negative resonance numbers indicate bound resonances, E_0 stands for the resonance energy, Γ_n and Γ_γ for the neutron and radiative width, respectively.

Res. #		Relative Value A1	Relative Value A2	Uncertainty (%) Atlas	Uncertainty (%) A1	Uncertainty (%) A2
-2	E_0	1.000	1.000	0.00	0.00	4.99
	Γ_n	1.000	1.031	0.00	0.00	48.71
	Γ_γ	1.000	1.030	0.00	0.00	48.41
-1	E_0	1.000	1.007	0.00	0.00	4.87
	Γ_n	1.000	1.317	0.00	0.00	28.29
	Γ_γ	1.000	1.317	0.00	0.00	28.29
1	E_0	.999	.999	.30	.30	.30
	Γ_n	1.015	1.001	2.19	2.11	2.18
	Γ_γ	1.130	1.009	6.45	4.64	6.31
2	E_0	.999	1.000	.18	.18	.18
	Γ_n	1.004	1.000	4.44	4.42	4.44
	Γ_γ	1.119	1.008	22.98	20.31	22.77
3	E_0	.999	.999	.22	.22	.22
	Γ_n	1.018	1.001	5.22	5.09	5.21
	Γ_γ	2.011	1.075	38.24	12.36	34.77

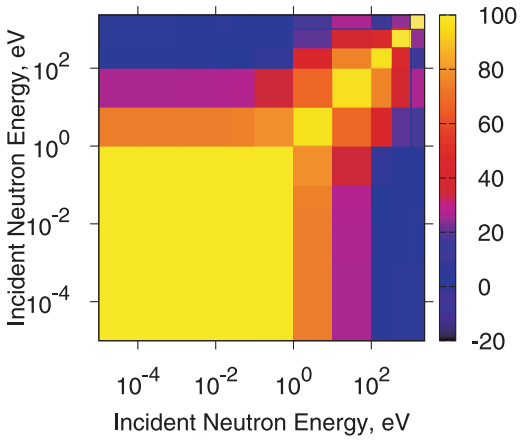

FIG. 4: Cross section correlations for ^{55}Mn(n,γ) in the low energy region for the full adjustment scenario (A2, Table I). The thermal region (bottom-left, in yellow) is fully correlated.

In spite of limited experience with the adjustment, we tend to favor the latter scenario. It achieves the consistency of uncertainties while minimizing changes to the original Atlas values and avoiding anti-correlations between positive resonances.

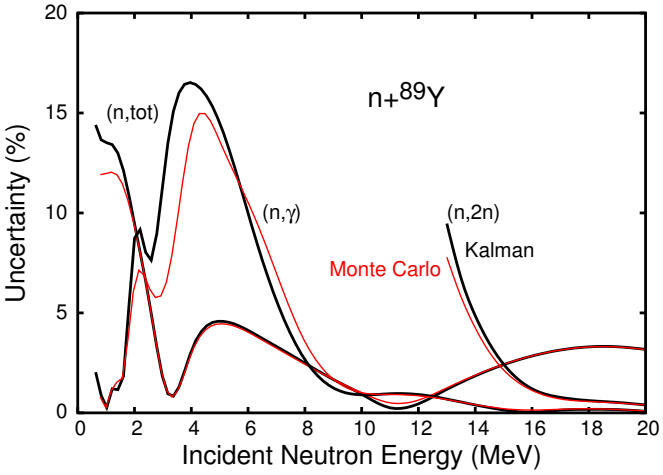

FIG. 5: Comparison of the model-based cross section uncertainties obtained with KALMAN (black) and Monte Carlo (red) methods for ^{89}Y+n reactions. Calculated uncertainties result from the variation of the real depth of the optical potential.

IV. FAST NEUTRON REGION

A. Comparison of model-based covariances obtained with Monte Carlo and KALMAN

It is of fundamental importance to compare KALMAN and MC approaches and understand any differences. The EMPIRE code was employed to perform nuclear reaction calculations, which enter both approaches, keeping inputs in both methods identical. Thus, the potential source of discrepancies, inevitable if two different reaction codes were used, was avoided. Calculations were performed for total, elastic, inelastic, (n,2n), capture, (n,p) and (n,α) reactions on ^{89}Y up to an incident energy of 20 MeV. The same uncertainties of model parameters were assumed and the MC parameters were sampled from a Gaussian distribution.

We have compared uncertainties of the considered cross sections resulting from the variation of a single model parameter. Fig. 5 shows such a comparison for one of the key parameters - depth of the real part of the optical potential. There is a reasonable agreement between model-based uncertainties obtained using the MC and KALMAN methods. Also, for the remaining parameters the results are close to each other. The only exception is the preequilibrium strength, for which the non-negligible differences were obtained. The reason for this discrepancy might be related to the fact that the relatively strong variation (20%) used in the calculations, together with the Gaussian distribution, allowed for values considerably far from the central value in the MC simulations. Because of this, the MC results may be demonstrating sensitivity to the non-linear dependence of the cross sections on the parameters.

Fig. 6 compares correlation matrices for the total cross sections. Again, both methods yield essentially equivalent results - the chess-board like pattern in the correlation matrix is the same in both methods. Only the transition between negative and positive correlations above 10 MeV is more gradual in the MC than in the KALMAN approach.

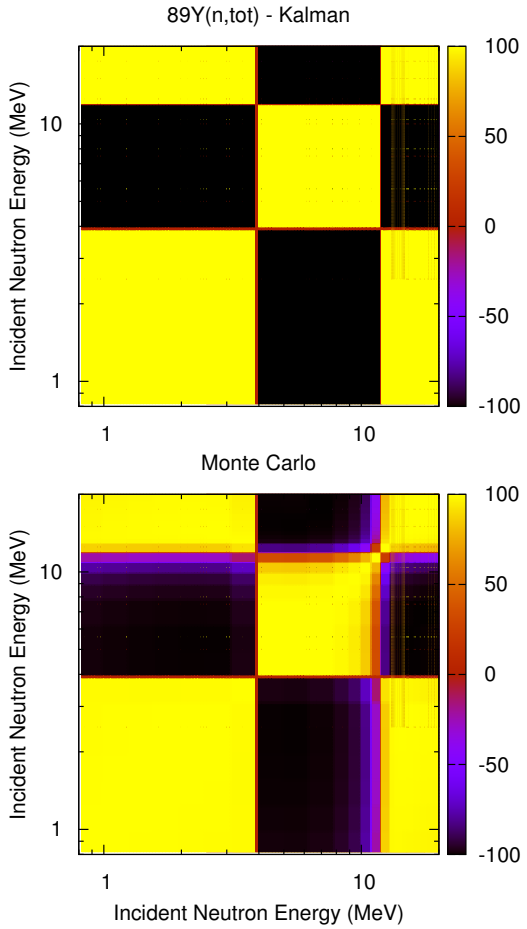

FIG. 6: Comparison of the model-based cross section correlations for ^{89}Y(n,tot) obtained with KALMAN (top) and Monte Carlo (bottom) methods. The correlations result from the variations of the real depth of the optical potential.

These numerical tests indicate that, in absence of experimental data, both methods are practically equivalent as long as the non-linearity (higher-order) effects in the KALMAN approach are taken into account. We found that to minimize the impact of non-linearity, the sensitivity matrix should be calculated using model parameter variations that are close to the parameter uncertainties.

B. Inclusion of experimental data

Inclusion of experimental data into the covariance determination still appears to be a major issue. The KALMAN method accounts for them naturally but suffers from the general deficiency of all least squares type approaches - uncertainties tend to reach values that are considered far too small if very many experimental data are included in the analysis. One practical remedy to this problem is to prevent uncertainties of the model parameters to fall below some sensible limit (say 3%). While this procedure is simple and effective, it in-

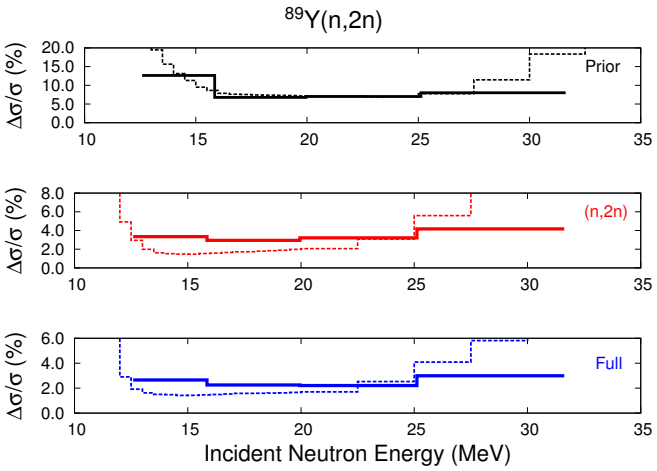

FIG. 7: Comparison of the ^{89}Y(n,2n) cross section uncertainties obtained with GANDR (solid lines) and KALMAN (dashed lines) illustrating inclusion of experimental data. The top panel shows the model-based uncertainties (prior), the middle panel includes (n,2n) data only, and the bottom panel includes experimental data for all reaction channels.

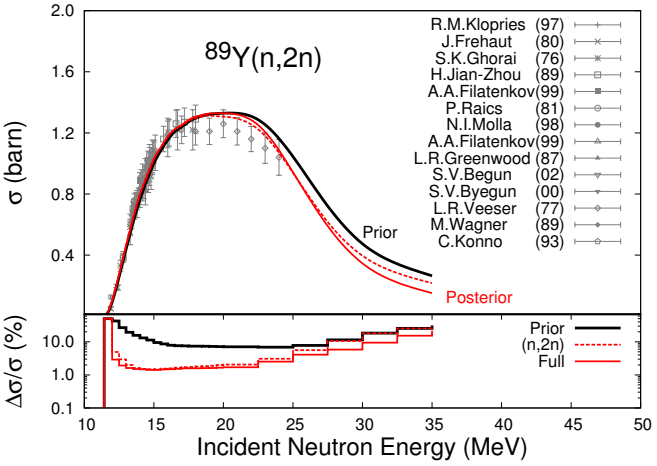

FIG. 8: Comparison of the ^{89}Y(n,2n) cross sections and uncertainties obtained with KALMAN. 'Prior' indicates default calculations and related model-based uncertainties, '(n,2n)' takes into account (n,2n) experimental data, and 'Full' includes experimental data for all reaction channels.

troduces a highly arbitrary component into the estimation of uncertainties. In the present comparison we have refrained from resorting to this solution.

The classical formulation of the MC approach does not account for the experimental data. Thus, in the present study, the prior (model-based cross section covariance), obtained with the EMPIRE-MC calculations, was fed into the Generalized Least Squares code ZOTT incorporated in a more general GANDR system by D.W. Muir [8]. In the following we refer to this approach as EMPIRE-MC-GANDR. The same nuclear reaction input was used to produce sensitivity matrices for KALMAN and the MC based priors for GANDR.

Fig. 7 illustrates effect of including experimental uncertainties of the ^{89}Y(n,2n) reaction estimated using the two methods. The pure model-based predictions are very similar. As expected, adding experimental data reduces uncertainties in both methods, but the reduction in the KALMAN approach is stronger than in the GANDR method. Inclusion of the experimental data for all the remaining channels (including nearly 1000 points for total) reduces (n,2n) uncertainties by about 30% in GANDR. In KALMAN this difference is practically negligible around 14-15 MeV, *i.e.*, in the range in which many (n,2n) measurements are available as can be seen in Fig. 8. This figure shows also the effect of including all experimental data on the posterior cross sections. Additional experimental points constrain model parameters so that the fit is slightly worse than in the case of using (n,2n) data only. There is a considerable advantage in reproducing all reaction channels simultaneously with the same set of model parameters, as cross correlations among various reaction channels are also produced.

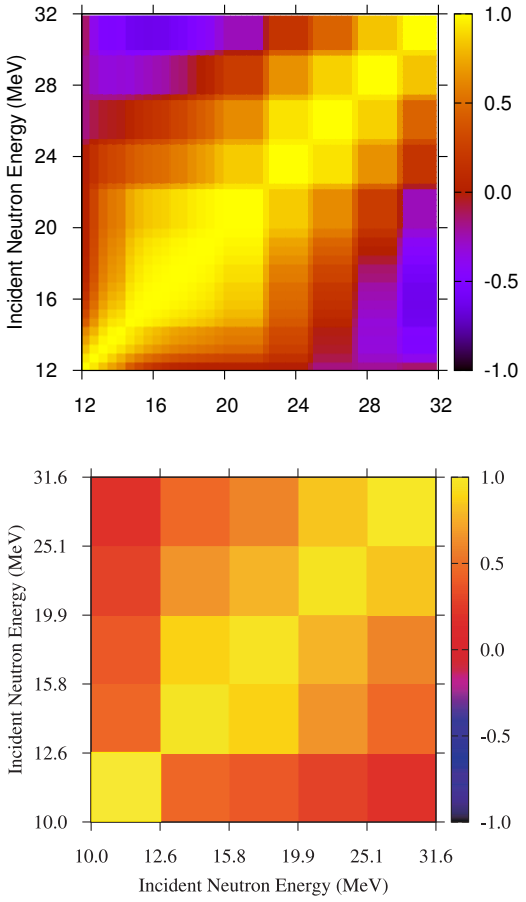

FIG. 9: The correlation matrix for the ^{89}Y(n,2n) reaction obtained with KALMAN using full set of experimental data for all reaction channels (top). The same for MC method (bottom).

Fig. 9 presents correlation matrices obtained with the two methods. The comparison is to some extent obscured by the low energy resolution in the case of GANDR, but the general structure of the two matrices can be considered similar. In the KALMAN matrix one notes relatively weak correlations

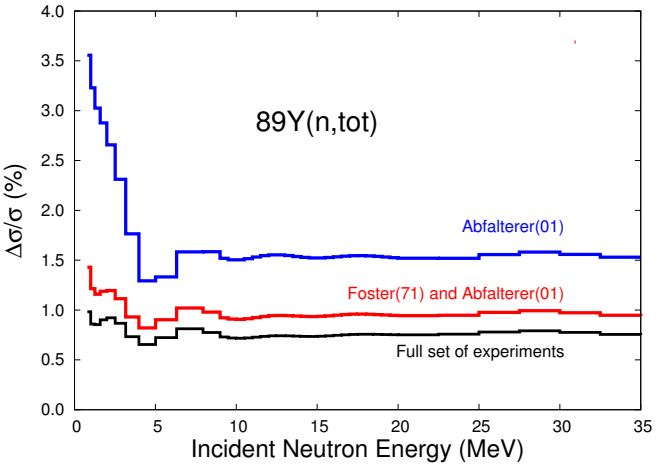

FIG. 10: Uncertainties of ^{89}Y(n,tot) cross sections obtained with KALMAN including (n,tot) data by Abfalterer (blue), (n,tot) data by Foster and Abfalterer (red), and full set of experimental data for all reaction channels (black).

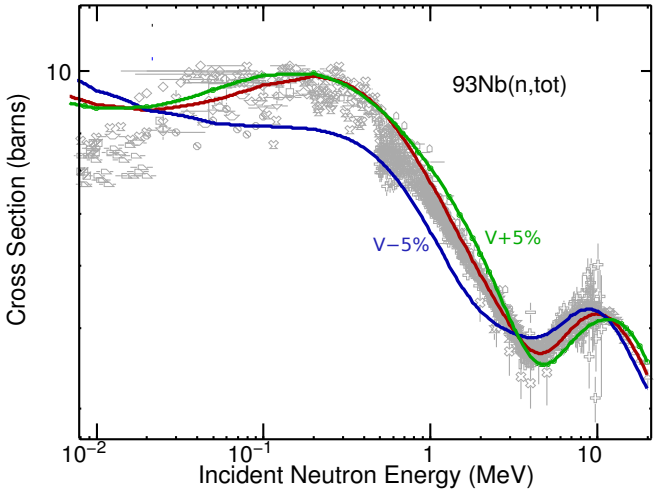

FIG. 11: Effect of 5% variation of the depth of the real optical potential on the ^{93}Nb(n,tot) cross section. The baseline values are in red.

below 15 MeV due to a large number of experimental data available in this region. At higher energies, the correlations are stronger as expected for the model dominated cases. The anticorrelations observed above 28 MeV can be explained as due to the preequilibrium emission that decreases (n,2n) cross sections in the maximum of the excitation function and increases them in the high energy tail.

Finally, in Fig. 10 we show ^{93}Nb(n,tot) and illustrate effect of including experimental data on the uncertainties of the total cross section using the KALMAN method. We note that 2.8% systematic error was assumed for all experiments but no cross correlations were allowed. Using the extended set of Abfalterer data (more than 400 points) the uncertainties are of the order of 1.5%. Adding about 200 points by Foster brings them down to about 1%, and including the remaining experiments results in a further reduction to about 0.75%. Many experimentalists would consider such low uncertainties as unrealistic.

C. Avoiding unreasonably low uncertainties

Quite often, Kalman filter analysis involving a vast amount of experimental data results in uncertainties that are far lower than systematic uncertainties even of the most precise measurement. This happens in spite of the fact that proper experimental covariances, accounting for systematic uncertainties, are supplied as an input to the KALMAN code.

One of the sources of the problem is the implicit Kalman filter assumption that the model itself is perfect. Thus, any uncertainties in model calculations are only due to the uncertainties of the model parameters. Often, the shape of a calculated excitation function is constrained. We illustrate this point on the example of the ^{93}Nb(n,tot) reaction in Fig. 11. The depth and radius of the real part of the optical model potential are essentially determining the shape and magnitude of the total cross section. The two quantities are known to be strongly correlated, therefore it is sufficient to consider only one of them. In Fig. 11 we show the change of total cross section in response to the variation of the real potential depth by 5%. One observes that this does not provide for scaling of the absolute value of the cross section. Such scaling is actually the degree of freedom that would be needed to accommodate systematic uncertainties in the measurements that in most cases amount to scaling cross sections up and down without changing its shape. Lack of this possibility might have a dramatic effect on parameter uncertainties - any scaling of the cross section appears incompatible with the model calculations since it can not be reproduced by any sensible variation of the model parameters. If the model were perfect we would have to conclude that the systematic experimental uncertainties are overestimated. To avoid such a reduction we introduce intrinsic model uncertainty by defining a fictitious model parameter, p_{mod}, that multiplies model predicted cross sections. The prior value of this parameter is one.

Our preliminary studies indicate that the Kalman filter adjusts the uncertainty of the fictitious model parameter, $\Delta p_{\rm mod}$, to reproduce the smallest systematic uncertainty. Thus, if the whole energy range is adequately covered by the experimental data the final result is well-defined. In the energy ranges without measurements the result, to some extent, depends on the initial (assumed) uncertainty of the new parameter, $\Delta p_{\rm mod}$. Naturally, if no experimental data are available the discussed contribution to the uncertainty is defined by $\Delta p_{\rm mod}$. In such a case, however, the cross section uncertainties are determined primarly by the propagation of uncertainties of the genuine model parameters, which are much larger than the intrinsic model uncertainties. The latter can, therefore, be neglected especially since there should be no uncertainties small enough to raise any concern. The procedure is particularly useful to simulate intrinsic uncertainties in the optical model, *i.e.*, it is meant to be applied to the total cross sections. These are often very well measured which, combined with the rigid shape of

the optical model predictions, results in extremely low uncertainties. There is no need to invoke such a procedure for other nuclear reaction models, e.g., compound nucleus and preequilibrium emission, since their formulations include parameters which, to a large extent, provide for a scaling degree of freedom.

A conceptually similar solution, correlated sampling of energy-dependent scaling parameters, has also been adopted for the MC approach in EMPIRE. In this way, the minimum uncertainty of the calculated cross-section is limited by the uncertainty of the scaling parameter which is taken as the model uncertainty.

An additional source of low uncertainties has been discussed in the contribution by Leeb [14] to the present Workshop - neglecting correlations among numerous experiments implies statistical independence of the respective systematic uncertainties and leads to reducing final uncertainty below individual systematic uncertainty. We refer to the original paper by Leeb for a description of an approximate method allowing one to avoid this source of underestimation.

V. APPLICATION TO COVARIANCE EVALUATIONS

The EMPIRE-KALMAN and EMPIRE-MC-GANDR system has been extensively applied for the generation of covariance data. We mention here covariances for 13 materials, ^{89}Y, ^{99}Tc, $^{152-158,160}$Gd, ^{191,193}Ir and ^{232}Th, included in the new ENDF/B-VII.0 library [11] released in 2006. In addition, there was a considerable effort to deliver preliminary covariances for the WPEC Subgroup 26 which resulted in covariance estimates for 36 materials. The more recent large-scale project was initiated by the U.S. Nuclear Criticality Safety Program to provide a 'low-fidelity', but complete, set of covariances that could be used to exercise processing methodologies and tools [15].

New evaluations for a full set of stable tungsten isotopes, $^{180,182-184,186}$W, in the neutron energy range up to 150 MeV were produced [16], with the covariance matrices generated using the EMPIRE-MC-GANDR approach. The NNDC produced new covariances for ^{55}Mn and ^{90}Zr in the fast neutron region using EMPIRE-KALMAN technique [17].

The NNDC and LANL are cooperating in preparation of covariances for the ENDF/B-VII.0 data adjustment within the GNEP project. This activity involves about 100 materials relevant to the design of the innovative fast actinide burner reactors.

VI. CONCLUSIONS

There has been considerable activity to reestablish covariance capabilities within the nuclear data comunity. Qualitative progress became possible due to the availability of advanced nuclear reaction codes supported by the comprehensive libraries of input parameters (RIPL) and by the compilation of resonance parameters (Atlas). The cross section covariance capabilities of the EMPIRE code cover the full energy range relevant to applications, including thermal, resonance and fast neutron regions. This puts EMPIRE in a unique position to provide complete sets of covariance data for most of the nuclei, such as the fission products and structural materials. The code is also well capable of treating actinides. The modules for estimating covariances for neutron multiplicities and for fission spectra are integrated into the EMPIRE code but need adequate parametrization.

The resonance module of EMPIRE closes the gap between the evaluated neutron resonance data for 381 isotopes contained in the Atlas of Neutron Resonances and applications by bringing Atlas data into the evaluated nuclear data files. In particular, the module produces covariances of the resonance parameters in the MF32 compact representation. When doing this, the module allows adjustment of the parameter uncertainties in order to ensure consistency with the uncertainties of the thermal cross sections. We have discussed several strategies for imposing such consistency and found that in most cases invoking correlations among positive and negative (bound) resonances is the least intrusive solution.

In the fast neutron region we discussed two complementary methods implemented in EMPIRE for determining covariances. The Kalman filter approach is based on variance minimization while the stochastic one is based on the Monte Carlo sampling followed by the GANDR least-squares fitting of experimental data. We have compared both approaches and concluded that model-based covariances obtained with the two methods are practically equivalent. There is also a possibility of using KALMAN generated model-based prior with the GANDR code.

Very serious concerns were raised regarding extremely low uncertainties resulting from the least-squares analysis using model-generated priors. We believe that these low uncertainties arise, in part, from the rigidity of the model predictions, *i.e.*, intrinsic model uncertainties which are not accounted for in the procedure. Our numerical experiments indicate that adding new degrees of freedom to the model has a desired effect on the output uncertainties and might be used to eliminate this deficiency.

The EMPIRE code system is entering a stage at which it can effectively be used for production of covariance data. Still, there is a number of issues that should be addressed. In the resonance region these include accounting for the uncertainties of the resonance integrals, and possible correlations among positive resonance parameters. The methodology in the unresolved resonance region should be addressed by adding capability to utilize average resonance parameters. In the fast neutron range, we should be seeking better insight into intrinsic model uncertainties and expand the space of perturbed parameters, *e.g.*, we should include the energy dependence on the model parameters. Protracted activities along these lines should eventually provide an extensive and consistent set of model parameters. Last, but not least, is the long standing problem of analyzing experimental data in order to extract critical information regarding statistical and systematic errors associated with these measurements, which are decisive in determining evaluated data.

The work at BNL was sponsored by DOE-NNSA, DOE-NE, and also by DOE-Office of Science under Contract No. DE-AC02-98CH10886 with Brookhaven Science Associates, LLC.

[1] M. Herman, R. Capote, B. Carlson, P. Obložinský, M. Sin, A. Trkov, H. Wienke, and V. Zerkin, "EMPIRE: Nuclear Reaction Model Code System for Data Evaluation," *Nuclear Data Sheets*, vol. **108**, no. 12, pp. 2655–2715, 2007.

[2] S. F. Mughabghab, *Atlas of Neutron Resonances: Thermal Cross Sections and Resonance Parameters*. Amsterdam: Elsevier, 2006.

[3] T. Kawano and K. Shibata, "Covariance Evaluation System." JAERI Data/Code, Japan Atomic Energy Research Institute, Tokai, Japan, 1997.

[4] D. Smith, "Covariance matrices for nuclear cross sections derived from nuclear model calculations," report ANL/NDM-159 November, Argonne National Lab, 2004.

[5] B. Pritychenko and A. Sonzogni, "Sigma: Web Retrieval Interface for Nuclear Reaction Data," *December 2008 issue of Nuclear Data Sheets*.

[6] R. Arcilla, A. Kahler, P. Obložinský, and M. Herman, "Processing of Neutron Cross Section Covariances Using NJOY-99 and PUFF-IV," *December 2008 issue of Nuclear Data Sheets*.

[7] T. Belgya, O. Bersillon, R. Capote, T. Fukahori, G. Zhigang, S. Goriely, M. Herman, A. Ignatyuk, S. Kailas, A. Koning, P. Obložinský, V. Plujko, and P. Young, "Handbook for Calculations of Nuclear Reaction Data, Reference Input Parameter Library-2," TECDOC-1506, IAEA, Vienna, 2005.

[8] D. W. Muir, A. Mengoni, and I. Kodeli, "Integration International Standards Evaluation into a Global Data Assessment," *December 2008 issue of Nuclear Data Sheets*.

[9] D. W. Muir, "Evaluation of correlated data using partinioned least squares: a minimum-variance derivation," *Nucl. Sci. Eng.*, vol. 101, pp. 88–93, 1989.

[10] S. Oh, J. Chang, and S. F. Mughabghab, "Neutron cross section evaluations of fission products below the fast neutron region," Tech. Rep. BNL-NCS-67469, Brookhaven National Lab., 2000.

[11] M. Chadwick, P. Obložinský, M. Herman, *et al.*, "ENDF/B-VII.0: Next generation evaluated nuclear data library for nuclear science and technology," *Nuclear Data Sheets*, vol. 107, no. 12, pp. 2931–3118, 2006.

[12] M. Herman, S. Mughabghab, P. Obložinský, M. Pigni, and D. Rochman, "Neutron cross section covariances in the resolved resonance region," Report BNL-80173-2008, Brookhaven National Laboratory, 2008.

[13] S. F. Mughabghab and P. Obložinský, "Neutron Cross Section Covariances in the Thermal and Resonance Regions," *December 2008 issue of Nuclear Data Sheets*.

[14] H. Leeb, "Consistent procedure for evaluation based on modeling," *December 2008 issue of Nuclear Data Sheets*.

[15] R. Little *et al.*, "Low-fidelity Covariance Project," *December 2008 issue of Nuclear Data Sheets*.

[16] A. Trkov, R. Capote, I. Kodeli, and L. Leal, "Evaluation of Tungsten Nuclear Reaction Data with Covariances," *December 2008 issue of Nuclear Data Sheets*.

[17] M. Pigni, M. Herman, and P. Obložinský, "Estimated ^{55}Mn and ^{90}Zr Covariances in the Fast Neutron Region," *December 2008 issue of Nuclear Data Sheets*.

Appendix B

Thermal and Resonance Parameter Uncertainties

Neutron Cross Section Uncertainties in the Thermal and Resonance Regions

S.F. Mughabghab* and P. Obložinský
National Nuclear Data Center, Brookhaven National Laboratory, Upton, NY 11973-5000
(Dated: September 2, 2008)

In the *Atlas of Neutron Resonances*, special care was expended to ensure that the resonance parameter information reproduces the various measured thermal cross sections, as well as the infinite dilute resonance integrals for Z = 1-100. In contrast, the uncertainties of the recommended quantities do not match those generated from the uncertainties of the resonance parameters. To address this problem, the present study was initiated to achieve consistency for 15 actinides and 21 structural and coolant moderator materials. This is realized by assigning uncertainties to the parameters of the negative-energy resonances and changing, if necessary, significantly the uncertainties of the low-lying positive-energy resonances. The influence of correlations between parameters on the derived uncertainties is examined and discussed.

I. INTRODUCTION

The National Nuclear Data Center produced a set of preliminary neutron covariance estimates for the international project, Nuclear Data Needs for Reactor Systems. The project is sponsored by the OECD Nuclear Energy Agency (NEA), Paris, under the Subgroup 26 of the International Working Party on Evaluation Cooperation (WPEC), chaired by M. Salvatores, ANL and CEA Cadarache. These preliminary covariances are described in the recent BNL report [1]. The project is interested in 53 materials (isotopes) which include 19 actinides and 34 structural, coolant and moderator materials. Out of them, the NNDC produced covariance estimates for 36 materials.

In the low-energy region, the NNDC used the method developed by BNL and LANL [2] that combines the recent information in the *Atlas of Neutron Resonances* [3] and the Bayesian code Kalman by Kawano and Shibata [4]. The idea of this approach is to use uncertainties of various parameters given in Ref. [3] and propagate them to cross section covariances. This can be done in two ways. First, one starts with cross sections and produces covariances straight in ENDF-6 file MF33 [1]. Second, as proposed in Ref. [5], one works purely with resonance parameters, produces covariances in MF32 and leaves up to processing codes the generation of cross section covariances.

As emphasized in [3], the absolute values of various recommended quantities, such as thermal capture, fission and scattering cross sections, as well as capture and fission resonance integrals, exhibit internal consistency with values calculated from the resonance parameters. However, no attempt was made to achieve consistencies between the various uncertainties of these quantities. Such inconsistencies would then propagate into the resulting cross section covariances rendering them less reliable.

In this study, consistencies between uncertainties of thermal cross sections and resonance parameters for capture and fission, but not scattering, cross sections were achieved for the following 36 nuclei: ^{19}F, ^{23}Na, ^{27}Al, ^{28}Si, ^{52}Cr, ^{55}Mn, ^{56,57}Fe, ^{58}Ni, ^{90,91,92,94}Zr, ^{166,167,168,170}Er, ^{206,207,208}Pb, ^{209}Bi, ^{233,234,236}U, ^{237}Np, ^{238,240,241,242}Pu, ^{241,242m,243}Am and ^{242,243,244,245}Cm.

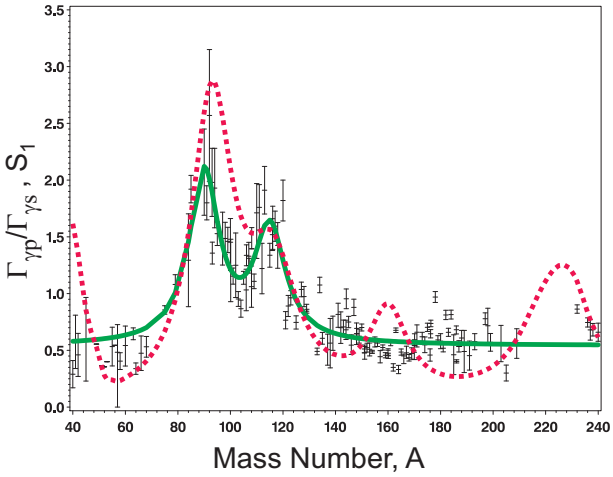

FIG. 1: Novel systematics for the average capture widths [6]. The ratio of the p-wave and s-wave radiative widths, displayed as a function of mass number, is designated by a solid green line. The p-wave strength function S_1, multiplied by 0.4×10^4, is shown by a broken red line.

II. METHODOLOGY

In this section, a brief account of the methodology and procedure considered in the analysis of covariances is presented.

- The starting point of the uncertainty analysis is an examination of the electronic file of the resonance parameters [3] in question to search for missing information.
- Where entries of the individual resonance parameters, such as radiative or scattering widths, are absent due to lack of measurements, then data based on the systematics described in [3] or other sources are supplied or estimated.
- In addition to the average resonance parameters and the systematics reported in [3], a recent detailed study [6]

*Corresponding author: mugabgab@bnl.gov

revealed for the first time a novel relationship between the average p- and s-wave radiative widths, as illustrated in Fig. 1. The observed structures for the ratio of the p-wave to s-wave radiative widths, $\Gamma_{\gamma p}/\Gamma_{\gamma s}$, at mass numbers 90 and 114 are associated with the splitting of the 3p single-particle state into its $3p_{1/2}$ and $3p_{3/2}$ components due to the nuclear spin-orbit interaction. Since these peaks are correlated with the p-wave strength function (Fig. 1), the p-wave radiative widths in the mass region 80-120 exhibit non-statistical effects in the neutron radiative capture mechanism. The background term for the ratio is interpreted in terms of the contribution of the giant dipole resonance to the capture process [6]. This significant information can be utilized in determining either the s- or p-wave radiative widths, when one is known with better accuracy than the other. Furthermore, for certain nuclei where information is lacking, scattering widths can be estimated from the reported measured capture kernels.

- The Atlas file is then converted into an ENDF-6 format with the aid of the computer program PTANAL [7]. In this procedure, average s- and p-wave radiative widths are supplied when such data is missing, and spin assignments of resonances of undetermined values are randomly made with the condition that the (2J+1) law for level density is followed.

- The utility code RECENT and a PSY-325 program are applied to determine the various contributions to the thermal cross sections and resonance integrals from individual resonances.

- The reported uncertainties of the thermal cross sections are attributed to the uncertainties of the bound levels and/or few low-energy resonances.

- Adjustments of the resonance parameter uncertainties are carried out iteratively until the calculated uncertainties of the thermal capture or fission cross sections converge to the measured ones.

The total uncertainty of the capture (fission) cross section in terms of the uncertainties of the individual resonance parameters, E_0, Γ_n, Γ_γ, and Γ_f, is expressed by Eq.(1) and Eq.(2), when correlations do not exist between the parameters; otherwise, additional terms, such as Eq.(3) and Eq.(4), have to be considered.

Since a large number of resonance uncertainties contribute to the scattering uncertainty, only the capture and fission uncertainties were treated in this study; for an explanation, refer to Eq.(1.9) and Eq.(1.14) in [3].

At the start, the correlations between the parameters were not considered; their effects are studied later on for some nuclei. Also in this study, the Breit-Wigner relations for capture and fission are utilized for the determination of the partial derivatives in Eqs. (1-4).

$$(\Delta\sigma_\gamma)^2 = \left(\frac{\partial\sigma_\gamma}{\partial E_0}\Delta E_0\right)^2 + \left(\frac{\partial\sigma_\gamma}{\partial\Gamma_n}\Delta\Gamma_n\right)^2 + \left(\frac{\partial\sigma_\gamma}{\partial\Gamma_\gamma}\Delta\Gamma_\gamma\right)^2 + \left(\frac{\partial\sigma_\gamma}{\partial\Gamma_f}\Delta\Gamma_f\right)^2 \quad (1)$$

$$(\Delta\sigma_f)^2 = \left(\frac{\partial\sigma_f}{\partial E_0}\Delta E_0\right)^2 + \left(\frac{\partial\sigma_f}{\partial\Gamma_n}\Delta\Gamma_n\right)^2 + \left(\frac{\partial\sigma_f}{\partial\Gamma_\gamma}\Delta\Gamma_\gamma\right)^2 + \left(\frac{\partial\sigma_f}{\partial\Gamma_f}\Delta\Gamma_f\right)^2 . \quad (2)$$

The calculated uncertainties for the thermal capture and fission cross sections due to all the individual s-wave resonances, reported in [3], are determined by these relations and then combined in quadratures to obtain the total uncertainty.

When correlations do exist between the various resonance parameters, such as between Γ_γ and Γ_n or Γ_f and Γ_γ, then the following additional terms, Eqs. (3)-(4) have to be added to Eqs. (1-2)

$$(\Gamma_\gamma,\Gamma_n) = 2\left(\frac{\partial\sigma_\gamma}{\partial\Gamma_n}\Delta\Gamma_n\right)\left(\frac{\partial\sigma_\gamma}{\partial\Gamma_\gamma}\Delta\Gamma_\gamma\right)\rho(\Gamma_\gamma,\Gamma_n)\,, \quad (3)$$

$$(\Gamma_f,\Gamma_\gamma) = 2\left(\frac{\partial\sigma_f}{\partial\Gamma_f}\Delta\Gamma_f\right)\left(\frac{\partial\sigma_f}{\partial\Gamma_\gamma}\Delta\Gamma_\gamma\right)\rho(\Gamma_f,\Gamma_\gamma)\,, \quad (4)$$

where $\rho(\Gamma_\gamma,\Gamma_n)$ and $\rho(\Gamma_f,\Gamma_\gamma)$ are the correlation coefficients between Γ_γ and Γ_n or between Γ_f and Γ_γ, respectively. The origin of these types of correlations is discussed briefly in the following section.

III. SOME SOURCES OF CORRELATIONS

In this section, a brief discussion of the sources of correlations between the various parameters, emanating from the analysis of the measurements, is presented.

- In capture measurements when the experimental resolution function is larger than the natural width of a resonance, area analysis yields a capture kernel, defined by $A_\gamma = g\Gamma_n\Gamma_\gamma/\Gamma$, where g is the statistical spin factor. If $A_\gamma < g\Gamma_\gamma$, then a scattering width can be evaluated from this relation by assuming an average capture width, derived from the systematics [3, 6], and a

spin value for the considered resonance. In this case, $\rho(\Gamma_n, \Gamma_\gamma)$ is negative.

- In combined capture and fission measurements, capture and fission kernels are determined, in which case Γ_f/Γ_γ is found. The fission widths are subsequently derived on the basis of an assumed average capture width, as, for example, in the case of the isotopic curium measurements of [8]. In this case $\rho(\Gamma_f, \Gamma_\gamma)$ is positive.

- Neutron sensitivity corrections, applied to capture measurements, are generally made with the help of the relation

$$\Gamma_\gamma^{\rm exp} = \Gamma_\gamma + k\Gamma_n \,,$$

where k is obtained experimentally. If k is not determined correctly, then $\rho(\Gamma_n, \Gamma_\gamma)$ can be positive. A Γ_γ-Γ_n correlation analysis, as well as theoretical calculations [9], has to be performed to determine as to whether the correlation exists. If affirmed, a determination has to be made as to whether it is due to neutron sensitivity or valence capture [9].

- In determining the parameters of bound levels, for nuclei where the positive-energy resonances also contribute significantly to the thermal capture cross section, then a negative correlation exists between the parameters of the positive-energy and bound resonances. Relations similar to those of Eqs. (3-4) can be employed to take into account their effects on the uncertainties.

IV. RESULTS

Our experience in the adjustment procedure is presented and the outstanding issues resulting from the present analysis are discussed for the following nuclei: ^{55}Mn, ^{56}Fe, and ^{167}Er.

A. ^{55}Mn

Adopted as a standard in neutron activation analysis, the thermal capture cross section of ^{55}Mn, σ_γ^0 = 13.36 $\pm$ 0.05 b (0.37%), is measured with high accuracy. As noted in a footnote in the Atlas [3], the adoption of the capture widths measured at ORNL [10], which were the only available data at the time, leads to a calculated resonance capture integral of 11.7 b. This value is discrepant with a measured value of 13.4$\pm$0.5 b [3]. To resolve this discrepancy, adjustments in the capture widths of [10] were made; the results are shown in column 5 of Table I.

In addition, two bound s-wave levels with spins 2 and 3 are invoked in order to account for the coherent and incoherent scattering amplitudes of ^{55}Mn. The contributions to the thermal capture cross section due to the bound levels, as well as the 3 positive-energy resonances, are presented in the last column of Table I. With these parameters and those in [3] above 3 keV, the calculated capture cross section in the energy region from 0.01 eV to 20 keV is displayed in Fig. 2 and is compared with the measurements of [11] below 300 eV.

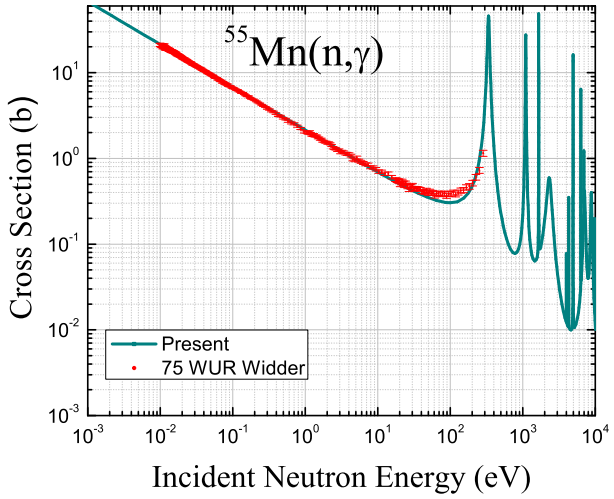

FIG. 2: The measured capture cross section of ^{55}Mn in the energy region 0.01 to 300 eV. The solid line represents the present calculations based on the resonance parameters of Table I and in Ref. [3] above 2.4 keV.

TABLE I: ^{55}Mn resonances and their contribution to the thermal capture cross section. In the present notation, a = data from the Atlas [3], and b = quantities evaluated in the present study. The energy uncertainty of the 337.3 eV resonance is altered from 1.0 eV [3] to 0.7 eV.

E_0 (eV)^a	$2g\Gamma_n$ (eV)^a	$2g\Gamma_n$ (eV)^b	Γ_γ(eV)^a	Γ_γ (eV)^b	σ_γ (b)^b
-16150	6255	6255	.75 $\pm$.0%	.79$\pm$.0	0.32
-202	1.15	1.15	.75 $\pm$.0%	.79$\pm$.0	3.38
337.3 $\pm$0.7	18.3 $\pm$2.2%	18.3$\pm$.2%	.31 $\pm$6.5%	.40$\pm$.0	7.44
1099 $\pm$ 2.0	18.0 $\pm$4.0%	18.0 $\pm$.4%	.435 $\pm$23.0%	.40$\pm$.0	1.50
2327 $\pm$ 5.0	460 $\pm$5.2%	460 $\pm$.2%	.34 $\pm$38.2%	.40$\pm$.0	0.17

To account for a 0.37% uncertainty in the thermal capture cross section, the uncertainties of the resonance parameters have to be drastically reduced. It is significant to note that consistency between the two uncertainties can be achieved by changing the energy uncertainty of the resonance at 337.1 eV from 1.0 eV to 0.7 eV.

This procedure presents an outstanding issue. To overcome this problem, one can invoke an anti-correlation between the parameters of the positive-energy and bound levels, which can alleviate this problem. Such a procedure entailed imposing large uncertainties on the parameters of the bound parameters while retaining, with minor adjustments, the uncertainties of the positive energy resonances as reported in [3]. The latter procedure is justifiable on physical grounds. For details, refer to [12].

B. ^{56}Fe

In this simple case, the thermal capture cross section section of ^{56}Fe, σ_γ^0 = 2.59±0.14 b, is dominated by a bound level, specified at an energy of -6.52 keV. The positive-energy resonance contributions due to all resonances up to an energy of 850 keV is only 0.09 b [3]. The pointwise capture cross section in the energy region 0.007 eV to 1.41 keV was measured by [13]. The computed and measured cross sections are depicted in Fig. 3. Note that the resonance at 1.147 keV has a p-wave assignment, and hence does not have a contribution to the thermal capture cross section of ^{56}Fe.

The 5.4% uncertainty of the thermal capture cross section can be propagated by assigning a 3.82% uncertainty to both the scattering and capture widths of the bound level only. The positive-energy resonances then maintain their original uncertainties [3]. In this case, it is not necessary to invoke an anti-correlation between the bound and positive energy resonances.

At this point, we point out the similarity of the capture cross sections of ^{52}Cr and ^{56}Fe in that both are dominated by bound levels; refer to the discussion in section V.

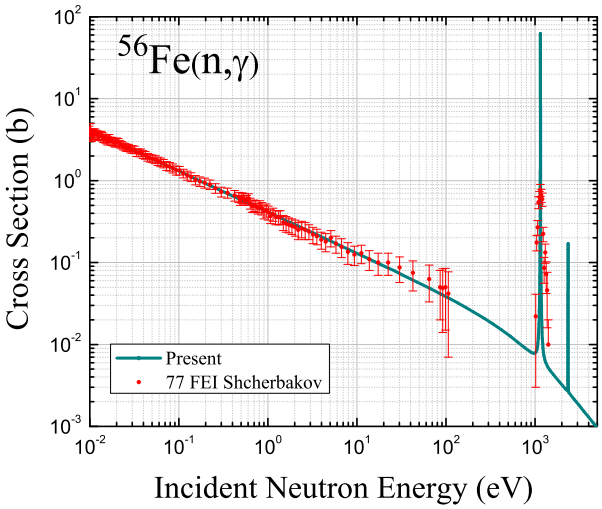

FIG. 3: The measured capture cross of ^{56}Fe in the energy region 0.01-3000 eV [13]. The solid line represents the calculations on the basis of the resonance parameters of the Atlas [3].

C. ^{167}Er

The thermal capture cross section of ^{167}Er, σ_γ^0 = 649±8 b(1.2%) is dominated by two positive-energy resonances at 0.460 eV and 0.584 eV. The scattering and capture widths of these two resonances are determined recently [14] by applying shape fit analysis to the transmission data, obtained for a natural Er sample in the energy region from 0.03-20 eV. To propagate a 1.2% uncertainty for σ_γ^0, the uncertainties of the capture widths of the bound level and the resonance at 0.460 eV were changed as shown in column 3 of Table II. The uncertainties of the scattering widths were maintained at the Atlas values.

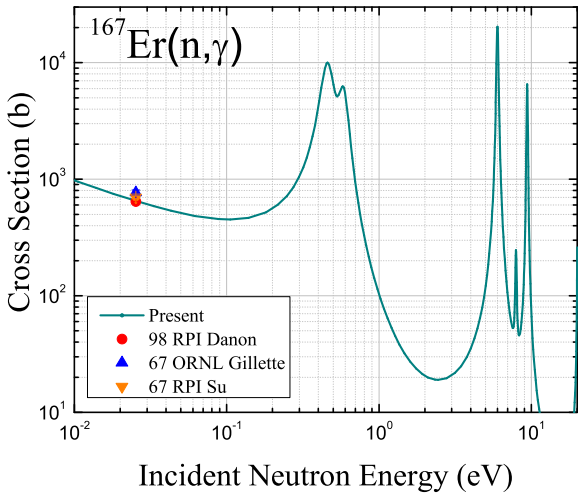

FIG. 4: The measured capture cross of ^{167}Er in the energy region from 0.001 to 10 eV. The solid line represents the calculations on the basis of the resonance parameters of the Atlas [3].

TABLE II: ^{167}Er resonances and their contribution to the thermal capture cross section. The two quantities in parentheses in columns 2 and 3 are the % uncertainties in the Atlas and the present study, respectively.

E_0 (eV)	$2g\Gamma_n$ (meV)	Γ_γ(meV)	σ_γ (b)
-23.6	117 (0.0, 10.0)%	88.0 (0.0, 11.0)%	7.9
0.460 ±0.002	0.3031 (0.33, 0.33)%	87.12 (0.2, 0.4)%	423
0.584 ±0.001	0.2163 (0.46, 0.46)%	86.20 (0.4, 0.4)%	161

V. CORRELATION EFFECTS ON CALCULATED UNCERTAINTIES

A correlation analysis between capture and scattering widths for the following nuclei ^{52}Cr, ^{55}Mn, ^{56}Fe, ^{167}Er and ^{237}Np was carried out. The correlation coefficients are, respectively, 0.63±0.09 (8 s-wave resonances), 0.700±0.001 (49), 0.20±0.58 (10), 0.35±0.01 (54), 0.12±0.12 (147). Note that the significance levels for ^{52}Cr and ^{56}Fe are high and null, respectively. For this reason, ^{56}Fe is replaced by ^{52}Cr in this analysis. In addition, we believe that the high significance level of the correlation coefficient for ^{55}Mn is due to neutron sensitivity correction and not arising from valence capture.

The effects of the correlation between the capture and scat-

TABLE III: Effects of correlations between Γ_γ and Γ_n on the thermal capture cross section uncertainties of ^{52}Cr, ^{55}Mn, and ^{237}Np for three values of the correlation coefficients, 0.0, -1.0, and 1.0.

nucleus	σ_γ (b)	$\Delta\sigma_\gamma$ (b)	$\Delta\sigma_\gamma$ (b)	$\Delta\sigma_\gamma$ (b)
$\rho(\Gamma_\gamma, \Gamma_n)$		0.0	-1.0	+1.0
^{52}Cr	0.86±0.02	0.020	0.018	0.023
^{55}Mn	13.36±0.05	0.047	0.047	0.049
^{237}Np	178.7±3.0	3.0	1.6	4.0

tering widths of the same resonance on the capture uncertainties for three nuclei, ^{52}Cr, ^{55}Mn, and ^{237}Np, were studied and summarized in Table III. The case for $\rho(\Gamma_\gamma, \Gamma_n) = 0$ corresponds to the results of the main study with no correlations, where the calculated uncertainties reproduce those of the recommendations [3]. In columns 4 and 5 of Table III are the results for $\rho(\Gamma_\gamma, \Gamma_n)$= -1 or +1. As shown, the correlations produce negligible effects for ^{52}Cr, ^{55}Mn. This is a result of the fact that the final adjusted uncertainties for the capture widths are set to zero; refer to Eq.(3). On the other hand, a non-negligible change occurs in the uncertainties of ^{237}Np.

VI. CONCLUSIONS

Internal consistency between the uncertainties of thermal capture and fission cross sections and the uncertainties of resonance parameters is achieved for 15 actinides and 21 coolant and structural materials. This was realized by re-assigning uncertainties to the parameters of bound levels and low-energy resonances. If the major contribution to the thermal capture cross section is due to the positive-energy resonances, then their uncertainties are significantly changed from values reported in [3]; this pauses certain challenge as to what extent these changes are physically justifiable. Such a situation can be resolved by invoking an anti-correlation between the bound and positive energy resonances, as determined for ^{55}Mn [12].

In other cases, where the thermal capture cross section is dominated by bound levels, as in ^{52}Cr and ^{56}Fe, the uncertainties of the positive-energy resonances are unaffected from those reported in [3]. The correlations between parameters of the same resonance are studied and their effect on the adjusted uncertainties is determined for some cases

Acknowledgments

The support of B. Pritychenko with LaTex is gratefully acknowledged. Work at Brookhaven National Laboratory was sponsored by the Office of Nuclear Physics, Office of Science of the U.S. Department of Energy under Contract No. DE-AC02-98CH10886 with Brookhaven Science Associates, LLC.

[1] D. Rochman, M. Herman, P. Obložinský and S. F. Mughabghab, *Preliminary Cross Sections and Nubar Covariances for WPEC Subgroup 26*, Report BNL-77407- 2007-IR, January 2007.

[2] M. B. Chadwick, P. Obložinský, M. Herman et al., *ENDF/B-VII.0: Next Generation of Evaluated Nuclear Data Library for Nuclear Science and Applications*, NUCLEAR DATA SHEETS, **107**, 2931-3060 (2006).

[3] S. F. Mughabghab, ATLAS OF NEUTRON RESONANCES: RESONANCE PARAMETERS AND THERMAL CROSS SECTIONS Z=1-100, Elsevier, Amsterdam 2006.

[4] T. Kawano and K. Shibata , *Covariance Evaluation System* , in Japanese, JAERI Report JAERI- Data/Code 97-037(1997).

[5] M. Herman, S. F. Mughabghab, P. Obložinský, M. T. Pigni and D. Rochman, *Neutron Cross Section Covariances in the Resolved Resonance Region*, Report BNL-80173-2008, April 2008.

[6] S. F. Mughabghab, *Spin-Orbit Splitting of the 3P Single Particle State: Non-statistical Effects in Radiative Neutron Capture*, Report BNL-80311-2008-JA, July 2008; submitted for publication.

[7] S. Oh, J. Chang and S. F. Mughabghab, *Neutron Cross Section Evaluations of Fission Products Below the Fast Energy Region*, Report BNL-NCS-67469, April 2000.

[8] M. Moore and J. Keyworth, *Analysis of the Fission and Capture Cross Sections of the Curium Isotopes*, Phys. Rev. C 3, 1656 (1971).

[9] A. M. Lane and S. F. Mughabghab, *Relation between the Optical Model and the Valence Model of E1 Neutron Capture at and between Resonances*, Phys. Rev. C 10, 412 (1974).

[10] R. L. Macklin, *Resonance Neutron Capture by Manganese below 2.5 keV*, Nucl. Sci. Eng. 89, 362 (1985).

[11] F. Widder, *Neutron Capture Cross-Section Measurements from 0.01 to 10 Electron Volts*, Second Neutron Capture Gamma-Ray Spectroscopy and Related Topics, p. 757 Petten, The Netherlands, Sept 2-6, 1974.

[12] M. Herman, M.T. Pigni, P. Obložinský et al., *Development of Covariance Capabilities in EMPIRE Code*, this issue of Nuclear Data Sheets.

[13] A. Scherbakov, and A. N. Glukhovec, *Slow Neutron Total and Radiative Capture Cross Section of* ^{56}Fe, Report YFI-24, 3 (1977).

[14] Y. Danon et al., *Neutron Total Cross Section Measurements and Resonance Analysis of Holmium, Thulium and Erbium from 0.001 to 20 eV*, Nucl. Sci. Eng. 128, 61 (1998).

Appendix C

Covariance Evaluations of ^{55}Mn and ^{90}Zr

Estimated ^{55}Mn and ^{90}Zr cross section covariances in the fast neutron energy region

M.T. Pigni,* M. Herman, and P. Obložinský
National Nuclear Data Center, Brookhaven National Laboratory, Upton, NY 11973-5000
(Dated: August 27, 2008)

We completed estimates of neutron cross section covariances for ^{55}Mn and ^{90}Zr, from keV range to 25 MeV, considering the most important reaction channels, total, elastic, inelastic, capture, and (n,2n). The nuclear reaction model code EMPIRE was used to calculate sensitivity to model parameters by perturbation of parameters that define the optical model potential, nuclear level densities and strength of the pre-equilibrium emission. The sensitivity analysis was performed with the set of parameters which reproduces the ENDF/B-VII.0 cross sections. The experimental data were analyzed and both statistical and systematic uncertainties were extracted from almost 30 selected experiments. Then, the Bayesian code KALMAN was used to combine the sensitivity analysis and the experiments to obtain the evaluated covariance matrices.

I. INTRODUCTION

Neutron cross section covariances are highly demanded by applications, probably the most prominent being the Global Nuclear Energy Partnership (GNEP) and the U.S. Nuclear Criticality Safety Program (NCSP). In GNEP, improved nuclear concepts are being considered with fuel and reactor characteristics that are well outside the design envelope of existing and prior systems. Therefore, a wide effort in advanced simulations must be preceded with the adequate adjustment of the recently released ENDF/B-VII.0 library [1]. Nuclear data covariances (uncertainties and correlations) are essential for such adjustment. NCSP is developing computational tools to enhance criticality safety predictive capabilities. For testing these tools an extensive amount of covariance data is needed, giving rise to the recent "low-fidelity project" [2].

This project was charged to provide a rough set of covariances covering all relevant reaction channels for all 393 materials in the ENDF/B-VII.0 library, emphasizing completeness rather than precision. In addition, NCSP needs high-quality covariances for specific materials, such as ^{55}Mn and ^{90}Zr. This need was partly met by the new ORNL evaluation of ^{55}Mn in the resonance region [3], including also ^{55}Mn(n,γ) dosimetry reaction for which covariance re-evaluation is required [4].

The present work is addressing covariances for ^{55}Mn and ^{90}Zr in the fast neutron region. Although the low-fidelity project was useful starting point, we made an important step forward by including almost 30 sets of experimental data.

The paper is organized as follows. In Section II, we describe the methodology used to produce the cross section covariances, while Section III and IV discuss, respectively, the results and the conclusions.

II. METHODOLOGY

Our methodology is based on the nuclear reaction model code EMPIRE [5], Bayesian code KALMAN [6] and due inclusion of experimental data, see adjacent paper for more details [7]. The EMPIRE code system incorporates an extensive set of nuclear reaction models capable of describing all relevant reaction mechanisms, coupled to the up-to-date library of input model parameters [8] and providing reasonable overall description of nuclear observables even if default parametrization is used. EMPIRE was used to calculate neutron cross sections and sensitivity matrices. Then, these sensitivity matrices were used as prior by KALMAN in order to incorporate, one by one, experimental data including their statistical and systematic uncertainties.

We emphasize that our goal is to produce covariance estimates, not to re-evaluate cross sections. Therefore, our modeling and parametrization aims to reproduce ENDF/B-VII.0 somewhat approximately, just giving us enough confidence in covariance estimates.

A. Reaction Models and Parameters

Four nuclear reaction models were adopted that should sufficiently well describe the physics of nuclear reactions at neutron energies from 10 keV to 25 MeV for both ^{55}Mn and ^{90}Zr. The spherical optical model, in case of ^{90}Zr, and the coupled channels formalism, in case of ^{55}Mn, take care of the total cross sections and neutron scattering. The Hauser-Feshbach statistical model describes the bulk of particle emission, and the exciton pre-equilibrium model describes major features of fast particle emission at higher incident energies.

TABLE I: *Prior* optical-model parameter uncertainties (in %): r - radius, a - diffuseness, V - real depth, W - imaginary depth. The subscripts v, s, and w, respectively, denote real volume, real surface, and imaginary surface. The superscripts, $tg \equiv$ n + $^{A}_{Z}$ and $np \equiv$ p + $^{A+1}_{Z-1}$, identify nucleon-nucleus interaction.

Δr_s^{tg}	Δr_v^{tg}	Δr_w^{tg}	ΔV_v^{tg}	ΔW_s^{tg}
3-5	5	5	5	3-5
ΔW_v^{tg}	Δa_s^{tg}	Δa_v^{tg}	ΔV_v^{np}	ΔW_s^{np}
5	5	5	5	5

The parametrization was taken from RIPL-3 [8]. For ^{55}Mn

*Electronic address: pigni@bnl.gov; http://www.nndc.bnl.gov/nndcpeople/pigni.html

we used optical model parameters of Koning-Delaroche [9] and for ^{90}Zr the dispersive potential used by us earlier [1]. Parameter uncertainties were those used in Ref. [2]. The optical model parameters, for which uncertainties (3% or 5%) were considered, are listed in Tab. I. The list of 8 parameters relevant for the Hauser-Feshbach and the exciton model plus a parameter taking into account the deformation of ^{55}Mn, is shown in Table II. The uncertainties given in Tabs. I, II represent the *prior* information on the model parameters required as a starting point in the Bayesian update procedure.

TABLE II: *Prior* parameter uncertainties (in %) used for the Hauser-Feshbach and exciton models: $\tilde{a}$ - total level density, $\tilde{g}$ - single-particle level density, f_γ - gamma-ray strength functions, and mfp - nucleon mean-free path; Def - deformation in the DWBA. The superscripts refer to $cn \equiv$ compound, $tg \equiv$ target, $n2n \equiv$ (n,2n) residue, $np \equiv$ (n,p) residue.

$\Delta\tilde{a}^{cn}$	$\Delta\tilde{a}^{tg}$	$\Delta\tilde{a}^{n2n}$	$\Delta\tilde{a}^{np}$	$\Delta\tilde{g}^{np}$	$\Delta\tilde{g}^{tg}$	Δf_γ	Δmfp	ΔDef
15	15	15	15	15	15	10-15	25	35

B. Sensitivities and Bayesian Update

Matrix elements $s_{i,j}$ of the sensitivity matrix $\mathbf{S}$ were calculated as

$$s_{i,j} = \frac{\partial\sigma(E_i,\mathbf{p})}{\partial p_j}\,, \tag{1}$$

where σ is the cross section, E_i is the energy and $\mathbf{p}$ is the vector of model parameters including p_j. The partial derivatives were computed numerically, by varying the parameters as defined by the uncertainties given in Tabs. I and II.

The Bayesian update procedure was used to update prior results by taking into account new data. We used the code KALMAN which is based on the iterative generalized least-squares approach. Applying the Bayesian equations is straightforward, an update being a simple algebraic operation,

$$\begin{aligned}\mathbf{p}_{n+1} &= \mathbf{p}_n + \mathbf{P}_n\mathbf{S}^{\mathrm{T}}\mathbf{Q}_{n+1}(\boldsymbol{\sigma}^{\mathrm{exp}}_{n+1} - \boldsymbol{\sigma}(\mathbf{p}_n))\\ \mathbf{P}_{n+1} &= \mathbf{P}_n - \mathbf{P}_n\mathbf{S}^{\mathrm{T}}\mathbf{Q}_{n+1}\mathbf{S}\mathbf{P}_n\,.\end{aligned} \tag{2}$$

Here, $\mathbf{p}_n$ is the vector of model parameters, $\mathbf{P}_n$ is their covariance matrix and $\boldsymbol{\sigma}^{\mathrm{exp}}_{n+1}$ is the new experimental data set. The updated (posterior) values are denoted by the superscript $n+1$. The matrix $\mathbf{Q}_{n+1}$ is defined as an inverse of the covariance matrix $\mathbf{C}_n$ and the experimental covariance matrix $\mathbf{C}^{\mathrm{exp}}_{n+1}$

$$\mathbf{Q}_{n+1} = (\mathbf{C}_n + \mathbf{C}^{\mathrm{exp}}_{n+1})^{-1}\,. \tag{3}$$

Then, the updated (posterior) cross section covariance matrix is obtained by the well known "sandwich" equation

$$\mathbf{C}_{n+1} = \mathbf{S}\mathbf{P}_{n+1}\mathbf{S}^{\mathrm{T}}\,. \tag{4}$$

The experimental data were analyzed and both statistical and systematic uncertainties were extracted for selected experiments. The covariance matrix of the n^{th}-experiment is

$$\mathbf{C}^{\mathrm{exp}}_n = \mathbf{U}_n + \mathbf{W}_n\,, \tag{5}$$

where $\mathbf{U}_n$ and $\mathbf{W}_n$ are the covariance matrices of the statistical and systematic uncertainties, respectively. In the explicit notation and omitting the subscript n, the matrix elements are given by

$$c^{\mathrm{exp}}_{i,j} = \begin{cases} u_{i,j} + w_{i,j} & i = j \\ w_{i,j} & i \neq j\,, \end{cases} \tag{6}$$

where the off-diagonal terms are obtained assuming that the systematic uncertainties are fully correlated.

The quality and consistency of the evaluated cross sections can be assessed by scalar quantity

$$\chi^2 = \sum_n (\boldsymbol{\sigma}^{\mathrm{exp}}_{n+1} - \boldsymbol{\sigma}(\mathbf{x}_n))^{\mathrm{T}} (\mathbf{C}^{\mathrm{exp}}_{n+1})^{-1} (\boldsymbol{\sigma}^{\mathrm{exp}}_{n+1} - \boldsymbol{\sigma}(\mathbf{x}_n))\,. \tag{7}$$

High value of χ^2 per one degree of freedom suggests that the obtained uncertainties are under-estimated and it is fairly common practice to use this factor to rescale these uncertainties to get their final values.

III. RESULTS AND DISCUSSION

We calculated neutron cross sections and their covariance matrices for ^{55}Mn and ^{90}Zr at 63 incident energies between 1 keV and 25 MeV, considering the five reaction channels, total, elastic, inelastic, (n,2n), and capture. We used data from 22 experiments for ^{55}Mn and 7 experiments for ^{90}Zr. First, we discuss ^{55}Mn and focus on energies above the ORNL evaluation [3], that is, above 122 keV.

Fig. 1 compares our cross sections with ENDF/B-VII.0 and three sets of experimental data [10–12] found to be the basis of the ENDF/B-VII.0 evaluation. Due to the necessity of retaining validated ENDF/B-VII.0 cross sections, our estimation of covariances exclusively depends on these selected experiments. The optical model predicts a smooth, averaged behavior of cross sections and cannot reproduce fluctuating values extending as high as 4 MeV and adopted by the ENDF/B-VII.0. Accordingly, below 4 MeV we adopted the uncertainties deduced from the experiments. Since related experimental information was limited, we estimated these uncertainties conservatively as 5%. At higher energies, our uncertainties are based on KALMAN and take into account careful measurement by Cierjacks *et al.* [10].

In Fig. 2, ^{55}Mn(n,n') reaction is shown. Our cross sections are in reasonable agreement with the ENDF/B-VII.0 evaluation. Relative uncertainties are fairly large at the threshold region, while in the energy range of about 0.7-10 MeV they drop to about 15-30%. As expected, the uncertainties rise at higher energies where cross sections become small.

Cross sections for ^{55}Mn(n,2n), obtained with EMPIRE-KALMAN using the experimental data of Refs. [13–24], appear to agree well with ENDF/B-VII.0 as shown in Fig. 3.

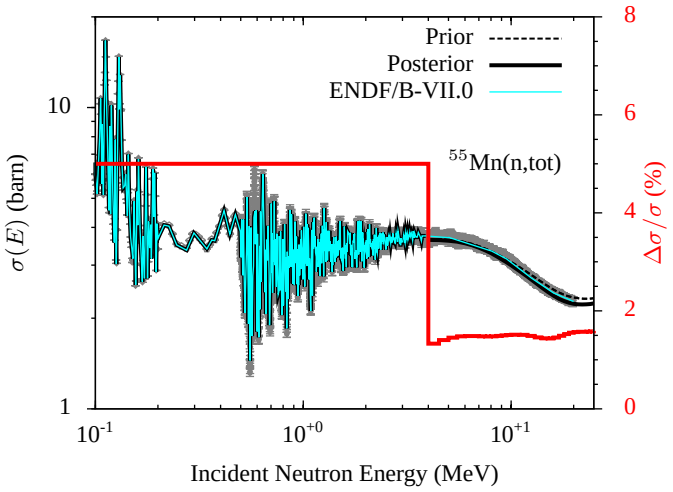

FIG. 1: Reaction ^{55}Mn(n,tot). *Prior*, *posterior*, and ENDF/B-VII.0 cross sections are compared with experimental data [10–12]. Relative uncertainties are in red (point-wise representation).

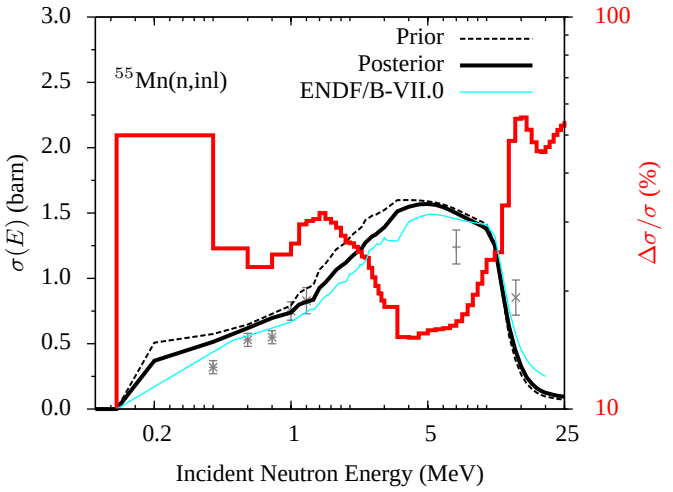

FIG. 2: Reaction ^{55}Mn(n,inl). *Prior*, *posterior*, and ENDF/B-VII.0 cross sections are compared with experimental data. Relative uncertainties are in red.

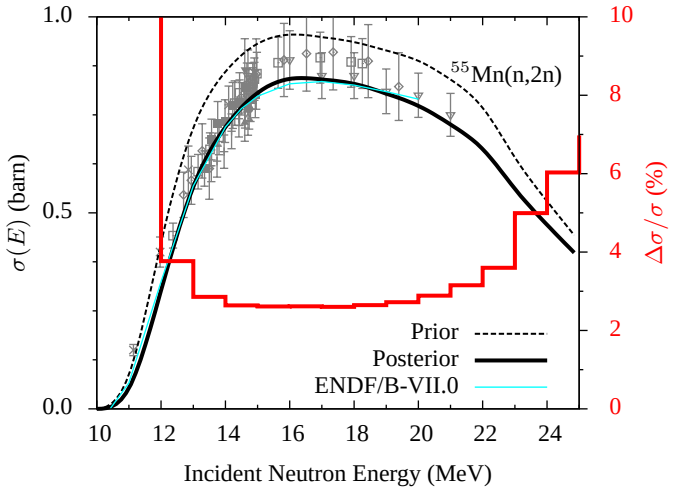

FIG. 3: Reaction ^{55}Mn(n,2n). *Prior*, *posterior*, and ENDF/B-VII.0 cross sections are compared with experimental data [13–24]. Relative uncertainties are in red.

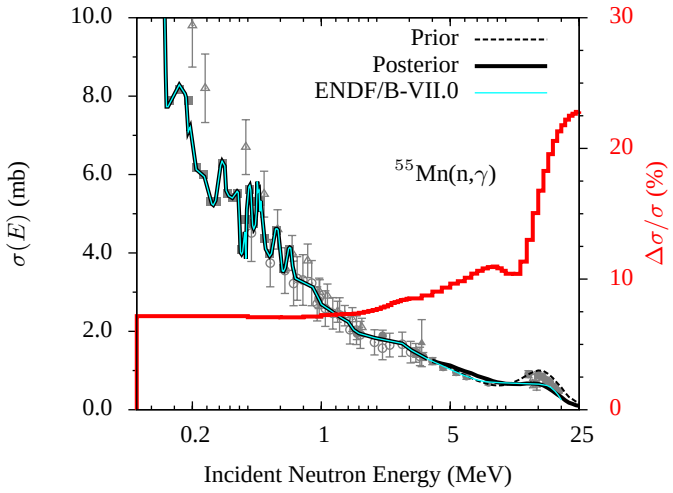

FIG. 4: Reaction ^{55}Mn(n,γ). *Prior*, *posterior*, and ENDF/B-VII.0 cross sections are compared with experimental data. Relative uncertainties are in red.

Relative uncertainties exhibit expected U-shape, starting with large values at the threshold region of ∼10 MeV, at energies ≲22 MeV being essentially flat. At higher energies, in the absence of experimental data, the uncertainties again increase.

Fig. 4 displays ^{55}Mn radiative capture cross sections and their uncertainties. Similar to (n,tot) reaction, below 1 MeV the ENDF/B-VII.0 adopted fluctuating cross sections following the experiment by Garg *et al.* [25]. Consequently, we adopted Garg's experimental uncertainties. At higher energies EMPIRE-KALMAN method was adopted. Relative uncertainties are lower than 10% in the energy range of 0.1-15 MeV, followed by expected sharp increase at higher energies.

We proceed with the discussion of ^{90}Zr reactions showing first ^{90}Zr(n,tot) and ^{90}Zr(n,el) in Figs. 5 and 6. Total as well as elastic cross sections compare well with ENDF/B-VII.0 and experimental data. Except for the low energy region, the uncertainties are fairly flat around 2.5%. In contrast, uncertainties for (n,inl) are much larger throughout the whole energy range (Fig. 7) since no experimental data were used. Generally, uncertainties should be low whenever a wealth of experimental data is used in the evaluation.

Finally, in Fig. 8 the ^{90}Zr(n,2n) cross sections obtained with EMPIRE-KALMAN method are shown. Compared are *prior*, *posterior*, and ENDF/B-VII.0 cross sections with experimental data [30–34] included in our evaluation showing good agreement with both ENDF/B-VII.0 and data. Relative cross section uncertainties exhibit expected U-shape.

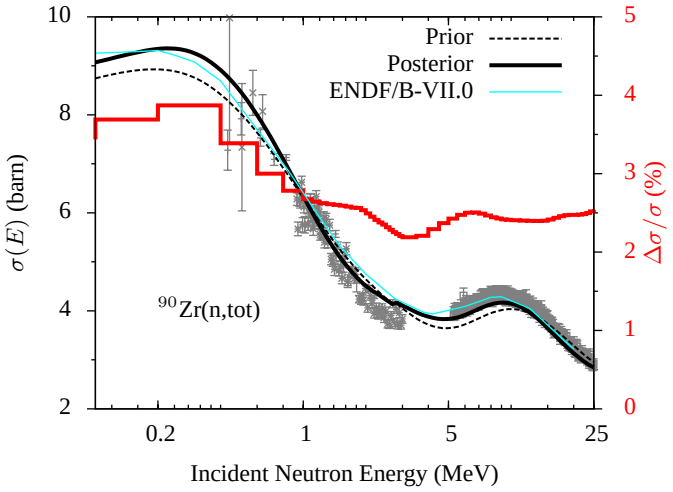

FIG. 5: Reaction ^{90}Zr(n,tot). *Prior*, *posterior*, and ENDF/B-VII.0 cross sections are compared with experimental data [26–29]. Relative uncertainties are shown in red.

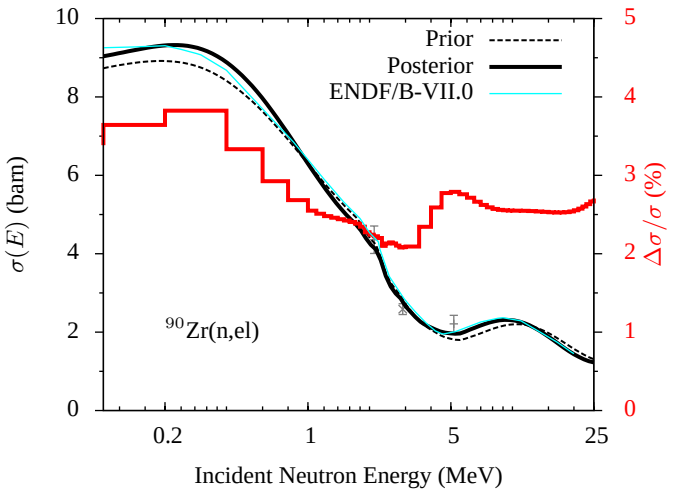

FIG. 6: Reaction ^{90}Zr(n,el). *Prior*, *posterior*, and ENDF/B-VII.0 cross sections are compared with experimental data. Relative uncertainties are shown in red.

IV. CONCLUSIONS

We produced estimates of neutron cross section covariances for ^{55}Mn and ^{90}Zr in the fast neutron energy region. This work was primarily motivated by the needs of the U.S. Nuclear Criticality Safety Program, though the results are of interest for other applications such as GNEP and dosimetry. Our results are based on the EMPIRE-KALMAN approach using statistical and systematic uncertainties taken from almost 30 selected experiments.

Our covariances should be considered as being of intermediate quality. For high-fidelity results one should perform complete re-evaluation of cross sections simultaneously with covariances, and preceded with detailed analysis of all experimental data. ^{55}Mn represents additional challenge due to many data available, including high resolution measurements that exhibit strong fluctuations up to a few MeV.

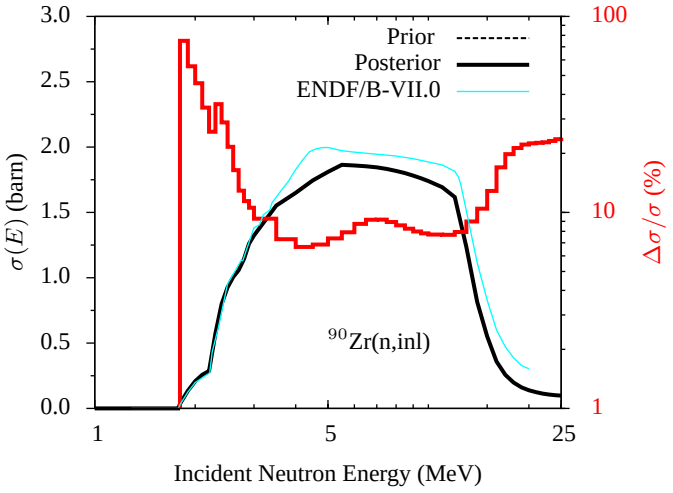

FIG. 7: Reaction ^{90}Zr(n,inl). Shown are *prior*, *posterior*, and ENDF/B-VII.0 cross sections. Relative uncertainties are in red.

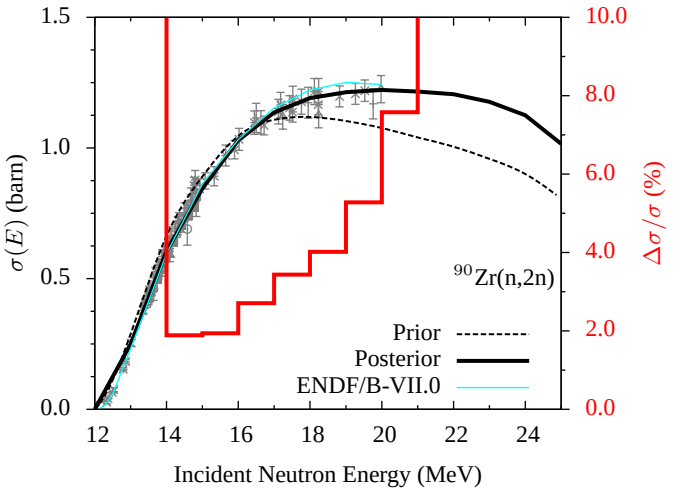

FIG. 8: Reaction ^{90}Zr(n,2n). *Prior*, *posterior*, and ENDF/B-VII.0 cross sections are compared with experimental data [30–34]. Relative uncertainties are shown in red.

Acknowledgments

This work was supported in part by the U.S. Nuclear Criticality Safety Program. Support from the DOE-Office of Science under the Contract No. DE-AC02-98CH10887 with Brookhaven Science Associates, LLC., is gratefully acknowledged.

[1] M.B. Chadwick, P. Obložinský, M. Herman, et al., "Next Generation Evaluated Nuclear Data Library for Nuclear Science and Technology," *Nuclear Data Sheets*, **107**, 2931 (2006).

[2] M.T. Pigni, M. Herman, P. Obložinský, "Extensive Set of Cross Section Covariance Estimates in the Fast Neutron Region," accepted by *Nucl. Sci. Eng.* (2008).

[3] H. Derrien at al., "Evaluation of the Resonance Parameters of 55-Mn in the Energy Range from 0 to 122 keV", included in ENDF/A library, March 2008.

[4] I. Kodeli and A. Trkov, "Validation of the IRDF-2002 Dosimetry Library," *Nucl. Instr. and Meth.*, **577**, 664 (2007).

[5] M. Herman, R. Capote, B.V. Carlson, et al., "EMPIRE: Nuclear Reaction Model Code System for Data Evaluation," *Nuclear Data Sheets*, **108**, 2655 (2007).

[6] T. Kawano and K. Shibata, "Covariance Evaluation System [in Japanese]," Lab. report JAERI-Data/Code 97-037, Japan Atomic Energy Research Institute (1997).

[7] M. Herman, M.T. Pigni, P. Obložinský, et al., "Development of Covariance Capabilities in EMPIRE Code," *Nuclear Data Sheets*, to be published.

[8] T. Belgya, O. Bersillon, R. Capote, et al., "Handbook for Calculations of Nuclear Reaction Data, Reference Input Parameter Library-2," Tech. report IAEA-TECDOC-1506, Vienna 2006.

[9] A.J. Koning and J.P. Delaroche, "Local and Global Nucleon Optical Model from 1 keV to 200 MeV," *Nucl. Phys. A*, **713**, 231 (2003).

[10] S. Cierjacks, P. Forti, D. Kopsch, et al., "High Resolution Total Neutron Cross Sections for Na, Cl, K, V, Mn and Co between 0.5 and 30 MeV," Kernforschungszentrum Karlsruhe Reports, 1000, supp. 2, (1969).

[11] W.F.E. Pineo, M. Divadeenam, E.G. Bilpuch, et al, "Neutron Strength Functions and Average Total Cross Sections II. The behavior of the Average Cross Sections and the S-wave Scattering Lengths," *Ann. Phys.*, **84**, 165 (1974).

[12] J.B. Garg, J. Rainwater, W.W. Havens Jr,"Neutron Resonance Spectroscopy in Vanadium, Manganese, and Cobalt," *Nucl. Sci. Eng.*, **65**, 76 (1978).

[13] A.A. Filatenkov, S.V. Chuvaev, V.N. and AKSENOV, et al., "Systematic Measurement of Activation Cross Sections at Neutron Energies from 13.4 to 14.9 MeV ,"Khlopin Radiev. Inst., Leningrad Reports (1999).

[14] M. Bostan and S.M. Qaim, "Excitation Functions of Threshold Reactions on ^{45}Sc and ^{55}Mn Induced by 6 to 13 MeV Neutrons," *Phys. Rev.* C **49**, 266 (1994).

[15] I. Kimura and K. Kobayashi, "Calibrated Fission and Fusion Neutron Fields at the Kyoto University Reactor," *Nucl. Sci. Eng.*, **106**, 332 (1990).

[16] Lu Han-Lin, Huang Jian-Zhou, Fan Pei-Guo, et al., "Measurement of Cross Sections for the (n,2n) Reaction of ^{55}Mn, ^{58}Ni, ^{59}Co, ^{93}Nb, ^{181}Ta and ^{197}Au," Chinese report to the I.N.D.C., 16, (1989).

[17] Y. Ikeda, C. Konno, K. Oishi, et al., "Activation Cross Section Measurements for Fusion Reactor Structural Materials at Neutron Energy from 13.3 to 15.0 MeV Using FNS Facility," JAERI Reports 1312 (1988).

[18] L.R. Greenwood, "Recent Research in Neutron Dosimetry and Damage Analysis for Materials Irradiations," American Soc. of Testing and Materials Reports 956, 743 (1987).

[19] J.W. Meadows, D.L. Smith, M.M. Bretscher, et al., "Measurement of 14.7 MeV Neutron-Activation Cross Sections for Fusion," *Ann. Nucl. Energy*, **14**, 489 (1987).

[20] B.M. Bahal and R. Pepelnik, "Cross Section Measurements of Cr, Mn, Fe, Co, Ni for an Accurate Determination of These Elements in Natural and Synthetic Samples Using a 14 MeV Neutron Generator," series GKSS (Ges.Kernen.-Verwertung, Schiffbau and Schiffahrt), 84E (1984).

[21] M. Berrada, "Measurement and Analysis of 14 MeV Neutron Nuclear Reaction Cross-Sections by X and Gamma Spectroscopy," Private communication, (1984).

[22] G.F. Auchampaugh, D.M. Drake, L.R. Veeser, "Neutron Cross Section Programs in the Energy Region from 1 to 24 MeV at the LASL Van de Graaff Facilities," Symp. on Neutr. Cross-Sect. 10-40 MeV, Brookhaven 1977, 231 (1977).

[23] G.N. Maslov, F. Nasyrov, N.F. Pashkin, "The Experimental Cross Sections of the Nuclear Reactions for 14 MeV Neutrons," *Yadernye Konstanty*, **9**, 50 (1972).

[24] H.O. Menlove, K.L. Coop, H.A. Grench et al., "Activation Cross Sections for the ^{19}F(n,2n)^{18}F, ^{23}Na(n,2n)^{22}Na, ^{55}Mn(n,2n)^{54}Mn, ^{115}In(n,2n)^{114m}In, ^{165}Ho(n,2n)^{164m}Ho, ^{115}In(n,n)^{115m}In, and ^{27}Al(n,α)^{24}Na reactions," *Phys. Rev.*, **163**, 1308 (1967).

[25] J.B. Garg, R.L. Macklin, J Halperin, "Neutron capture cross section of manganese," *Phys. Rev.* C, **19**, 2079 (1978).

[26] R.W. Stooksberry and J.H. Anderson, "Measurement of the Neutron Total Cross Sections of Zircaloy-2, Zirconium-90 and C between 0.4 and 2.0 MeV," *Nucl. Sci. Eng.*, **51**, 235 (1973).

[27] M.V. Pasechnik, M.B. Fedorov, V.D. Ovdienko, et al., "Total Neutron Cross-Sections for Molybdenum and Zirconium at Low Energies," 5.All Union Conference on Neutron Physics, Kiev, 15-19 Sep. 1980, **1**, 304 (1980).

[28] P. Guenther, A. Smith, and J. Whalen, "^{90}Zr and ^{92}Zr: Neutron Total and Scattering Cross Sections," *Phys. Rev.* C, **12**, 1797 (1975).

[29] R. W. Finlay, W.P. Abfalterer, G. Fink, et al., "Neutron Total Cross Sections at Intermediate Energies," *Phys. Rev.* C, **47**, 237 (1993).

[30] A. Pavlik, G. Winkler, H. Vonach, "Precise Measurement of Cross Sections for the ^{90}Zr(n,2n)^{89}Zr Reaction from Threshold to 20 MeV," *Nucl. and Part. Phys.*, **8**, 1283 (1982).

[31] Zhao Wen-Rong, Lu Han-Lin, and Fan Pei-Guo, "Measurement of Cross Section for the Reaction ^{90}Zr(n,2n)^{89}Zr," *Chinese J.of Nuclear Physics (Beijing)*, **6**, 80 (1984).

[32] N.I. Molla, R.U. Miah, M. Rahman, et al., "Excitation Functions of Some (n,p), (n,2n) and (n,α) Reactions on Nickel, Zirconium and Niobium Isotopes in the Energy Range 13.63-14.83 MeV," Int. Conf. on Nuclear Data for Science and Tech., Jülich, Germany, 13-17 May, 1991, Proc. 355 (1991).

[33] K. Kobayashi and I. Kimura, "Activation Cross Sections Measured with 14.1 MeV Neutrons from 6-LiD Converters," Japanese report to NEANDC **116** (1988).

[34] B.P. Bayhurst, J.S. Gilmore, R.J. Prestwood, et al., "Cross Sections for (n,xn) Reactions between 7.5 and 28 MeV," *Phys. Rev.* C, **12**, 451 (1975).

Appendix D

Covariances in Resolved Resonance Region

BNL-80173-2008

Neutron cross section covariances in the resolved resonance region

M. Herman, S.F. Mughabghab, P. Obložinský, M.T. Pigni
D. Rochman*

National Nuclear Data Center, Brookhaven National Laboratory
Upton, New York, 11973-5000, U.S.A.
www.nndc.bnl.gov

April 2008

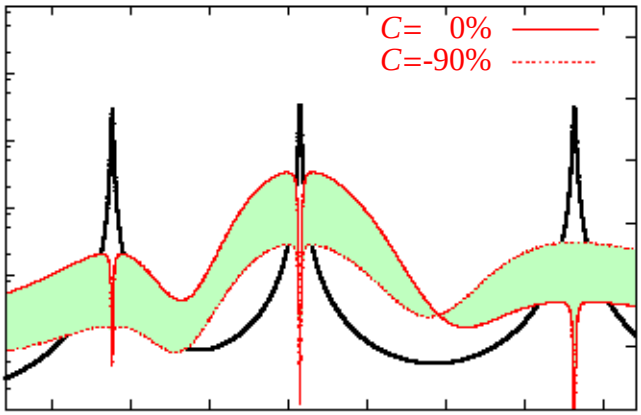

* Address since September 2007: Nuclear Research and Consultancy Group, NRG, P.O. Box 25, 1755 ZG Petten, The Netherlands.

DISCLAIMER

Contents

Abstract

We present a detailed analysis of the impact of resonance parameter uncertainties on covariances for neutron capture and fission cross sections in the resolved resonance region. Our analysis uses the uncertainties available in the recently published Atlas of Neutron Resonances employing the Multi-Level Breit-Wigner formalism. We consider uncertainties on resonance energies along with those on neutron-, radiative-, and fission-widths and examine their impact on cross section uncertainties and correlations. We also study the effect of the resonance parameter correlations deduced from capture and fission kernels and illustrate our approach on several practical examples. We show that uncertainties of neutron-, radiative- and fission-widths are important, while the uncertainties of resonance energies can be effectively neglected. We conclude that the correlations between neutron and radiative (fission) widths should be taken into account. The multi-group cross section uncertainties can be properly generated from both the resonance parameter covariance format MF32 and the cross section covariance format MF33, though the use of MF32 is more straightforward and hence preferable.

Editorial note: The ideas on which this paper is based were put forward during numerous discussions between the scientists of the National Nuclear Data Center, BNL in the first half of 2007. This was part of an intensive effort devoted to developing neutron cross section covariance methodology in the resolved resonance region. The backbone of this methodology is the use of the uncertainty information contained in the Atlas of Neutron Resonances (author S. Mughabghab, Elsevier 2006). The present report was drafted in summer 2007, near final version followed in September 2007. Three months later, in December 2007, a paper by D. Rochman and A.J. Koning, NRG Petten, was submitted to Nucl. Instr. Methods A using many of our original ideas without mentioning our work. The NNDC learned about it from an on-line version of NIM-A in March 2008. This prompted publishing the present report in order to secure our priority in this matter.

Chapter 1

Introduction

The recent revival of interest in neutron cross section covariances (uncertainties and correlations) is driven by the needs of advanced reactor systems and fuel cycles [1, 2], data adjustment for the Global Nuclear Energy Partnership (GNEP) project as well as nuclear criticality safety. This interest is strongly enhanced by recent advances in computer technology and progress in radiation transport codes allowing to perform fast numerical simulations. Such simulations can substantially reduce expensive and time consuming measurements on mock-up assemblies. For these simulations to be useful, neutron cross section evaluations have to come with a trusted estimate of uncertainties.

It appears that the covariance information is very incomplete even in the most recent nuclear data libraries. For example, the brand new ENDF/B-VII.0 library [3] contains neutron cross section covariances only for 13 old and 13 newly evaluated materials out of 393. The consequence of the lack of covariance information in the user community is a common misuse assuming that a given old covariance file, obtained under specific conditions, for specific cross sections or other nuclear data, can be used with a new data file, obtained under different assumptions. To remedy this problem, it is important to create new reliable covariance files, consistent with mean values to which they refer to.

The new neutron cross section covariances included in the ENDF/B-VII.0 library are sample covariance evaluations that represent a prerequisite for a much broader effort anticipated for ENDF/B-VII.1 release. In the resolved resonance region these evaluations were obtained by three different methods. The direct SAMMY was used for the covariance evaluation of ^{232}Th, the retroactive SAMMY for ^{152,153,154,155,156,157,158,160}Gd, and the Atlas-KALMAN method was used for evaluation of ^{89}Y, ^{99}Tc and ^{191,193}Ir.

The first method, direct SAMMY, is the most suitable for new measurements, where the analysis of raw experimental data can be performed with powerful R-matrix codes. The best known is the ORNL code SAMMY [4], which automatically produces full covariance information [5]. For comparison, the European code REFIT [6] has similar capabilities in data analysis [7], but produces diagonal covariance terms only. The code SAMMY preforms a multilevel multichannel R-matrix fit to neutron data using the Reich-Moore formalism. Experimental conditions such as resolution function, finite size sample, non-uniform thickness of sample, multiple scattering, self-shielding, normalization, background are taken into account. An important distinction of the SAMMY is the usage of the Bayes' equations, or the generalized least squares rather than the least-squares equations to update resonance parameters [8].

The second method is based on the idea to generate experimental data "retroactively" and then proceed with the direct evaluation as described above [9]. The motivation behind this somewhat unorthodox method, termed retroactive SAMMY [3], is to benefit from the power of SAMMY and from huge experience accumulated over years in experimental facilities such as ORELA. An intention is to apply this method to those cases where suitable experimental data are not available. In doing so one first generates artificial experimental cross sections using the R-matrix theory with already-determined values of resonance parameters. Statistical and systematical uncertainties are assigned to each data point, estimated from past experience. Transmission, capture, fission and other data are calculated assuming realistic experimental conditions such as Doppler broadening and resolution function. Then, the SAMMY code is used to generate resonance-parameter covariance matrix.

The third method, pursued by the National Nuclear Data Center, is focusing on many cases where the use of the above two methods may not be practical. It is based on the idea to utilize another resource of information on neutron resonances, namely, the recently published Atlas of Neutron Resonances [10]. This monumental work by S.F. Mughabghab represents the 5^{th} edition of what was previously well known as the Brookhaven National Laboratory BNL-325 Reports. The point is that Atlas contains not only the resonance parameters, frequently adopted by many evaluations in major evaluated data libraries, but also their uncertainties. The idea is to make use of these uncertainties and convert them into neutron cross section covariances. Such a task has several distinct perspectives.

- One perspective is that we deal with a specific case of nuclear reaction modeling that one would ideally encounter when using the nuclear reaction

model code EMPIRE originally designed for evaluations in the fast neutron region [11]. In EMPIRE, one is far away from a situation of having perfect model, perfect parametrization along with solid model parameter uncertainties. Yet, the resolved resonance region is pretty close to this ideal situation. One has a model, such as the Multi-Level Breit-Wigner (MLBW) formalism, with a set of well determined model parameters along with their uncertainties directly deduced from experiments. Hence, one should built on experience from coupling EMPIRE with the Bayesian code KALMAN [12] to produce covariances in the fast neutron region and expand it to the resonance region. This led to the development of the Atlas-KALMAN method, used to evaluate four materials for ENDF/B-VII.0 [3] and also to produce preliminary set of covariances for advanced reactor systems [13].

- Another perspective is that one encounters a typical processing problem, with converting resonance parameters (file MF2 as defined in the ENDF-6 format [14]) and the resonance parameter uncertainties (file MF32) into cross sections and cross section covariances. To this end, one should employ a suitable processing code such as PUFF [15] or ERRORJ [16]. This approach, however tempting, does not provide sufficient insight into the role of the resonance parameter uncertainties unless one is sufficiently familiar with the processing code itself.

- Still another perspective is that one deals with the task where straightforward analytical solutions are possible. This should shed sufficient light on the role of the resonance parameter uncertainties and this is the primary objective of the present paper. On practical level, such an analysis would bring us to the previous item by providing justification for conversion of uncertainty information from the Atlas of Neutron Resonances into MF32 covariances. This procedure is straightforward and should be preferred over our earlier approach of using MF33.

This paper is organized as follows. In Chapter 2 we summarize formalism for neutron capture and fission cross sections. In Chapter 3 we consider single resonances and analyze the impact of the resonance parameter uncertainties and resonance parameter correlations on the neutron cross section uncertainties and correlations. Then, in Chapter 4 we extend this analysis to many resonances. Our conclusions are given in Chapter 5.

Chapter 2

Capture and fission cross sections

We restrict ourselves to the MLBW formalism as defined in the ENDF-6 format [14]. This is justified by a wide use of MLBW in all major evaluated nuclear data libraries and its dominant use also in the Atlas of Neutron Resonances. Furthermore, MLBW is sufficiently representative for our purposes and relatively easy to implement analytically. Although our analysis could be extended to a more sophisticated Reich-Moore formalism, it would hardly change any of our findings.

For a simplicity we restrict ourselves to s-wave processes, first discuss a single resonance, then proceed with a multi-resonance case. We will provide expressions for capture cross sections, with the understanding that the expressions for fission cross sections can be obtained by a simple transformation. For the purposes of the present paper all examples shown to illustrate our points are s-wave resonances.

For a single resonance at the energy E_0 and the neutron incident energy E, the capture cross section can be expressed by the Breit-Wigner formula as

$$\sigma_\gamma(E) = \pi\lambda\!\!\!^{-2} \frac{g\Gamma_n(E)\Gamma_\gamma}{(\Gamma(E)/2)^2 + (E - E_0)^2}\,, \tag{2.1}$$

where we dropped all indices related to quantum numbers. Here, $\lambda\!\!\!^{-}$ is the neutron wavelength,

$$\lambda\!\!\!^{-} = \frac{\hbar}{\sqrt{2mE}}\,, \tag{2.2}$$

m being the neutron reduced mass and $\hbar$ the Planck constant, the spin statistical factor is given by

$$g = \frac{2J + 1}{2(2I + 1)}\,, \tag{2.3}$$

with J being the spin of the resonance and I the spin of the target nucleus, and the energy-dependent neutron width for s-wave neutrons is

$$\Gamma_n(E) = \Gamma_n \sqrt{\frac{E}{E_0}}\,, \tag{2.4}$$

where Γ_n denotes the neutron width at E_0. The energy dependence of the total resonance width, $\Gamma(E)$, can be neglected when compared to the strong energy term in the denominator of Eq. 2.1, giving

$$\Gamma(E) = \Gamma = \Gamma_n(E_0) + \Gamma_\gamma + \Gamma_f\,, \tag{2.5}$$

being Γ_γ and Γ_f the radiative and fission width respectively. Eq. (2.1) can be rewritten to its final form

$$\sigma_\gamma(E) = \frac{2\pi\hbar^2}{m}\left(\frac{1}{EE_0}\right)^{1/2} \frac{g\Gamma_n\Gamma_\gamma}{(\Gamma_n + \Gamma_\gamma + \Gamma_f)^2 + 4(E-E_0)^2}\,, \tag{2.6}$$

where one can explicitly see all quantities of interest to our analysis. These quantities, along with their uncertainties, can in general be found in the Atlas of Neutron Resonances [10] and include the resonance parameters E_0, Γ_n, Γ_γ, Γ_f and the capture kernel $g\Gamma_n\Gamma_\gamma/\Gamma$.

For the case of several resonances the above expression can be generalized by performing summation over the individual resonances, denoted by the subscript r,

$$\begin{aligned}\sigma_\gamma(E) &= \sum_r \sigma_{\gamma r}(E) \\ &= \frac{2\pi\hbar^2}{m}\sum_r \left(\frac{1}{EE_{0r}}\right)^{1/2} \frac{g_r\Gamma_{nr}\Gamma_{\gamma r}}{\Gamma_r^2 + 4(E-E_{0r})^2}\,.\end{aligned} \tag{2.7}$$

This is justified by the observation that there are no interference effects in neutron capture, generally when the number of primary γ-ray transitions is large.

For fission cross sections the same formalism, after interchanging the subscripts γ and f in the above equations, can be applied.

Chapter 3

Cross section covariances for a single resonance

The energy-energy covariance between capture cross sections, $\sigma_\gamma(E)$ and $\sigma_\gamma(E')$ at the neutron energies E and E', is given by

$$\langle \delta\sigma_\gamma(E)\, \delta\sigma_\gamma(E') \rangle = \sum_{i,j} \frac{\partial \sigma_\gamma(E)}{\partial p_i} \langle \delta p_i\, \delta p_j \rangle \frac{\partial \sigma_\gamma(E')}{\partial p_j}\,, \tag{3.1}$$

where p_i stands for the resonance parameters E_0, Γ_n, Γ_γ, Γ_f, and $\langle \delta p_i\, \delta p_j \rangle$ is their covariance matrix. Assuming that the resonance parameters are uncorrelated,

$$\langle \delta p_i\, \delta p_j \rangle = \begin{cases} (\Delta p_i)^2 & i = j \\ 0 & i \neq j\,, \end{cases} \tag{3.2}$$

one gets

$$\langle \delta\sigma_\gamma(E)\, \delta\sigma_\gamma(E') \rangle = \sum_{i} \frac{\partial \sigma_\gamma(E)}{\partial p_i} (\Delta p_i)^2 \frac{\partial \sigma_\gamma(E')}{\partial p_i} \tag{3.3}$$

that defines all elements of the energy-energy cross section covariance matrix. The diagonal terms, $E = E'$, contain cross section uncertainties, while the off-diagonal terms, $E \neq E'$, contain cross section correlations.

3.1 Cross section uncertainties

The diagonal terms of the energy-energy covariance matrix are cross section uncertainties. Using a more explicit notation, this diagonal term defined by Eq. (3.3)

can be written for non-fissile nuclei as

$$(\Delta\sigma_\gamma)^2 = \left(\frac{\partial\sigma_\gamma}{\partial E_0}\Delta E_0\right)^2 + \left(\frac{\partial\sigma_\gamma}{\partial\Gamma_n}\Delta\Gamma_n\right)^2 + \left(\frac{\partial\sigma_\gamma}{\partial\Gamma_\gamma}\Delta\Gamma_\gamma\right)^2 . \tag{3.4}$$

Here, $\partial\sigma_\gamma/\partial E_0$, $\partial\sigma_\gamma/\partial\Gamma_n$, and $\partial\sigma_\gamma/\partial\Gamma_\gamma$ are the partial derivatives and ΔE_0, $\Delta\Gamma_n$, and $\Delta\Gamma_\gamma$ are the standard deviations (uncertainties) of the resonance energy, neutron, radiative width, respectively. We note that the above equation can be easily generalized to describe actinides by adding fission term.

Considering Eq. (2.6), the first term of Eq. (3.4), after normalizing it to the capture cross section, gives the relative capture cross section uncertainty

$$\frac{\partial\sigma_\gamma}{\partial E_0}\frac{\Delta E_0}{\sigma_\gamma} = \left(\frac{8E_0(E-E_0)}{\Gamma^2+4(E-E_0)^2} - \frac{1}{2}\right)\frac{\Delta E_0}{E_0}, \tag{3.5}$$

which shows strong E-dependence. Thus, for the neutron energies far away from E_0 the cross section uncertainty is small, -(5/2)$\Delta E_0/E_0$ at $E = 0$ and -(1/2)$\Delta E_0/E_0$ at $E >> E_0$. For the interim energies, the leading term is $2\Delta E_0/(E - E_0)$ and this explains the initial rapid growth in the relative cross section uncertainty, followed by equally rapid decrease, with a deep minimum at $E = E_0$.

As an example, in Fig. 3.1 we show ^{152}Gd(n,γ) for the single s-wave resonance with the resonance energy E_0=173.8 eV known to 0.06% precision, see Table 3.1, while Γ and Γ_γ are treated as exactly known quantities. Although the cross section

Table 3.1: The resonance parameters and their uncertainties for E_0 = 173.8 eV s-wave resonance in ^{152}Gd+n [10].

E_0 (eV)	$g\Gamma_n$ (meV)	Γ_γ (meV)
173.8±0.1	86±2	30±2

uncertainties tend to be very large, in practice they can be neglected since there is a strong anti-correlation with respect to E_0 (see Sec. 3.2). This anti-correlation virtually annihilates contribution to cross section uncertainties due to ΔE_0 once the cross section averaging is done even over the fairly narrow energy interval around E_0.

The second term in Eq. (3.4), the energy dependence of the relative capture cross section uncertainty due to $\Delta\Gamma_x$, reads

$$\frac{\partial\sigma_\gamma}{\partial\Gamma_x}\frac{\Delta\Gamma_x}{\sigma_\gamma} = \left(1 - \frac{2\Gamma_x\Gamma}{\Gamma^2+4(E-E_0)^2}\right)\frac{\Delta\Gamma_x}{\Gamma_x} . \tag{3.6}$$

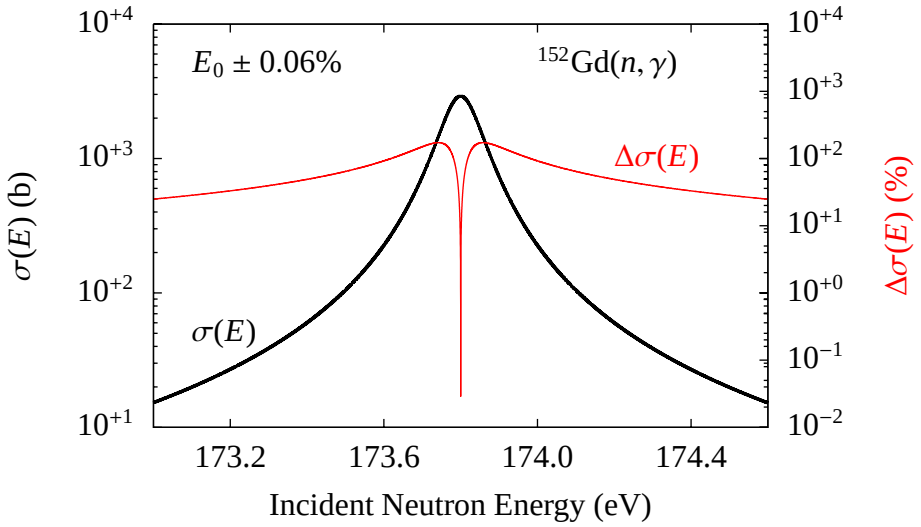

Figure 3.1: The ^{152}Gd(n,γ) cross sections for the single resonance E_0 = 173.8 eV (left scale) and their relative uncertainties due to the resonance energy uncertainty 0.06% (right scale).

where the index x stands either for n or γ. This expression gives the cross section uncertainties that are fairly constant. For the neutron energies far away from E_0 one gets $\Delta\Gamma_x/\Gamma_x$ for cross section uncertainty, the interim energy region is fairly flat, with somewhat complex shape close to E_0 depending on the actual value of the term $(1 - 2\Gamma_x/\Gamma)$.

An example is given for ^{152}Gd(n,γ) for the single resonance E_0=173.8 eV, with $\Delta\Gamma_n/\Gamma_n$=2.3% and $\Delta\Gamma_\gamma/\Gamma_\gamma$=6.6%, see Table 3.1. Shown in Fig. 3.2 is the impact of $\Delta\Gamma_n$ which yields complex shape around E_0 caused by Γ_n/Γ being close to unity. Fig. 3.3 shows the contribution caused by $\Delta\Gamma_\gamma$ that drops at E_0 since Γ_γ/Γ is relatively small.

3.2 Cross section correlations

The correlation between capture cross sections is given by the non-diagonal terms, $E \neq E'$, of the energy-energy covariance matrix, Eq. (3.3). Two possibilities will be discussed. First, we will consider the uncorrelated resonance parameters. Then, we will examine the correlation between Γ_n and Γ_γ using the constraint given by the capture kernel.

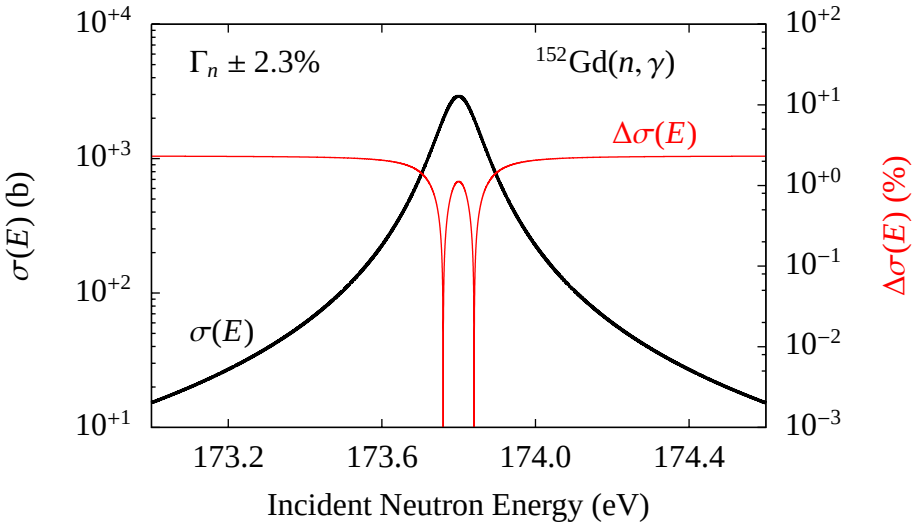

Figure 3.2: The ^{152}Gd(n,γ) cross sections for the single 173.8 eV resonance (left scale) and their relative uncertainties due to the neutron width Γ_n = 86 meV±2.3% (right scale).

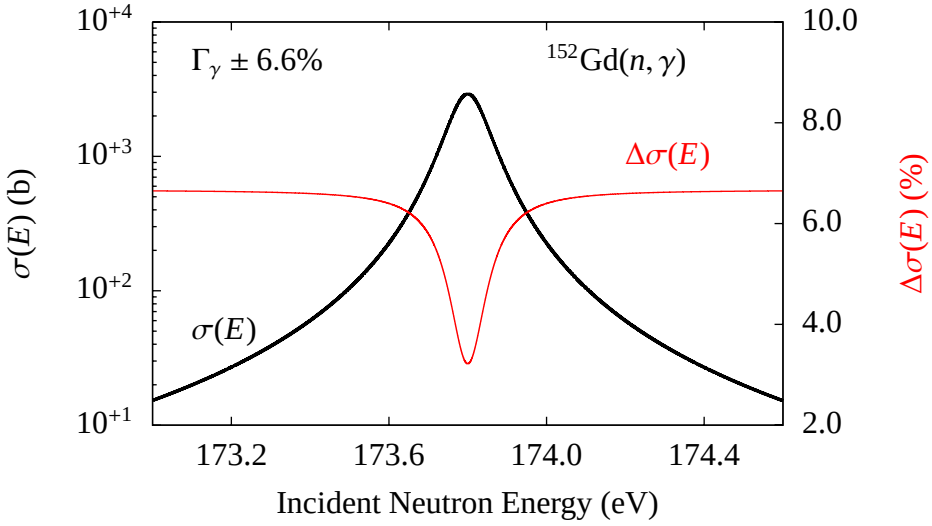

Figure 3.3: The ^{152}Gd(n,γ) cross sections for the single 173.8 eV resonance (left scale) and their relative uncertainties due to the radiative width Γ_γ = 30 meV±6.6% (right scale).

For the uncorrelated resonance parameters, and following the usual practice to normalize the covariance matrix so that the matrix elements are between -1 and +1, one gets correlation matrix

$$\frac{\langle \delta\sigma_\gamma(E)\,\delta\sigma_\gamma(E')\rangle}{\Delta\sigma_\gamma(E)\,\Delta\sigma_\gamma(E')} = \sum_i \frac{\partial\sigma_\gamma(E)}{\partial p_i}\frac{(\Delta p_i)^2}{\Delta\sigma_\gamma(E)\Delta\sigma_\gamma(E')}\frac{\partial\sigma_\gamma(E')}{\partial p_i}\,, \tag{3.7}$$

where $p_i = E_0, \Gamma_n, \Gamma_\gamma$. For illustration we continue to analyze ^{152}Gd(n,γ) at E_0=173.8 eV. In Fig. 3.4, to the right, we show the relative cross section uncertainties due to both the neutron and radiative widths uncertainties, $\Delta\Gamma_n$ and $\Delta\Gamma_\gamma$, while the resonance energy E_0 is considered to be known exactly. Then, in Fig. 3.5 we show a complete case, where also the resonance energy uncertainty, ΔE_0, is considered. This has striking impact, showing up as strong anti-correlation with respect to the energy E_0. As a consequence this anti-correlation annihilates the impact of ΔE_0 on the averaged cross section uncertainties.

Next, we examine the correlation between the resonance widths. In capture measurements the capture kernel,

$$A_\gamma = \frac{g\Gamma_n\Gamma_\gamma}{\Gamma}\,, \tag{3.8}$$

shows that there is negative correlation between Γ_n and Γ_γ. This correlation may or may not be strong, depending on the values of the resonance widths involved. Thus, if either Γ_n/Γ or Γ_γ/Γ is close to the unity, the correlation is weak. If, however, these ratios are approximately equal, then the correlation between Γ_n and Γ_γ will be strong. The corresponding expression for the cross section uncertainty reads

$$(\Delta\sigma_\gamma)^2 = \left(\frac{\partial\sigma_\gamma}{\partial\Gamma_n}\Delta\Gamma_n\right)^2 + 2\frac{\partial\sigma_\gamma}{\partial\Gamma_n}\langle\delta\Gamma_n\,\delta\Gamma_\gamma\rangle\frac{\partial\sigma_\gamma}{\partial\Gamma_\gamma} + \left(\frac{\partial\sigma_\gamma}{\partial\Gamma_\gamma}\Delta\Gamma_\gamma\right)^2\,, \tag{3.9}$$

where $\langle\delta\Gamma_n\,\delta\Gamma_\gamma\rangle$ is a covariance matrix and again we dropped the fission term for simplicity.

The approach described here to calculate the correlation term between the resonance widths applies the generalized least squares method from the Bayesian theorem [12]. The initial values of Γ_n, Γ_γ, A_γ as well as their uncertainties, $\Delta\Gamma_n$, $\Delta\Gamma_\gamma$ and ΔA_γ, can be taken from the Atlas of Neutron Resonances. The following relations hold for the prior covariance matrix of the resonance widths, Ψ, and the

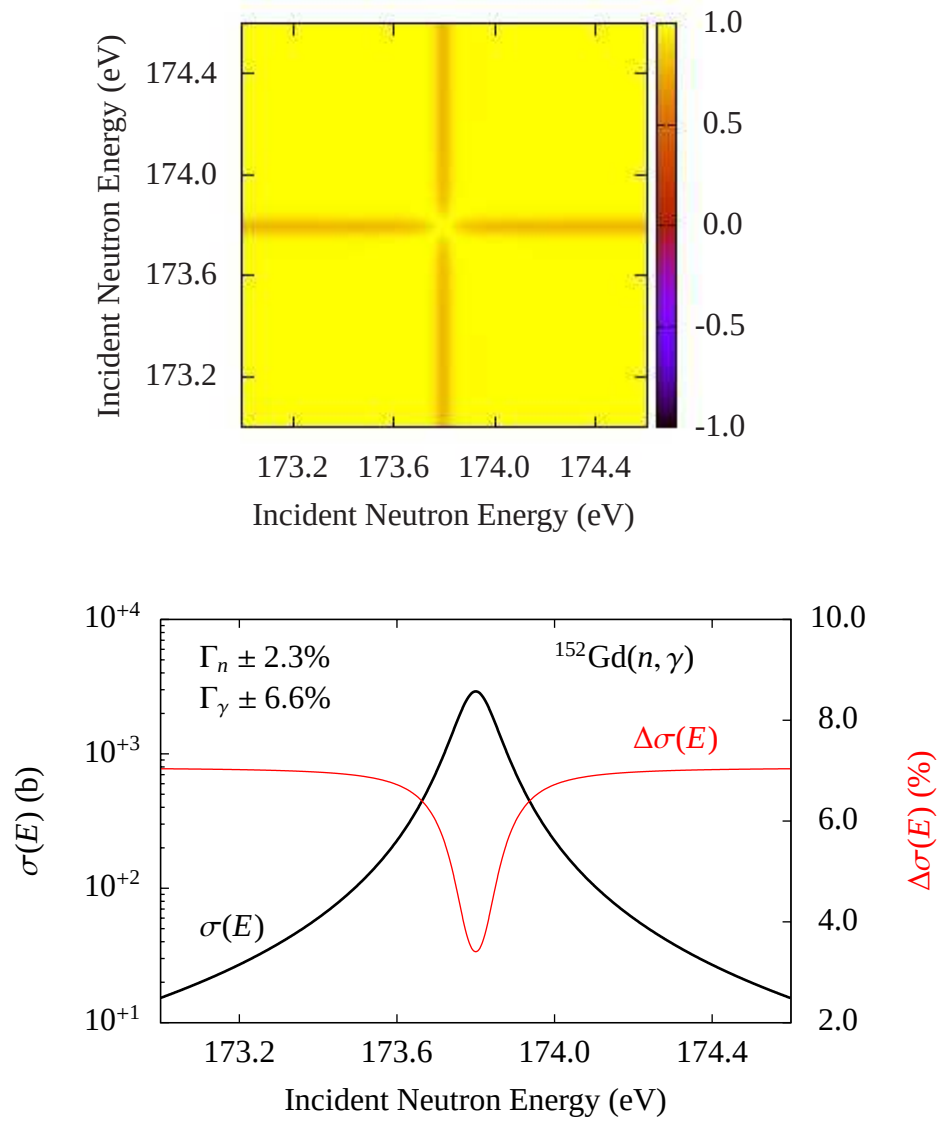

Figure 3.4: Top: The ^{152}Gd(n,γ) cross section correlations due to uncorrelated Γ_n and Γ_γ for the single 173.8 eV resonance. Bottom: The same for relative cross section uncertainties.

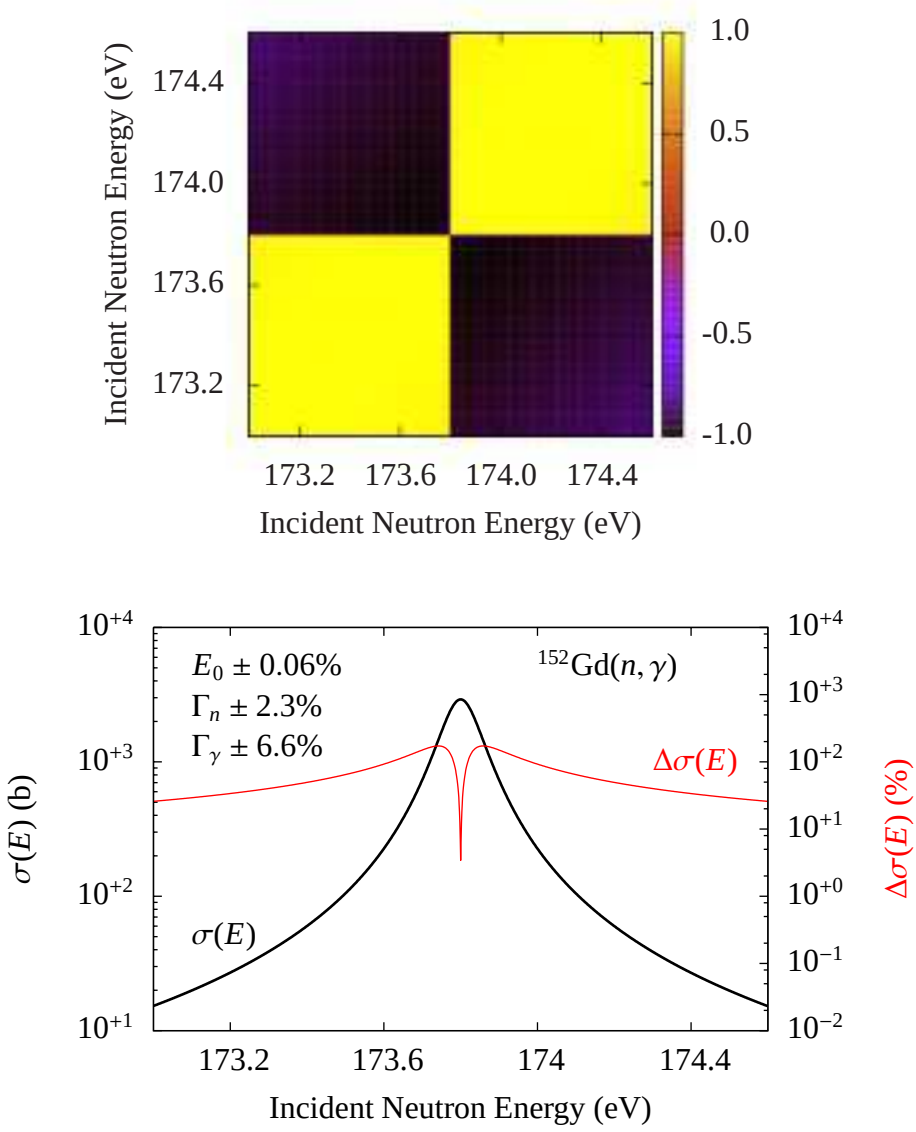

Figure 3.5: Top: The ^{152}Gd(n,γ) cross section correlations due to uncorrelated E_0, Γ_n and Γ_γ for the single 173.8 eV resonance. Bottom: The same for relative cross section uncertainties.

posterior matrix, $\tilde{\Psi}$,

$$\begin{aligned} \tilde{\chi} &= \chi + \Psi S^{\mathrm{T}} V[A - A(\chi)] \\ \tilde{\Psi} &= \Psi - \Psi S^{\mathrm{T}} V S \Psi \,, \end{aligned} \tag{3.10}$$

where $V = (S\Psi S^{\mathrm{T}} + (\Delta A)^2)^{-1}$. The vector $A(\chi)$ represents the capture kernel calculated for the set of parameters $\chi \equiv \{\Gamma_n, \Gamma_\gamma\}$. The quantity $A \equiv A_\gamma$ is the experimental value of the capture kernel with related variance $(\Delta A_\gamma)^2$, while S is the sensitivity matrix and S^{T} is its transpose given by

$$S^{\mathrm{T}} \equiv \left(\frac{\partial A_\gamma}{\partial \Gamma_n}, \frac{\partial A_\gamma}{\partial \Gamma_\gamma} \right) . \tag{3.11}$$

The covariance matrix for the resonance parameters is given as

$$\Psi = \begin{pmatrix} (\Delta\Gamma_n)^2 & \langle \delta\Gamma_n \, \delta\Gamma_\gamma \rangle \\ \langle \delta\Gamma_\gamma \, \delta\Gamma_n \rangle & (\Delta\Gamma_\gamma)^2 \end{pmatrix} . \tag{3.12}$$

We introduce the shortened notation for the correlation term between Γ_n and Γ_γ

$$C = \frac{\langle \delta\Gamma_n \, \delta\Gamma_\gamma \rangle}{\Delta\Gamma_n \, \Delta\Gamma_\gamma} . \tag{3.13}$$

The upper line of Eq.(3.10) represents the update of the Γ_n and Γ_γ parameters, while the lower line defines the covariance calculation for these parameters. In the prior matrix Ψ, the correlation term C is assumed to be equal to zero. Then, the calculation is iterated by replacing Ψ with the calculated $\tilde{\Psi}$ until convergence is achieved.

We illustrate impact of the $(\Gamma_n, \Gamma_\gamma)$ correlations on capture cross section uncertainties in Fig. 3.6. We choose ^{152}Gd(n, γ) reaction in the vicinity of the resonance at 173.8 eV and show the range of uncertainties when the correlation coefficient C varies between -0.1 and -0.9. One notes that low correlations result in higher uncertainties at both wings of the resonance while the opposite is true for the peak zone. The change in the cross section uncertainty can reach about 50% between physical limits of C (-1 to 0) but is less than 30% in the peak zone. Typical scale of the $(\Gamma_n, \Gamma_\gamma)$ correlation is shown in Table 3.2, in which we reproduce experimental values of C for several s-wave resonances in ^{152}Gd+n as reported in Ref. [18]. Generally, there is a strong negative correlation if Γ_n and Γ_γ are comparable and it weakens if one of the widths becomes much larger than the other.

Table 3.2: The resonance parameters and capture kernels of selected s-wave resonances for ^{152}Gd+n [10]. The correlation terms, C, between Γ_n and Γ_γ were taken from Ref. [18]. For all resonances $g = 1$.

E_0 (eV)	$g\Gamma_n$ (meV)	Γ_γ (meV)	A_γ (meV)	C	Comment
173.8	86±2	30±2	22.3±0.3	-0.91	
185.7	84±2	53±5	32.3±0.5	-0.95	
203.1	97±2	59±3	36.6±0.4	-0.95	
223.3	301±12	64±3	52.9±0.6	-0.75	$\Gamma_n >> \Gamma_\gamma$
231.4	46±4	62±8	26.4±0.9	-0.98	
1678.4	999±116	69±7	64.6±2.3	-0.60	$\Gamma_n >> \Gamma_\gamma$

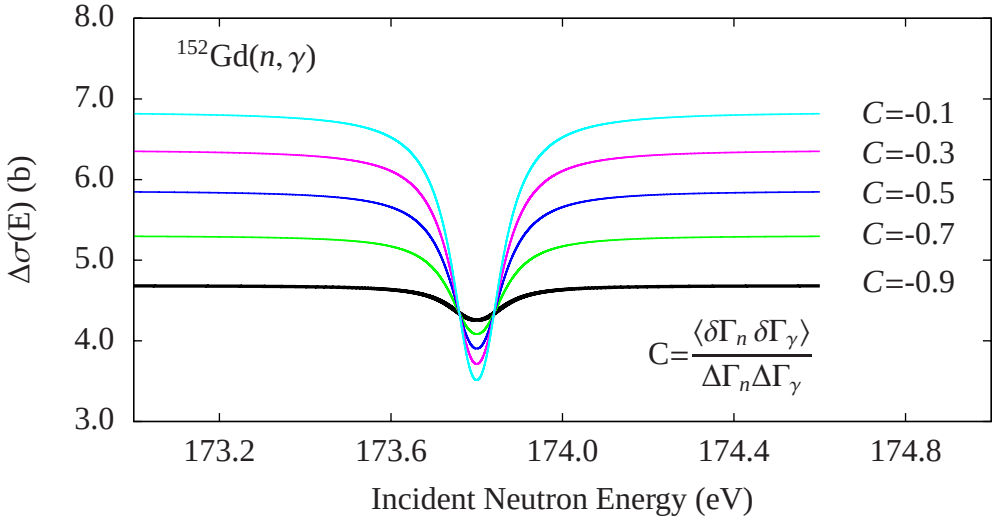

Figure 3.6: The ^{152}Gd(n,γ) relative cross section uncertainties for the single 173.8 eV resonance illustrating the impact of the correlation between Γ_n and Γ_γ.

3.3 Averaged values

Users of neutron cross section data are primarily interested in the group-averaged cross sections and their uncertainties. Therefore, it is of practical interest to examine the impact of the covariances on the cross sections that are averaged over a broader energy interval. The capture cross section averaged over the energy interval ΔE around the energy E_0 can be calculated as

$$\overline{\sigma_\gamma} = \frac{1}{\Delta E}\sum_i \sigma_\gamma(E_i)\Delta e\,, \tag{3.14}$$

where Δe is a sufficiently small energy step. Then, the averaged cross section uncertainty is

$$\overline{\Delta\sigma_\gamma} = \frac{\Delta e}{\Delta E}\sqrt{\sum_{i,j}\langle\delta\sigma_\gamma(E_i)\,\delta\sigma_\gamma(E_j)\rangle}\,. \tag{3.15}$$

It should be pointed out that typical widths of energy bins over which the averaging is done is much larger than the width of a single resonance. Thus, in our sample case that we choose to illustrate our results, ^{152}Gd(n,γ), the 173.8 eV resonance falls in the group-energy interval that is orders of magnitude larger than the resonance width $\Gamma_\gamma = 0.03$ eV. Indeed, in the 44-group structure used for nuclear criticality safety applications the relevant energy group has width orders of magnitude larger. In the 15-group structure, used in some advanced reactor systems studies, the relevant energy group spans the energy range from 22.6 eV to 454 eV, implying the bin widths more than 400 eV. The energy interval over which the cross section uncertainty is displayed in the above example, see Figs. 3.1-3.6 is less than 1 eV. This energy interval is sufficiently broad for our purposes, yet still pretty small when compared to the energy interval of any relevant group structure used in practice.

One important comment is in place. In calculating average quantities the role of correlations become important as can be seen in Eq.(3.15). As a consequence, averaged uncertainties are lower, sometimes considerably lower, than those intuitively expected considering purely diagonal terms.

Considering the anti-correlation caused by ΔE_0, it is clear that impact of ΔE_0 on the averaged cross section uncertainty is negligible. On the contrary, $\Delta\Gamma_n$ and $\Delta\Gamma_\gamma$ are important in view of the cross section uncertainties since the related cross section correlation matrix is positive and fairly uniform. Therefore there is no cancellation that eliminates the effect of ΔE_0. The impact of the correlation between

Γ_n and Γ_γ may be significant and reduces the average cross section uncertainty for negative C.

Chapter 4

Cross section covariances for multiple resonances

The previous analysis can be extended to a more realistic case with many resonances. We will discuss the cross section uncertainties and then proceed with the correlations.

4.1 Cross section uncertainties

Using Eq. (3.4), the cross section uncertainty for the multi-resonance case can be worked out fairly easily. Two cases will be discussed, first we would assume uncorrelated resonance parameters, afterwards we will consider correlation between Γ_n and Γ_γ. For the uncorrelated resonance parameters one has

$$(\Delta\sigma_\gamma)^2 = \sum_r \left[\left(\frac{\partial\sigma_\gamma}{\partial E_{0r}} \Delta E_{0r} \right)^2 + \left(\frac{\partial\sigma_\gamma}{\partial \Gamma_{nr}} \Delta\Gamma_{nr} \right)^2 + \left(\frac{\partial\sigma_\gamma}{\partial \Gamma_{\gamma r}} \Delta\Gamma_{\gamma r} \right)^2 \right], \tag{4.1}$$

where r denotes the individual resonances. Following Eqs. (3.5) and (3.6) the partial contributions to $(\Delta\sigma)^2$ can be readily obtained and, after some rearrangement and dropping subscript γ, written as

$$\frac{\partial\sigma}{\partial E_{0r}} \frac{\Delta E_{0r}}{\sigma} = \frac{\sigma_r}{\sigma} \left(\frac{8E_0(E - E_{0r})}{\Gamma_r^2 + 4(E - E_{0r})^2} - \frac{1}{2} \right) \frac{\Delta E_{0r}}{E_{0r}} \tag{4.2}$$

and

$$\frac{\partial\sigma}{\partial \Gamma_{xr}} \frac{\Delta\Gamma_{xr}}{\sigma} = \frac{\sigma_r}{\sigma} \left(1 - \frac{2\Gamma_{xr}\Gamma_r}{\Gamma_r^2 + 4(E - E_{0i})^2} \right) \frac{\Delta\Gamma_{xr}}{\Gamma_{xr}}, \tag{4.3}$$

where σ_r is the cross section of the resonance r and $x = n, \gamma$. The ratio σ_r/σ modifies the behavior of the cross section uncertainty far from the resonance energy E_{0r}. If the neutron energy E is close to E_{0r}, then the ratio σ_r/σ is almost equal to unity and Eqs. (4.2, 4.3) become similar to Eqs. (3.5, 3.6). For the energy E far from E_{0r}, the σ_r/σ becomes small in the presence of another resonance and the effect of the r^{th} resonance on the cross section uncertainty is also small.

We will discuss two examples, each showing three s-wave resonances. Our first example continues with the case of ^{152}Gd(n,γ). We already discussed the 173.8 eV resonance, now we proceed by adding 185.7 eV and 203.1 eV resonances. For these three resonances, the calculated capture cross sections and the calculated relative uncertainties are shown in Fig. 4.1. One can see three broad peaks in the uncertainty curve with narrow dips at the resonance energies. Possible impact of the correlation between Γ_n and Γ_γ is displayed by the shadowed band that corresponds to the range of values C=0.0 and -0.9.

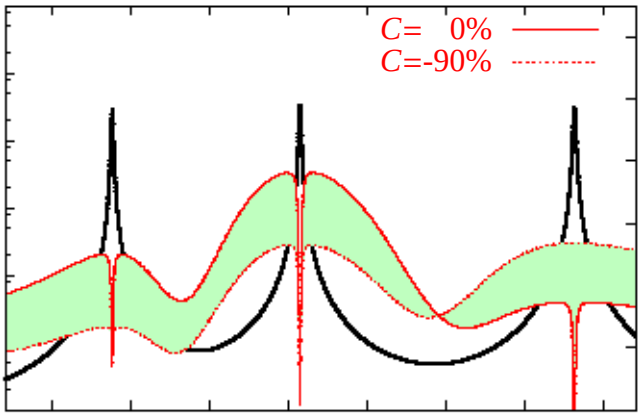

Figure 4.1: The ^{152}Gd(n,γ) cross sections and their relative uncertainties for three s-wave resonances, E_0=173.8, 185.7 and 203.1 eV. The resonance energy uncertainties, ΔE_0, were not considered. The shadowed band illustrates the impact of the $(\Gamma_n, \Gamma_\gamma)$ correlation.

Our second example discusses fission. In Fig. 4.3 we show ^{241}Am(n,f) cross sections and their uncertainties considering three resonances as well as the bound level. The resonance parameters and their uncertainties are given in Table 4.1. The contribution of the bound level to the cross sections is clearly visible. One

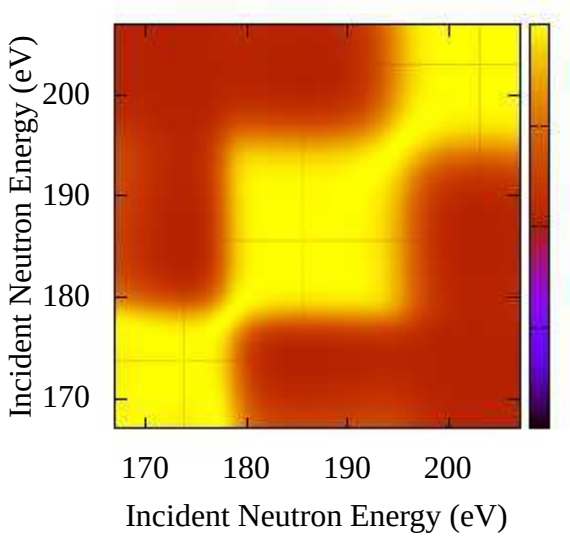

Figure 4.2: Cross section correlation due to uncorrelated Γ_n and Γ_γ for ^{152}Gd(n,γ) for three s-wave resonances, E_0=173.8, 185.7 and 203.1 eV.

Table 4.1: The resonance parameters and their uncertainties for three s-wave resonances in ^{241}Am(n,f) [10], fission kernels A_f are not available. Also shown are parameters for the bound state which are considered to be known exactly. Shown in the last column are correlation coefficients, C, between Γ_n and Γ_f.

E_0(eV)	$2g\Gamma_n$ (meV)	Γ_γ (meV)	Γ_f(meV)
-0.425	0.641	40	0.215
0.307 ±0.002	0.0560 ±0.0005	46.8±0.3	0.29±0.03
0.574 ±0.004	0.0923 ±0.0020	47.2±0.3	0.14±0.02
1.268 ±0.004	0.3200 ±0.0080	48.9±0.7	0.37±0.02

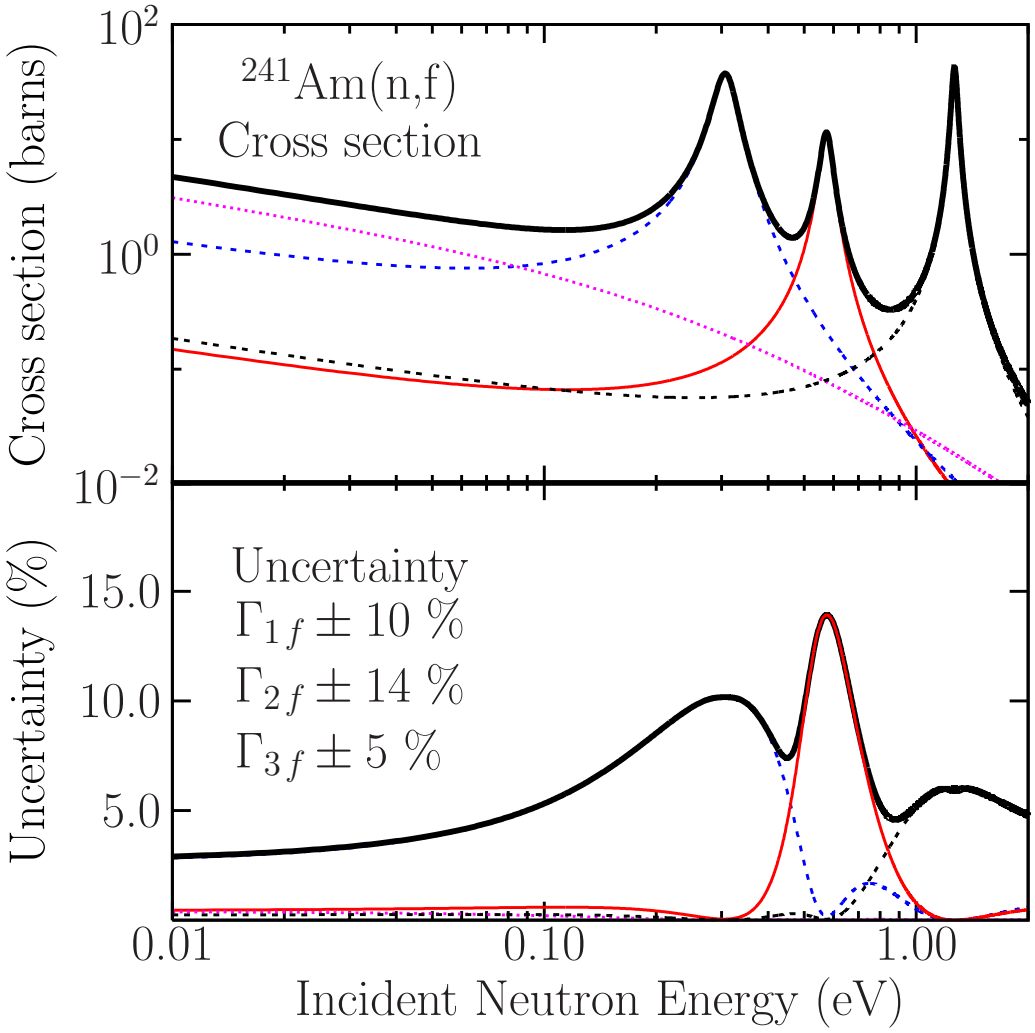

Figure 4.3: The ^{241}Am(n,f) cross sections and their relative uncertainties for three s-wave resonances (0.307, 0.574 and 1.268 eV) and the bound level. Γ_{if} stands for the fission width for the *i*-th resonance. The resonance energy uncertainties, ΔE_0, were not considered.

can see that there are no local mimima at the resonance energies, in line with our earlier discussion of the single resonances as $\Delta\Gamma_f/\Gamma$ is close to zero. Since the resonances are close to each other the local structures are washed out due to the uncertainties of individual resonances.

Table 4.1 shows the resonance parameters for three s-wave resonances in ^{241}Am(n,f) as well as the bound level and we expect $(\Gamma_n, \Gamma_\gamma)$ to be strongly anti-correlated.

4.2 Cross section correlations

The energy-energy correlation between capture (fission) cross sections for many resonances can be obtained readily using Eq. (3.7) and performing summation of contributions from single resonances r. One has

$$\frac{\langle \delta\sigma(E)\,\delta\sigma(E')\rangle}{\Delta\sigma(E)\Delta\sigma(E')} = \sum_r \sum_\nu \frac{\partial\sigma(E)}{\partial p_{\nu r}} \frac{(\Delta p_{\nu r})^2}{\Delta\sigma(E)\Delta\sigma(E')} \frac{\partial\sigma(E')}{\partial p_{\nu r}}, \qquad (4.4)$$

where the subscript ν denotes different resonance parameters. When discussing correlations one can consider three options, although they may not be fully supported by the data available in the Atlas of Neutron Resonances. These options are:

- Uncorrelated parameters for each individual resonance,
- Correlations between parameters of a single resonance (short range correlation), and
- Correlations between parameters of various resonances (long range correlation).

The first option is illustrated on ^{241}Am(n,f) reactions in Fig. 4.4. The resonance parameters and their uncertainties, given in Table 4.1, are treated as uncorrelated. Strong and localized anti-correlation can be seen close to the resonance energies. For ^{241}Am(n,f), the cross section uncertainty in the thermal energy region is dominated by the 0.307 eV resonance. Consequently, the thermal cross section and uncertainty are almost fully dominated by the first positive resonance at 0.307 eV. The second option could be illustrated by continuing in the above example and including the effect of Γ_n and Γ_f correlation. It appears that, when looking on the

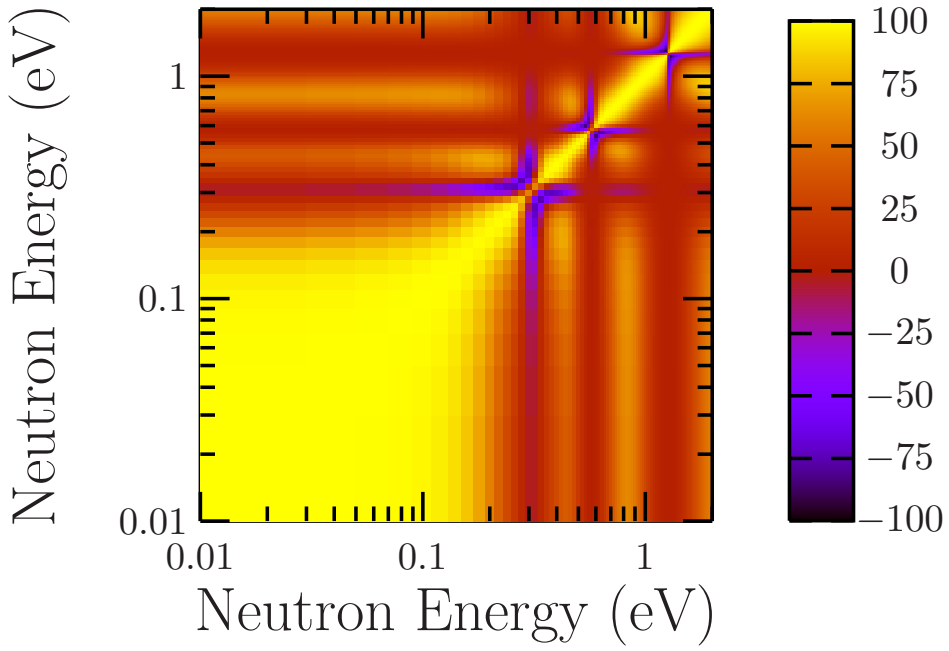

Figure 4.4: Fission cross section correlations for ^{241}Am(n,f) considering three resonances (0.307, 0.574 and 1.268 eV) and the bound level. The uncertainties of all resonance parameters were assumed to be uncorrelated.

correlation plot similar to Fig. 4.4, the effects are relatively small and hence not shown here.

The third option takes into account also long-range correlations. Obviously one could consider the resonance energies as they are determined by the neutron flight path, but this effect in practice is very small and can be neglected. Of more interest would be to consider another correlation, indicated by the Atlas of Neutron Resonances, though without any strict guidance. This correlation can be inferred from the fact that often the radiative widths are assumed to be constant. In this case, the radiative widths of all resonances should be strongly correlated. Such correlations can be only estimated using *ad hoc* assumptions as no guidance is given in the Atlas of Neutron Resonances and we are not attempting to do so here.

4.3 Averaged values

As already mentioned the users require multi-group cross sections. The reason is that large simulation codes are not designed for point-wise cross sections that are far too detailed, rather one needs suitably averaged values, the multi-group cross sections. To this end, the processing codes such as PUFF [15] and ERRORJ [16] and NJOY [17]should be employed.

From the above discussion it is clear that the two possible ways how to obtain multi-group cross section uncertainties in the resonance region should be equivalent. If one choses to produce MF32 covariances, then PUFF or ERRORJ should be used to obtain multi-group cross section covariances from covariances of resonances parameters. If, alternatively, one chose to produce MF33 covariances, then either of the above codes can be used to obtain multi-group cross section covariances. We are not resorting to show this on any single case as such an example might not be considered as sufficiently general and it is beyond the scope of this report to go to extensive analysis of this point.

In practice, MF32 is more straightforward and provides more flexibility. Hence its use, unless prohibited by huge size of the file, such as in the case of ^{235}U, is preferable.

Chapter 5

Conclusions

The cross section uncertainties and correlations for neutron capture and fission in the resolved resonance region were examined. Our goal was to make maximum use of the information available in the Atlas of Neutron Resonances. We used the MLBW formalism that allowed analytical solutions, complemented with the numerical calculations whenever necessary.

We studied the impact of the resonance parameter $(E_0, \Gamma_\gamma, \Gamma_n)$ uncertainties and examined the possibility to introduce resonance parameter correlations by utilizing the capture kernel (A_γ). We have shown that the uncertainties of the resonance energies, ΔE_0, can be neglected in the averaged cross sections. The uncertainties of the other resonance parameters should be taken into account. This is also true for the correlations between Γ_n and Γ_γ in cases where these widths have comparable values.

The use of the resonance parameter covariances, file MF32, is a logical step forward in developing our covariance methodology in the neutron resolved resonance region. So far, we have been using the cross section covariance representation, file MF33. These two ways are equivalent in the sense of providing the same multi-group values, but the use of MF32 is more straightforward and more flexible and it should be given the preference.

We conclude that the Atlas of Neutron Resonances contains the wealth of information that can be effectively utilized in the evaluation of neutron cross section covariances in the resolved energy region.

List of Figures

List of Tables

Acknowledgments

The authors wish to thank Toshihiko Kawano, LANL for the stimulation and encouragement. We gratefully acknowledge useful discussions with G. Chiba, Japan Atomic Energy Agency (JAEA). This manuscript has been authored by Brookhaven Science Associates, LLC, under contract DELACO2-98CH10886 with the U.S. Department of Energy.

Bibliography

[1] M. Salvatores, G. Aliberti, G. Palmiotti, D. Rochman, P. Obložinský, M. Herman, P. Talou, T. Kawano, L. Leal, A. Koning, I. Kodeli, "Nuclear Data Needs for Advanced Reactor Systems. A NEA Nuclear Science Committee Initiative", Proceedings of the International Conference on Nuclear Data for Science and Technology, Nice, France, April 22-27, 2007, to be published.

[2] G. Aliberti, G. Palmiotti, M. Salvatores, T. K. Kim, T. A. Taiwo, M. Anitescu, I. Kodeli, E. Sartori, J. C. Boscp and J. Tommasi, Annals of Nuclear Energy **33** (2006) 700.

[3] M.B. Chadwick, P. Obložinský, M. Herman *et al.*, "ENDF/B-VII.0: Next Generation of Evaluated Nuclear Data Library for Nuclear Science and Technology", Nuclear Data Sheets **107** (2006) 2931.

[4] N.M. Larson, "Updated Users' Guide for SAMMY: Multilevel R-Matrix Fits to Neutron Data Using Bayes' Equations", Report ENDF-364 and ORNL/TM-9179/R6, Oak Ridge National Laboratory, Oak Ridge, TN (May 2003). Also report ORNL/TM-9179/R7 (2006).

[5] N.M. Larson, "Use of Covariance Matrices in SAMMY", Workshop on Nuclear Data Evaluation for Reactor Applications, WONDER 2006, 9-11 October 2006, Château de Cadarache, Saint-Paul-lez-Durance, France, unpublished.

[6] M.C. Moxon and J.B. Brisland, "REFIT, a least square fitting program for resonance analysis of neutron transmission and capture data", Technical Report AEA-INTEC-0630, AEA Technology (1991).

[7] A. Borella, G. Aerts, F. Gunsing, M. Moxon, P. Schillebeeckx and R. Wynants, Nucl. Inst. Meth. **A 577** (2007) 626.

[8] P. Schillebeeckx, private communication, July 2007.

[9] T. Kawano, L.C. Leal *et al*, "Covariance matrix evaluation and processing in the resolved/unresolved resonance region", Report WPEC-Subgroup 20, NEA/WPEC-20, OECD, Paris, 2006.

[10] S.F. Mughabghab, "Atlas of Neutron Resonances: Thermal Cross Sections and Resonance Parameters", Elsevier Publisher, Amsterdam, 2006.

[11] M. Herman, R. Capote, B. Carlson *et al*, "EMPIRE: Nuclear Reaction Model Code System for Data Evaluation", Nuclear Data Sheets **108** (2007) 2655.

[12] T. Kawano and K. Shibata, "Covariance Evaluation System", in Japanese, JAERI Report JAERI-Data/Code 97-037 (1997).

[13] D. Rochman, M. Herman, P. Obložinský, S. Mughabghab, "Preliminary Cross Section and Nubar Covariances for WPEC Subgroup 26 (Nuclear Data Needs for Advanced Reactor Systems)", Internal Report BNL-77407-2007-IR (2007).

[14] M. Herman (editor), "ENDF-6 Formats Manual: Data Formats and Procedures for the Evaluated Nuclear Data File ENDF/B-VI and ENDF/B-VII", Tech. Report BNL-NCS-44945-05-Rev, Document ENDF-102, Brookhaven National Laboratory, 2005.

[15] D. Wiarda and M.E. Dunn, "PUFF-IV: A Code for Processing ENDF Uncertainty Data into Multigroup Covariance Matrices", Report ORNL/TM-2006/147 (2006).

[16] G. Chiba, "ERRORJ-2.2 Manual Report on JENDL-3.2 Covariance Matrices", Report JAERI-Research 2003-001 (2003).

[17] R.E. McFarlane and D.W. Muir, "The NJOY Nuclear Data Processing System, Version 91", Los Alamos National Laboratory, Report LA-12740-M (1994), and more recent updates.

[18] R.L. Macklin, "Neutron Capture Resonances of ^{152}Gd and ^{154}Gd", Nucl. Sci. Eng. **95** (1987) 304.

Appendix E

Covariance Estimates in Fast Neutron Region

Extensive set of cross section covariance estimates in the fast neutron region

M.T. Pigni *, M. Herman, P. Obložinský

National Nuclear Data Center, Brookhaven National Laboratory
Upton NY 11973-5000, U.S.A.

Abstract

We generated, for the first time, a very comprehensive set of estimates of cross section covariance data in the neutron energy range of 5 keV - 20 MeV. The covariance matrices were obtained for 307 materials, from ^{19}F to ^{209}Bi, covering structural materials, fission products, and heavy non-fissile nuclei. These results offer model-based, consistent assessments of covariance data for nuclear criticality safety applications. The evaluation methodology combines the nuclear reaction model code EMPIRE that calculates the sensitivity of the cross sections to nuclear reaction model parameters, and the Bayesian code KALMAN that propagates uncertainties of the model parameters to these cross sections. Taking into account the large number of materials studied, we refer only marginally to experimental data. The covariances were derived from the perturbation of several key model parameters selected by the sensitivity analysis. These parameters refer to the optical model potential, the level densities, and the strength of the pre-equilibrium emission. Our work represents the first attempt to generate neutron cross section covariances on such a large scale.

Key words: neutron cross section covariances, nuclear criticality safety, ENDF/B-VII.0
PACS: 25.40.-h, 28.20.-v

1. Introduction

Two factors can explain the recent revival of research on neutron cross section covariances. First, there is intensive renewed interest in nuclear technology applications, such as designing a new generation of nuclear power reactors along with enhanced requirements on nuclear criticality safety. Second, considerable advances in computer technology and in neutronics simulation codes now allow refined predictions of integral quantities that start to probe the uncertainties of basic nuclear data.

Neutron cross section covariances (uncertainties and correlations) are necessary for several distinct types of applications [1]. Probably the most important is the need to assess the uncertainties of integral quantities, such as the design and operational parameters of nuclear power reactors. Estimates of the accuracy of predictions of such applied quantities due to uncertainties in the basic data can be viewed as the forward propagation of uncertainties. To this end, sensitivity coefficients are computed for the integral quantity, R, with respect to cross sections and the integral variance is obtained as

$$(\Delta R)^2 = \mathbf{s}_R^{\mathrm{T}} \mathbf{D} \mathbf{s}_R \,, \qquad (1)$$

where $\mathbf{s}_R^{\mathrm{T}}$ is the transpose of the sensitivity coefficient vector, $\mathbf{s}_R$, and $\mathbf{D}$ is the cross section covariance matrix.

The same approach, albeit in the reverse order, can be used to identify nuclear data requirements. In doing so, one starts from the target uncertainties of integral quantities and propagates them backwards to the desired precision of the neutron cross sections. Salvatores et al.'s [2] recent international collaboration applied this approach to identify the data needed for designing advanced reactor systems.

Data adjustment represents another important use of neutron covariance data. Here, one would start with the basic evaluated data library, such as the recently released ENDF/B-VII.0 [3], analyze suitable integral experiments, calculate sensitivities for observed integral quantities, account for covariance data, and produce an adjusted multi-group library constrained by these integral experiments. Such an adjusted library then could be used for neutronics simulations of the new systems. Ideally, if the adjustments were propagated backward to the basic library, integral quantities could be predicted for systems that go beyond current experience in terms of their material composition and neutron energy spectra. Currently, the Global Nuclear Energy Partnership (GNEP) is engaged in such a data adjustment project, focusing on fast, metal-cooled actinide burner reactors [4].

Although covariances were extensively studied in the 1970s,

* Reference author
Email address: pigni@bnl.gov (M.T. Pigni).
URL: http://www.nndc.bnl.gov/nndcpeople/pigni.html (M.T. Pigni).

this research virtually disappeared in the 1990s due to limited interest by users and scarce resources for data evaluation. Consequently, the availability of covariances in the major nuclear data libraries is very restricted. For example, the most recent ENDF/B-VII.0 library, released in December 2006, contains covariances for only 26 materials, i.e., for less than 7% of those in the neutron sub-library. Moreover, only 13 of these materials can be considered complete in that they provide covariances for all reaction channels important for applications. The lack of a consistent, complete set of covariances is a barrier that prevents using the sensitivity tools in developing innovative nuclear technologies, and discourages the advancement of the tools themselves.

The U.S. Nuclear Criticality Safety Program (NCSP) recently addressed the scarcity of neutron covariance data. An almost complete lack of these data not only prevents prediction of uncertainties in computing criticality but it also prevents development and testing relevant computational capabilities. To facilitate such development, cross section covariance data are essential. Even relatively crude approximations would be an enormous help for these advances. The goal is to produce a rough set of covariances covering all relevant reaction channels and materials (from thermal energy to 20 MeV), thereby affording a solid base for testing the new tools for advanced numerical simulations employing nuclear data uncertainties and correlations. The emphasis is on completeness rather than on precision - the latter should be addressed after the evaluation methodology is well established and adequate tools are available.

The large scale of our "low-fidelity" covariance project necessitated our basing the results on model calculations, with minimal reference to experimental data. Calculations by the code EMPIRE [5] with default set of parameters provide a complete set of cross sections, while the code KALMAN [6] generates their (co)variances. We stress that EMPIRE predictions of cross sections, many of which are very reasonable, do not coincide with any of the official evaluated libraries. Therefore, our covariances should not be associated with any cross sections recommended for applications. The almost complete neglect of experimental data, and the global nature of our model calculations also limits detailed comparison with the existing covariances generated from much more thorough analyses.

The low-fidelity covariance project produced cross section covariance matrices (MF33 in ENDF-6 format definition) for a complete set of 393 materials in the ENDF/B-VII.0 neutron sub-library. The data required by the project cover five major reaction channels, (n,el), (n,inl), (n,2n), (n,γ), plus (n,f) for actinides, with the understanding that (n,tot) is redundant. We note that (n,p) and (n,α) cross sections are in general fairly small, particularly for heavier nuclei, and their impact on total cross section covariances can be neglected except for a few light nuclei. The project involved four major U.S. national laboratories (BNL, ORNL, LANL, and ANL) with different responsibilities. Our role was to produce covariance estimates in the fast neutron region for 307 isotopes between ^{19}F and ^{209}Bi. This massive task was split into two parts. First, we derived covariances for 219 fission products [7,8] defined as the ENDF/B-VII.0 materials in the range of Z = 31 - 68, and second, for the remaining 57 structural and 31 heavy materials [9]. ORNL took care of the low neutron energy region (<5 keV) where the covariances were estimated from the standard deviation of the thermal cross sections and resonance integrals [10]. LANL produced covariances in the fast energy region for light nuclei (A$<$ 19) and actinides (A$>$ 209). Finally, ANL has responsibility for checking and reviewing. The project, including its justification and results, is summarized in the recent paper [11].

The paper is organized as follows. In Section 2, we describe the methodology, while Section 3 presents and discusses the calculations. Our conclusions are summarized in Section 4.

2. Evaluation methodology

Our methodology is based on the nuclear reaction model code EMPIRE [5] coupled to the Bayesian filtering code KALMAN [6]. For this extensive task, we based the results almost entirely on model calculations with marginal reference to experimental data. The EMPIRE code calculates neutron cross sections according to appropriately selected models and model parameters, while KALMAN propagates model parameter uncertainties into cross section (co)variances.

2.1. *Evaluation method*

The Bayesian update procedure is a standard tool used in statistics to modify prior results by taking into account any new data. In our case, the evaluation starts with the EMPIRE nuclear reaction model code which encompasses a wide range of nuclear models of different degrees of sophistication to assure an overall description of nuclear observables. The adopted models address specific reaction mechanisms, and depend on adjustable parameters. The most relevant ones are those related to optical potential and nuclear level densities. These parameters are varied to calculate partial derivatives of cross sections, defining the elements of the sensitivity matrices (see Eq. (6)). The calculated reaction cross sections, sensitivity matrices along with the model parameters and their uncertainties represent input quantities for the KALMAN code.

The KALMAN code is used as a nuclear data evaluation tool based on the iterative generalized least-squares approach. The procedure emphasizes the estimation of the uncertainties in the model parameters, and the corresponding correlations. It is applied to evaluating neutron cross sections and their covariance matrices for various reaction channels. Applying the Bayesian equations is straightforward, and the update is a simple algebraic operation,

$$\mathbf{p}_{n+1} = \mathbf{p}_n + \mathbf{P}_n\mathbf{S}^{\mathrm{T}}\mathbf{Q}_n(\boldsymbol{\sigma}_n^{\mathrm{exp}} - \boldsymbol{\sigma}(\mathbf{p}_n))$$

$$\mathbf{P}_{n+1} = \mathbf{P}_n - \mathbf{P}_n\mathbf{S}^{\mathrm{T}}\mathbf{Q}_n\mathbf{S}\mathbf{P}_n\,, \qquad (2)$$

where n denotes the n^{th}-step in the evaluation process according to the number of sets of experimental data to be included. The vector $\mathbf{p}_{n+1}$ contains the improved values of the parameters starting from the vector $\mathbf{p}_n$. Likewise, the matrix $\mathbf{P}_{n+1}$

is the updated covariance matrix of the parameters $\mathbf{p}_{n+1}$. The combination of the theoretical covariance matrix $\mathbf{D}$ and the experimental covariance matrix $\mathbf{D}^{\text{exp}}$ yields the updated covariance matrix,

$$\mathbf{Q} = (\mathbf{D}^{\text{exp}} + \mathbf{D})^{-1}\,, \tag{3}$$

and the vector $\boldsymbol{\sigma}(\mathbf{p})$ represents the set of cross sections for a specific reaction channel calculated for the set of parameters, $\mathbf{p}$.

In our calculations, the experimental data were virtually ignored, so considerably simplifying the evaluation procedure that then becomes driven by the theoretical cross section covariances. The theoretical cross section covariance matrix,

$$\mathbf{D} = \mathbf{SPS}^{\text{T}}\,, \tag{4}$$

is associated with the model calculation by the covariance matrix of the model parameters,

$$\mathbf{P} \equiv \langle \delta p_\ell\, \delta p_m \rangle\,, \tag{5}$$

and the sensitivity matrix, $\mathbf{S}$, with the elements,

$$s_{i,j} = \frac{\partial \sigma(E_i, \mathbf{p})}{\partial p_j}\,, \tag{6}$$

calculated as the partial derivative of the cross section σ at the energy E_i with respect to the parameter p_j. Then, the covariance matrix defined in the context of the present work can be identified readily with the theoretical covariance matrix, $\mathbf{D}$.

In the explicit notation, the elements of the cross section covariance matrix can be written as

$$d_{i,k} = \sum_{\ell,m=1}^{q} s_{i,\ell}\, \langle \delta p_\ell\, \delta p_m \rangle\, s_{k,m}\,, \tag{7}$$

wherein the covariance matrix of model parameters, $\mathbf{P}$, is diagonal, if model parameters are uncorrelated, as we assumed in the present work. Conveniently, the cross section covariance matrix can be separated into the diagonal terms - the cross section variances [*], $d_{i,i} \equiv \langle (\delta d_i)^2 \rangle$ - and the cross section correlation matrix defined as

$$\zeta_{i,k} = \frac{d_{i,k}}{\sqrt{d_{i,i}}\sqrt{d_{k,k}}}\,, \tag{8}$$

where the matrix elements lie, by definition, within the range $-1 \leq \zeta_{i,k} \leq 1$.

We note that the covariance matrix, likewise its correlation matrix, must be symmetric and positive definite. While the first requirement is easy to satisfy, the second is less transparent and means that

$$\mathbf{ZDZ}^{\text{T}} > 0\,, \tag{9}$$

for all non-zero real vectors $\mathbf{Z}$. This condition is achieved by ensuring that all matrix elements have positive values after diagonalizing them; otherwise, numerical rounding of errors in the calculation and normalization procedure can lead to inconsistencies, with the matrices $\boldsymbol{\zeta}$ not satisfying Eq. (9). We carefully checked all cross section covariance matrices to ensure positive-definitiveness.

[*] The cross section uncertainty (or standard deviation) is related to the variance via $\Delta d_i = \sqrt{d_{i,i}} = \sqrt{\langle (\delta d_i)^2 \rangle}$.

2.2. *Reaction models and parameters*

The EMPIRE code system [5] is a modern tool for modeling low and intermediate energy nuclear reactions. It incorporates an extensive set of nuclear reaction models able to describing all relevant reaction mechanisms, each of them conveniently coupled to the up-to-date library of input model parameters [12]. Therefore, EMPIRE provides reasonable overall description of nuclear observables, even if default parametrization is used. The code is suitable for massive calculations, is easy to use, has readily available default input values for all parameters, and it is applicable to a wide range of target nuclei and incident neutron energies from about 1 keV to 150 MeV.

In the context of this project, three nuclear reaction models were adopted:
– Spherical optical model,
– Hauser-Feshbach statistical model, and,
– Exciton pre-equilibrium model.
These three models sufficiently well describe the physics of nuclear reactions at neutron energies from 5 keV to 20 MeV for the entire set of nuclei. The spherical optical model takes care of the total cross sections and neutron elastic scattering, the Hauser-Feshbach statistical model describes the bulk of particle emissions, and the exciton pre-equilibrium model details major features of fast particle emission at higher incident energies.

To better describe the model parameters considered in our calculations, we briefly and simply outline the nuclear reaction models listed above. Then we discuss the model parameters and their uncertainties.

2.2.1. *Spherical optical model*

The optical model for nucleon-nucleus interaction is the starting ingredient in calculating cross sections. This model allows us to determine neutron elastic scattering as well as absorption cross sections and the transmission coefficients discussed later. The spherical optical model potential usually is defined as

$$\mathcal{U}(r,E) = -\mathcal{V}_v(r,E) - i\mathcal{W}_v(r,E) - i\mathcal{W}_s(r,E) + \mathcal{V}_{so}(r,E)\ell\cdot s + i\mathcal{W}_{so}(r,E)\ell\cdot s\,. \tag{10}$$

Here, all components are separated in E-dependent well depths and energy-independent radial parts according to

$$\begin{aligned}
\mathcal{V}_v &= V_v(E) f(r, R_v, a_v)\,,\\
\mathcal{W}_v &= W_v(E) f(r, R_v, a_v)\,,\\
\mathcal{W}_s &= -4a_s W_s(E) \frac{\mathrm{d}}{\mathrm{d}r} f(r, R_s, a_s)\,,\\
\mathcal{V}_{so} &= V_{so}(E) \left(\frac{\hbar}{m_\pi c}\right)^2 \frac{1}{r}\frac{\mathrm{d}}{\mathrm{d}r} f(r, R_{so}, a_{so})\,,\\
\mathcal{W}_{so} &= W_{so}(E) \left(\frac{\hbar}{m_\pi c}\right)^2 \frac{1}{r}\frac{\mathrm{d}}{\mathrm{d}r} f(r, R_{so}, a_{so})\,,
\end{aligned} \tag{11}$$

where the indices v, s, and so refer, respectively, to volume-central, surface-central, and spin-orbit potentials. The form-factor is given by the frequently used Woods-Saxon shape

$$f(r, R_i, a_i) = (1 + \exp[(r - R_i)/a_i])^{-1}, \qquad (12)$$

where the geometric parameters are the radius $R_i = r_i A^{1/3}$ and the diffuseness, a_i, with A being the atomic mass number.

2.2.2. *Hauser-Feshbach statistical model*

The decay of the compound nucleus is described in the framework of the formalism of Hauser-Feshbach statistical model, with many open channels contributing to the decay. Schematically, the cross section for a reaction (a,b) that proceeds through the compound nucleus (CN) mechanism can be written as

$$\sigma_{a,b} = \sigma_a \frac{\Gamma_b}{\sum_c \Gamma_c}. \qquad (13)$$

Here, σ_a is the absorption cross section, and the ratio expresses the chance of emitting particle b relative to all other reaction channels. For simplicity, we suppress the notation showing summation over the quantum numbers such as spin and parity, and integration over the energy. The decay width is given by

$$\Gamma_c = \int_0^{E-B_c} \frac{\rho_c(E')T_c(E - B_c - E')\mathrm{d}E'}{2\pi\rho_{\mathrm{CN}}(E)}, \qquad (14)$$

where B_c is the binding energy of particle c in the compound nucleus, ρ is the nuclear level density, and $T_c(\epsilon)$ represents the transmission coefficient for particle c having channel energy $\epsilon = E - B_c - E'$. Again, we dropped explicit reference to spin and parity. Since all evaluations extend up to 20 MeV, sequential multi-particle particle emissions had to be included in the Hauser-Feshbach calculations, which, in practice, implies an energy convolution of the multiple integrals of the type of Eq. (14).

EMPIRE offers several models describing nuclear level densities. We adopted the EMPIRE-specific approach [5] that uses the formalism of the super-fluid model below the critical excitation energy, and the Fermi gas model above this energy. The dominant term is

$$\rho(E) \propto a^{1/4} \exp\left(2\sqrt{\mathrm{const} \cdot a}\right), \qquad (15)$$

where the level density parameter, a, can be calculated from its asymptotic value, $\tilde{a}$, as

$$a = \tilde{a} \cdot [1 + f(U)\delta W/U]. \qquad (16)$$

The Eq. (16) accounts for the energy dependence of the level density parameter that results from the disappearance of the shell-correction δW with increasing excitation energy, as described by the f function.

2.2.3. *Exciton pre-equilibrium model*

In the exciton model, the composite nucleus follows a series of more and more complicated configurations wherein the excited states are characterized by the number of excited particles and holes (excitons) at each stage of the pre-equilibrium cascade. Restriction to two-body interactions leads to selection rules about the possible variation of the number of excitons during the cascade. The initial configuration is determined by the nature of the projectile. Assuming that the pre-equilibrium systems develops only in the direction of increasing exciton number, i.e., the "never-come-back" approximation, the convenient closed-form expression is obtained,

$$\frac{\mathrm{d}\sigma_{a,b}}{\mathrm{d}\epsilon} = \sigma_a \sum_{\substack{n \\ \Delta n=2}} \mathcal{D}_n \frac{W_b(n, \epsilon)}{W_{tot}(n) + \lambda^+(n)}, \qquad (17)$$

where $\mathcal{D}_n$ represents the depletion factor, $W_b(n, \epsilon)$ is the emission rate for particle b with the energy ϵ, and $W_{tot}(n)$ is the total emission rate. A somewhat simplified form of the internal transition rate reads

$$\lambda^+(n) = \frac{2\pi}{\hbar}|M|^2 g^3 E^2/(n + 1). \qquad (18)$$

Here, g is the single-particle level density, and $|M|^2$ is the average matrix element for the residual two-body interaction that often is parametrized through the nucleon mean-free path (mfp), as we adopted also in our work.

2.2.4. *Model parameters*

For the optical model, we used the recent parametrization based on Koning and Delaroche's [13] extensive analysis of spherical nuclei (or nearly spherical ones). The energy and mass dependencies of potential parameters that were employed by those authors are more flexible than those used in previous similar analyses. This feature engenders a reasonable description of total and elastic cross sections, as well as elastic angular distributions for spherical nuclei across the periodic table. The energy range extends well above 20 MeV that we adopted as the upper limit for the present work. In our calculations, we used results of Ref. [13] applying relative (multiplicative factor) perturbations to the final values of the major parameters (potential depths, radii, and diffusenesses) thereby preserving the original functional dependencies. Table 1 lists the varied optical model parameters, along with their respective uncertainties (3% or 5%), as determined by Koning from the Monte-Carlo analysis. We note that we have used the spherical optical model for all nuclei considered, including the deformed ones. Table 2

Table 1
Parameter uncertainties (in %) used in this work for the optical model: r - radius, a - diffuseness, V - real depth, W - imaginary depth. The subscripts, v, s, and w, respectively, denote real volume, real surface, and imaginary surface. The superscripts, $tg \equiv$ n + $\frac{A}{Z}$ and $np \equiv$ p + $\frac{A+1}{Z-1}$, refer to nucleon-nucleus interaction.

Δr_s^{tg}	Δr_v^{tg}	Δr_w^{tg}	ΔV_v^{tg}	ΔW_s^{tg}	ΔW_v^{tg}	Δa_s^{tg}	Δa_v^{tg}	ΔV_v^{np}	ΔW_s^{np}
3	3	3	3	5	5	3	3	3	3

lists the eight parameters relevant for the Hauser-Feshbach and the exciton model. This includes four nuclear level density parameters for the former and two single-particle level densities for the latter, each estimated to be known within 10%. The two remaining parameters, the γ-ray strength function and the mfp for the pre-equilibrium emission, are estimated to be known within 20%.

The Hauser-Feshbach statistical model is driven by nuclear level densities, and the estimated global uncertainties for the

Table 2
Parameter uncertainties (in %) used in this work for the Hauser-Feshbach and exciton models: $\tilde{a}$ - total level density, $\tilde{g}$ - single-particle level density, f_γ - gamma-ray strength functions, and mfp - nucleon mean-free path. The superscripts refer to $cn \equiv$ compound, $tg \equiv$ target, $n2n \equiv$ (n,2n) residue, $np \equiv$ (n,p) residue.

$\Delta\tilde{a}^{cn}$	$\Delta\tilde{a}^{tg}$	$\Delta\tilde{a}^{n2n}$	$\Delta\tilde{a}^{np}$	$\Delta\tilde{g}^{np}$	$\Delta\tilde{g}^{tg}$	Δf_γ	Δmfp
10	10	10	10	10	10	20	20

related parameters are based on a considerable experience accumulated while using EMPIRE code in neutron cross section evaluations for the ENDF/B-VII.0 library [3]. This experience also was employed to determine uncertainties for other model parameters. These estimates finally were validated by randomly comparing the calculated cross section uncertainties against the spread of experimental data; the correlations among model parameters were disregarded. This simplification is justified within the scope of this project, despite ignoring some well-known physical constraints (e.g., the anti-correlation between the radius (r_v) and the real depth (V_v) of the optical potential). Future work will quantify these correlations, and include them in the analysis.

2.3. *Cross section sensitivities*

We undertook cross section sensitivity calculations by considering the uncertainties for 18 model parameters that contribute most significantly to the major reaction cross sections. Thus, (n,el), which is composed of shape- and compound-elastic cross sections, exhibits sensitivity primarily to real optical model parameters. In the elastic reaction channel the sensitivity is dominated by the imaginary optical model parameters that determine creation of the compound nucleus. At the incident energies above about 10 MeV the pre-equilibrium emission starts to play a role and its strength, determined by the nucleon-mean free path, becomes important. For (n,2n) reactions the sensitivity to nuclear level density parameters is decisive. In capture, in addition to most of the above parameters, the sensitivities are driven by the gamma-ray strength function.

The uncertainties of model parameters, summarized in Tables 1 and 2, were adopted uniformly for all energies and all nuclei covered in the present work. These parameter uncertainties propagate into cross sections and define the diagonal matrix **P**. We note that model parameter sensitivities were studied already earlier [14] and were used to estimate uncertainties for some activation cross sections [15].

We quantify the effect of the perturbation of the model parameter p_j on the cross section via the relative quantity

$$\mathcal{S}(E_i, p_j) = \frac{\sigma^+(E_i, p_j) - \sigma^-(E_i, p_j)}{\sigma(E_i, \mathbf{p})}\,, \qquad (19)$$

where $\sigma(E_i, \mathbf{p})$ is the cross section calculated for the best (or default) set of parameters $\mathbf{p} = (p_1, \ldots, p_j, \ldots, p_q)$, while

$$\sigma^{\pm}(E_i, p_j) = \sigma(E_i; p_1, \ldots, p_j \pm \delta p_j, \ldots, p_q)$$

are the cross sections calculated with the value of the parameter p_j perturbed by its expected uncertainty δp_j. Then, the sensitivity matrix element $s_{i,j}$ is obtained as

$$s_{i,j} = \mathcal{S}(E_i, p_j)\frac{\sigma(E_i, \mathbf{p})}{2\,\delta p_j} \qquad (20)$$

that can be viewed as the measure of the cross section response to the physically sensible variation of the model parameter p_j.

The above sensitivity equations, adopted throughout the present paper, assume that the linearity approximation is valid. This appears to be fairly reasonable assumption. Recent comparison with Monte Carlo approach, which does not suffer from the non-linearity effects, demonstrated that a linear approximation holds well for majority of cases [16]. Though, one has to be careful and consider non-linearity effects when quality evaluations are performed for the limited amount of important materials.

As an example, we discuss neutron reactions on ^{89}Y. Fig. 2 shows the response of the (n,tot), (n,el), (n,abs), (n,n′), (n,γ), (n,2n), and (n,p) cross sections to the variation of the real depth (V_v^{tg}) of the optical potential for the target. There are remarkably different levels of sensitivity for various reactions, and strong energy dependencies. The sensitivities plotted in Fig. 2 are cumulative, and combine effects resulting from the incident (absorption) and outgoing (inelastic scattering) channels since both use the same optical potential. Figs. 3 and 4 depict individual contributions of the two channels. The salient effects that can be ascribed to the perturbation of V_v^{tg} are summarized below:

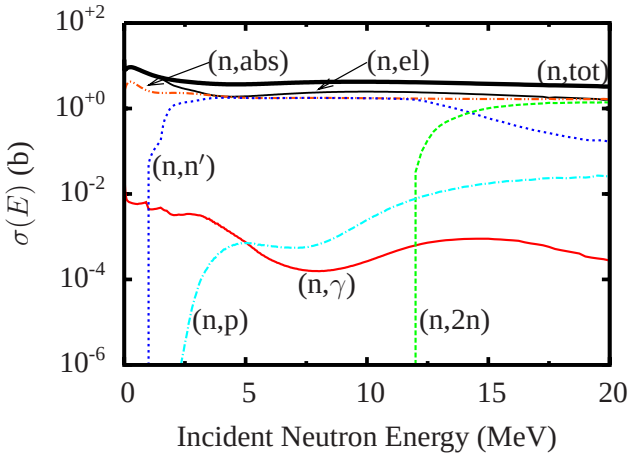

Figure 1. Calculated ^{89}Y+n cross sections for different reaction channels.

– The (n,γ) reaction channel exhibits high sensitivity; this is partially due to the very small cross sections (see Fig. 1) for neutron capture on ^{89}Y, which is a semi-magic nucleus (50 neutrons). Fig. 4 shows that the behavior of $\mathcal{S}(E, p)$ for (n,γ) reflects the competition of the inelastic scattering to the first excited states. These considerations can be extended to the (n,p) reaction, which essentially presents very similar behaviour.
– More detailed analysis shows that the dramatic sensitivity of absorption at energies below 2 MeV is due to the neutron p-wave strength function that rapidly changes with the strength of the real central potential.
– The outgoing (inelastic scattering) channel is responsible for the high sensitivities at the (n,n′), (n,p), and (n,2n) thresholds.

The incoming (absorption) channel seems only to affect the sensitivity for scattering to the first excited level in ^{89}Y.

– It is remarkable that Fig. 3 reveals the presence of nodes (around 4 and 11 MeV) at which points the sensitivities to the V_v^{tg} for all reaction channels converge.
– All sensitivities change sign several times between 0 and 20 MeV. The immediate consequence of this behavior is that at these zero-crossing points the real potential depth uncertainty (even if arbitrarily large) will not contribute to uncertainty in the cross section.

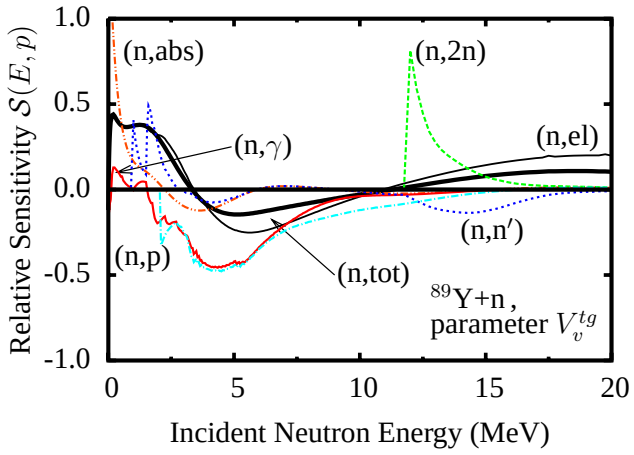

Figure 2. Relative sensitivity of the ^{89}Y+n cross sections to the $\pm 5\%$ perturbation of real depth (V_v^{tg}) optical model parameter for neutrons. Plotted sensitivities show cumulative effects resulting from the changes in the incident (absorption) and outgoing (inelastic scattering) channels.

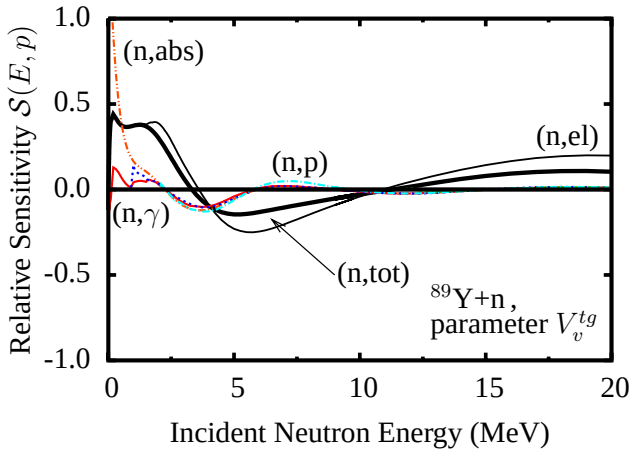

Figure 3. Relative sensitivity of the ^{89}Y+n cross sections to the $\pm 5\%$ perturbation of the real depth (V_v^{tg}) optical model parameter for neutrons resulting from the changes in the incident (absorption) channel.

Finally, Fig. 5 illustrates the response of neutron-radiative capture on ^{89}Y on the variation of the most important model parameters. Two fundamental nuclear reaction mechanisms are clearly evident. In the energy region below about 10 MeV, neutron capture is well described by the formation and decay of the compound nucleus. As expected, the nuclear level density parameters $\tilde{a}^{cn}$ and $\tilde{a}^{tg}$ play an important role, along with the depths of the real volume V_v^{tg} and imaginary surface W_s^{tg} components of the optical model potential. At higher energies, the

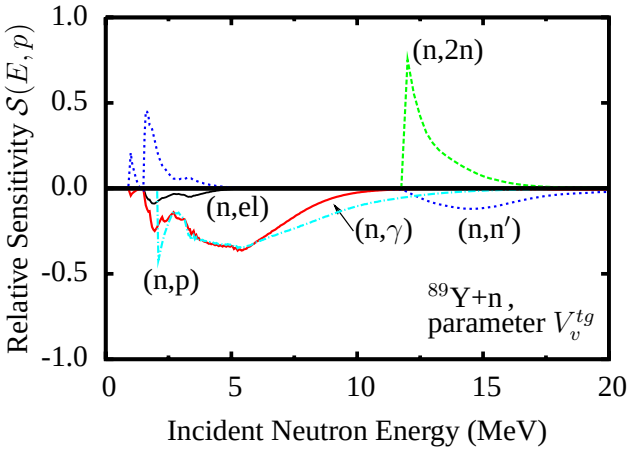

Figure 4. Relative sensitivity of the ^{89}Y+n cross sections to the $\pm 5\%$ perturbation of the real depth (V_v^{tg}) optical model parameter for neutrons resulting from the changes in the outgoing (inelastic scattering) channel.

pre-equilibrium emission mechanism dominates and the mfp parameter plays a major role. The effect of the radiative strength function is practically constant since f_γ enters both mechanisms as a multiplicative factor.

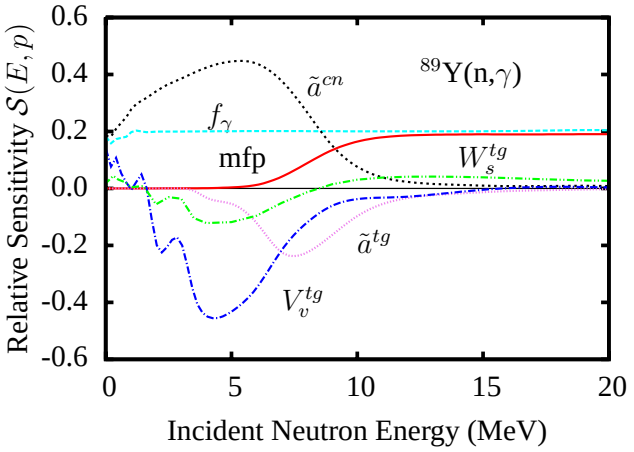

Figure 5. Relative sensitivity of the ^{89}Y(n,γ) cross section to $\pm$3-10% perturbation of the level density ($\tilde{a}^{tg}, \tilde{a}^{cn}$) and optical-model parameters (V_v^{tg}, W_s^{tg}), and to $\pm 20\%$ perturbations of the γ-ray strength function (f_γ) and the mfp in the pre-equilibrium model.

3. Calculations and discussion

3.1. *Calculations*

We calculated the neutron cross section covariances for 307 isotopes (see Table 3) at 30 incident energies between 5 keV and 20 MeV, considering the five reaction channels, total, elastic, inelastic, capture, and (n,2n). Altogether, 18 model parameters were varied. The results are fully based on model calculations and while experimental data were not taken into account, we occasionally consulted them to check the quality of our results. This approach is in line with the scope of the low-fidelity covariance project that aimed to produce consistently model-based estimates for an extensive set of covariances.

We note that cross-correlations were not considered, neither as the reaction-reaction correlations for a given material nor as the material-material correlations. This is widely considered to be a reasonable assumption. In general, users are not requesting cross-correlations except for a few important cases, where the cross-correlations do play a role. Thus, for major actinides the cross-correlation between fission and capture reaction channel is important as well as the material-material cross-correlation due to the ^{235}U(n,f) standard used in many measurements performed relative to this cross section.

We obtained covariances for all materials included in the new ENDF/B-VII.0 library, apart from actinides and light nuclei. The large set of 307 materials can be divided into three regions: structural materials, fission products, and heavy non-fissile nuclei (summarized in Table 3). Such distinction should guide in selecting nuclear reaction modeling and parametrization. Although the scope of this project did not allow such a level of complexity, it should be applied in future refinements of our results.

Table 3
List of 307 materials covered by BNL. It includes all materials from ^{19}F to ^{209}Bi in the neutron sub-library of ENDF/B-VII.0.

Materials	Nuclei	No. of isotopes
Structural	^{19}F - ^{nat}Zn *	57
Fission products	^{69}Ga - ^{170}Er	219
Heavy non-fissile nuclei	^{175}Lu - ^{209}Bi	31

3.2. *Discussion*

We first discuss a specific example, ^{56}Fe, for which detailed evaluations are available in several major evaluated data libraries. Then, we will proceed to a broader, yet very useful, view of the massive amount of data that we have produced.

3.2.1. *Example - ^{56}Fe*

We focus on the relative cross section uncertainties for ^{56}Fe+n, and start the discussion by showing our results. Then, we compare these findings with evaluations in the three major evaluated data libraries, ENDF/B-VI.8, JEFF-3.1, and JENDL-3.3.

Fig. 6 shows the relative uncertainties of the total cross section on ^{56}Fe. We note that the uncertainties tend to increase at low energies. In particular, we point to the presence of distinct minima in the uncertainties, i.e., the most striking features in Fig. 6. The latter structure is related to the oscillations in the cross sections that, in turn, result from the interference of the incident neutron wave traversing the nucleus with the wave which was scattered. This quantum-mechanical feature is naturally incorporated in the optical model. The widths and the positions of the cross section humps are directly related to the depth of the real potential well, and the nuclear radius.

* The ENDF/B-VII.0 library contains neutron cross sections for elemental Zn. Considering future needs for isotopic evaluations, we produced covariances for a full set of Zn isotopes, ^{64,66,67,68,70}Zn.

Fig. 6 also compares the calculated cross sections and uncertainties with the Harvey's [17] high-resolution experimental data. Due to the huge number of measurements in the EXFOR library, we avoided cluttering the plot by including only this data. The optical model only predicts a smooth, averaged behaviour, thus the comparison is meaningful only in the region lacking evident resonance-like structures. In the case of ^{56}Fe, such conditions are reached at relatively high energies, $\gtrsim$8 MeV. With this restriction in mind, the comparison is favorable and the predicted uncertainties apparently encompass the observed scatter of the experimental data. The calculated uncertainties probably are conservative (over-estimated) in line with the scope of this project. Fig. 7 graphs the relative uncertainties of neutron elastic scattering cross sections, along with

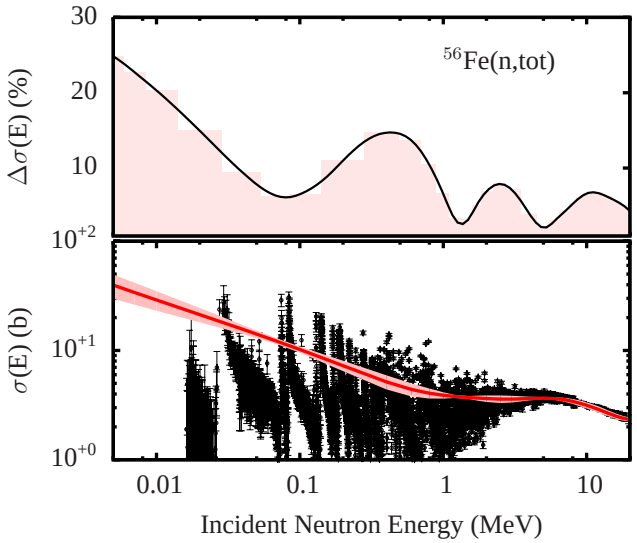

Figure 6. Relative uncertainties of ^{56}Fe(n,tot) cross sections obtained with the EMPIRE-KALMAN method. Also shown are cross sections compared with selected experimental data [17].

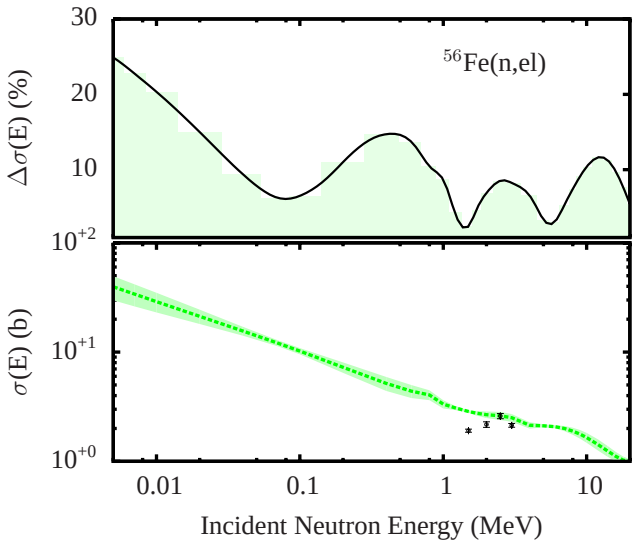

Figure 7. Relative uncertainties of ^{56}Fe(n,el) cross sections obtained with the EMPIRE-KALMAN method. Also shown are also cross sections compared with selected experimental data [18,19].

selected experimental data [18,19] above 1 MeV. Not unexpectedly, the uncertainties have the same oscillating structure as does the total cross section, since the same optical model governs both.

In Fig. 8, our results for the inelastic scattering are shown. The optical model oscillations still are seen although they much attenuated by the presence of the statistical mechanism that tends to wash-out the effect of wave interference in the absorption cross section. The uncertainties increase at the threshold region and at energies above 10 MeV, while at energies between 1 and 10 MeV they generally are lower than 10%. The uncer-

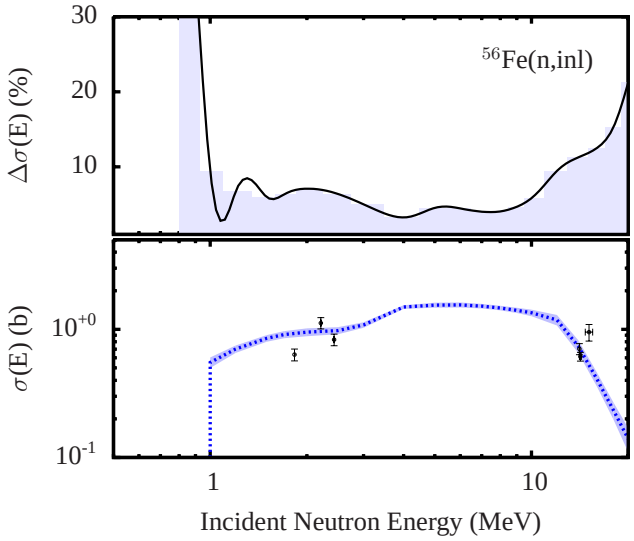

Figure 8. Relative uncertainties of ^{56}Fe(n,n′) cross sections obtained with the EMPIRE-KALMAN method. Also shown for reference are also cross sections and selected experimental data [20,21,22,23].

tainties of the (n,2n) reaction (Fig. 9) are essentially flat outside the threshold region. We note that the experimental cross sections fall within the calculated error band, and the optical-model's oscillations are not visible.

Fig. 10 summarizes the results for the capture cross sections by showing uncertainties as well as the calculated cross sections along with the experimental data. Certainly, the calculated capture cross sections cannot reproduce the experimental fluctuations observed in the high-resolution experiments below 0.1 MeV. Therefore, the uncertainty ($\gtrsim$20%) should be interpreted as an average over the broader energy range and not the point-wise form. As expected, uncertainties rise above 1 MeV.

Nuclear applications, including criticality safety, require neutron covariance matrices in the multi-group representation. These are just the averages of the point-wise covariance matrices, i.e., $\langle \delta\sigma(E)\,\delta\sigma(E')\rangle$, over union groups I, J,

$$\langle \delta\sigma_I\,\delta\sigma_J\rangle = \frac{\int_I\int_J \phi(E)\phi(E')\langle\delta\sigma(E)\,\delta\sigma(E')\rangle \mathrm{d}E\mathrm{d}E'}{\int_I\int_J \phi(E)\phi(E')\mathrm{d}E\mathrm{d}E'}\,, \quad (21)$$

where $\phi(E)$ is the flux "model" assumed for the multi-group calculations. It is useful to compare our model-based cross section uncertainties, e.g., for ^{56}Fe + n, with multi-group evalua-

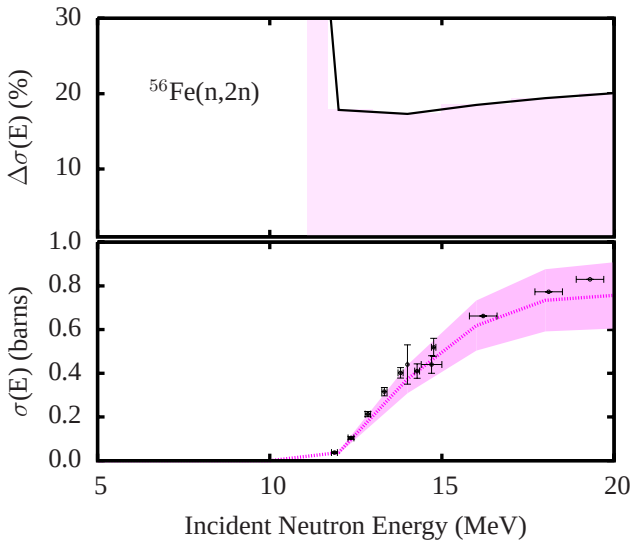

Figure 9. Relative uncertainties of ^{56}Fe(n,2n) cross sections obtained with the EMPIRE-KALMAN method. Also shown for reference are cross sections and selected experimental data [24,25,26].

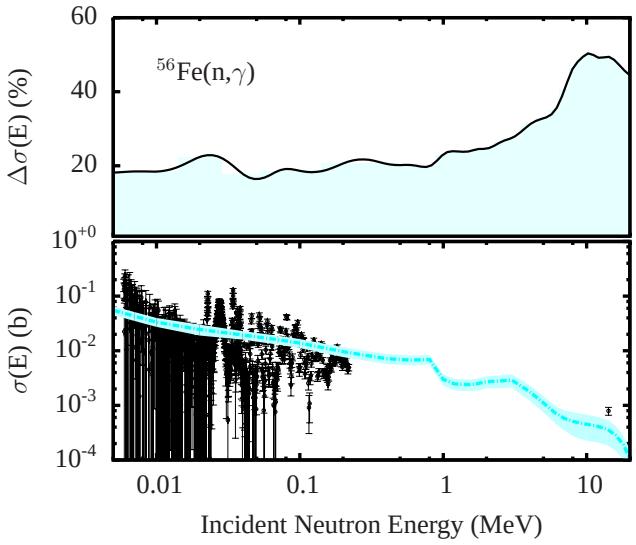

Figure 10. Relative uncertainties of ^{56}Fe(n,γ) cross sections obtained with the EMPIRE-KALMAN method. Also shown are cross sections and the high resolution experimental data [27,28,29].

tions undertaken for the three major nuclear data libraries. Our results are given in the point-wise form that includes 30 energy points above 5 keV. We extracted the results from the evaluated libraries with the Los Alamos code NJOY and processed them into a 44-energy group representation. We note that only a limited number of groups in this representation overlap with our energy range of 5 keV - 20 MeV. We also point out, that positive correlations decrease the multi-group uncertainties below the point-wise values.

Fig. 11 compares our results on ^{56}Fe(n,tot) cross section uncertainties with those in the ENDF/B-VI.8, JEFF-3.1, and JENDL-3.3 evaluations (the latter in the 44-energy group representation). As expected, our uncertainties are generally higher than the multi-group results from other libraries, particularly in the lower energy range. This discrepancy can easily be ex-

plained. First, contrary to the regular evaluations, our estimates do not explicitly use the experimental data and rely almost exclusively on model calculations employing global parameters. Sensitivity to the optical model parameters is particularly high

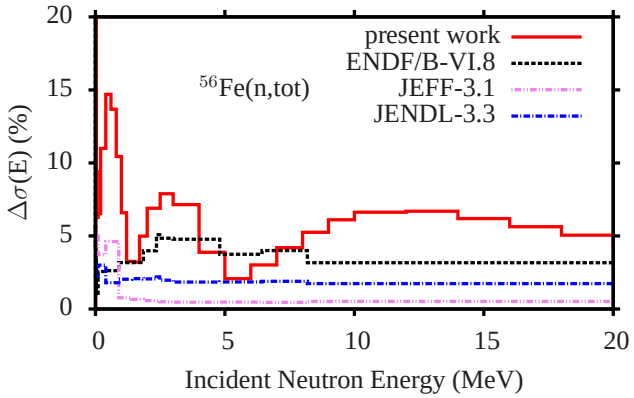

Figure 11. Relative uncertainties of ^{56}Fe(n,tot) cross sections compared to three major nuclear data libraries. The present results are in the point-wise form, while the other data are in the 44-energy group representation.

at low energies, and this translates into high cross section uncertainties. Accidentally, these higher uncertainties occur in the region where cross sections fluctuate due to resonance structure. Therefore, a big uncertainty is not unreasonable when ascribed to the smooth optical model's cross section that replaces fluctuating reality. On the other hand, true evaluations tend to reproduce experimental structure, and thus are much closer to the reality than optical model's predictions. This accounts for much lower uncertainties reported in the national libraries. Generally, uncertainties should be low whenever a wealth of experimental data are used in the evaluation.

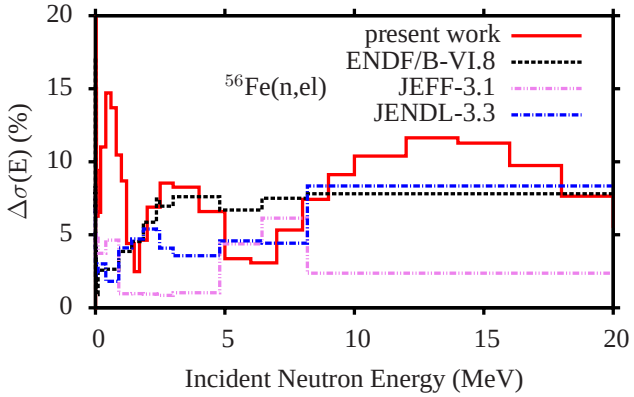

Figure 12. Relative uncertainties of ^{56}Fe(n,el) cross sections compared to three major nuclear data libraries. The present results are in the point-wise form, while the other data are in the 44-energy group representation.

Figs. 12 and 13 illustrate further comparisons between multi-group evaluations and our results. Except for the low energy region, our findings for elastic and inelastic scattering uncertainties agree reasonably with other evaluations. In contrast, uncertainties for the (n,2n) reaction channel are strongly overestimated throughout the whole energy range (Fig. 14). This simply reflects the fact that the extensive experimental information on the ^{56}Fe(n,2n) reaction, which drove other evaluations,

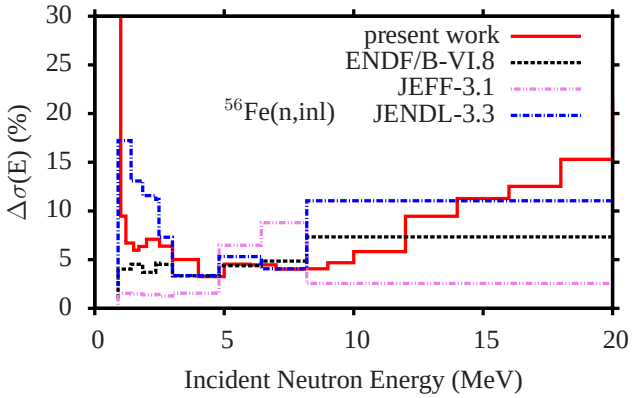

Figure 13. Relative uncertainties of ^{56}Fe(n,n′) cross sections compared to three major nuclear data libraries. The present results are in the point-wise form, while the other data are in the 44-energy group representation.

was totally ignored in our estimates. We reiterate that the basic aim underlying out the present work was to provide a complete set of approximate covariances derived from the global nuclear-model calculations. Finally, in Fig. 15 we compare cross sec-

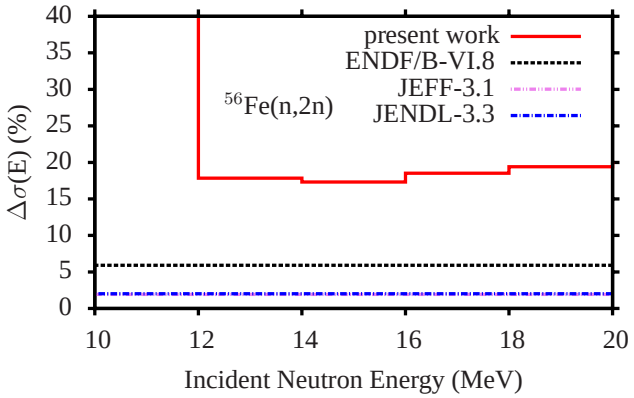

Figure 14. Relative uncertainties of ^{56}Fe(n,2n) cross sections compared to three major nuclear data libraries. The present results are in the point-wise form, while the other data are in the 44-energy group representation.

tion uncertainties for the ^{56}Fe(n,γ) reaction. The results are in acceptable agreement in view of the multi-group representation. In particular, we noted the same energy behavior as in the JENDL-3.3 library. This confirms our previous finding of reasonable agreement between our evaluations and that of others whenever little experimental evidence is available for analysis.

3.2.2. *Materials from ^{19}F to ^{209}Bi*

To present the overall picture of our results, we plotted contours in a single figure of the full set of nuclei over the entire range of incident energies studied. These plots show relative cross section uncertainties represented by different colors, from 0% shown in black to 100% shown in yellow. Using these plots, we depict in Figs. 16-20 the relative cross section uncertainties for the major reaction channels. The x- and y-axes refer, respectively, to the mass numbers of the complete list of 307 materials, and to all incident neutron energies.

Figs. 16 and 17 show total and neutron elastic scattering channels. For both, exceptionally high uncertainties are found

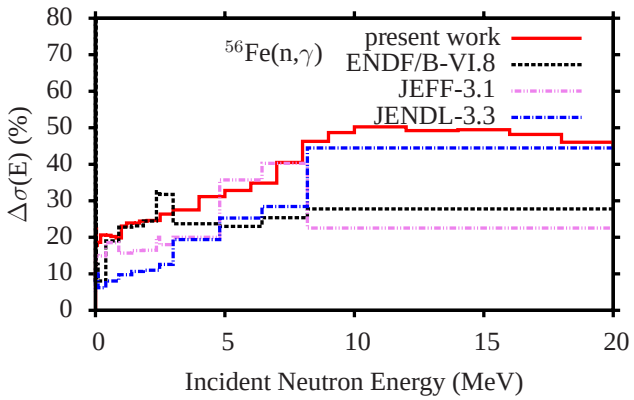

Figure 15. Relative uncertainties of ^{56}Fe(n,γ) cross sections compared to three major nuclear data libraries. The present results are in the point-wise form, while the other data are in the 44-energy group representation.

for nuclei between Xe and Eu at incident energies below 100 keV. This effect might be traced to the structure observed in the s- and/or d-wave neutron strength functions. For these two reaction channels, we also note very similar patterns characterized by regions where the uncertainties are particularly small. These intriguing structures are derived from the position of the minima discussed in the case of ^{56}Fe (see Figs. 6 and 7).

In Fig. 18, we summarize the neutron inelastic scattering by providing a contour plot for the complete list of materials. Inelastic scattering is the threshold reaction; hence, black color at below thresholds reflects perfect knowledge of the zero cross section. Some deviations from this pattern can be explained by metastable targets wherein the threshold for inelastic scattering is zero. At intermediate energies some structure is observed, while, at the highest energies, as the cross sections decline, the model's predictions become poor (shown as yellow areas).

Fig. 19 exhibits the cross section uncertainties for the (n,2n) reactions. The relative uncertainties basically are flat, but we note an isotopic effect represented on the plot by vertical lines of different intensities.

Fig. 20 summarizes the uncertainties for the neutron capture cross sections. Relatively good precision is achieved at lower energies, but the uncertainties increase with the incident neutron energy. Above 10 MeV, capture cross sections represent such tiny fraction of the absorption that the model-predicted uncertainties exceed 50%. We stress that this result is due only to the propagation of uncertainties in the model parameters and does not include numerical (rounding) errors. The latter supposedly are not a major issue for capture reactions below 20 MeV, but are known to create problems in the (n,α) reactions close to thresholds.

3.2.3. *Limitations of the covariance estimates*

The global approach adopted in the present work, which turned out to be so important for mass production of covariance estimates, has its natural limitations. First, we used the uniform definition of the fast neutron region and performed estimates for energies above 5 keV assuming that this suitably represents both the unresolved resonance region and the fast neutron region for each nucleus. Second, we used a simplified set of nuclear reaction models to describe cross sections above 5 keV. Third, we adopted uniform model parameter uncertainties for all energies and all nuclei. Fourth, we almost entirely ignored experimental cross section data, assuming that the default set of EMPIRE parameters already describes most of the cross sections well. These assumptions represent an obvious simplification and hence an obvious limitation in our covariance estimates. Clearly, in future, one should make a step forward and consider several regional sets of models, several regional sets of parameterization and perform at least basic comparison with experimental data. In view of these simplifications, our covariances should not be associated with the official U.S. evaluated library ENDF/B-VII.0, which strives to keep its high reputation of including quality data only.

An obvious request for comparison with other covariance libraries cannot be satisfied in vast majority of cases. The reason is that such libraries do not exist. Major evaluated nuclear reaction data libraries contain very limited amount of covariance data. For example, the new US library ENDF/B-VII.0, released in 2006, has complete covariance data for only 13 out of 393 materials. However, these data were obtained by more sophisticated methods, the most important difference being in due consideration of nuclear properties of each material and in due inclusion of experimental data.

Despite the above limitations, it should be noted that our results are already finding use in practical applications that go beyond the original scope of the low-fidelity project (development and testing of computational tools for nuclear criticality safety). The most striking example is the well-known ORNL reactor licensing code SCALE-6 [30]. Its latest release [31] adopted the covariance estimates for more than 200 nuclei reported in the present work, supplemented with ORNL low-fidelity estimates for energies below 5 keV. These combined low-fidelity data serve as welcome addition to covariance data adopted by SCALE-6 from major evaluated data libraries for a small number of the most important materials. Even though our covariance results represent simple estimates, SCALE-6 validation indicates that they are useful provided the related materials do not play dominant role in the system under consideration.

4. Conclusions and outlook

We applied the EMPIRE-KALMAN method to produce a simple, yet consistent set of estimates of fast neutron covariance for 307 materials, from ^{19}F to ^{209}Bi, included in the ENDF/B-VII.0 library. Our results are based on model calculations and depend on the assumed uncertainties of the model parameters.

Experimental data were used only globally and approximately to ensure that our calculated cross section uncertainties were reasonable in comparison to the spread of the measurements. We used the same global set of model parameters and their related uncertainties for all 307 nuclides. The calculated cross sections and their uncertainties often deviate from the evaluated ones derived from experimental data. This is the limitation of our global approach. Hence, our covariances should not be associated with the ENDF/B-VII.0 library.

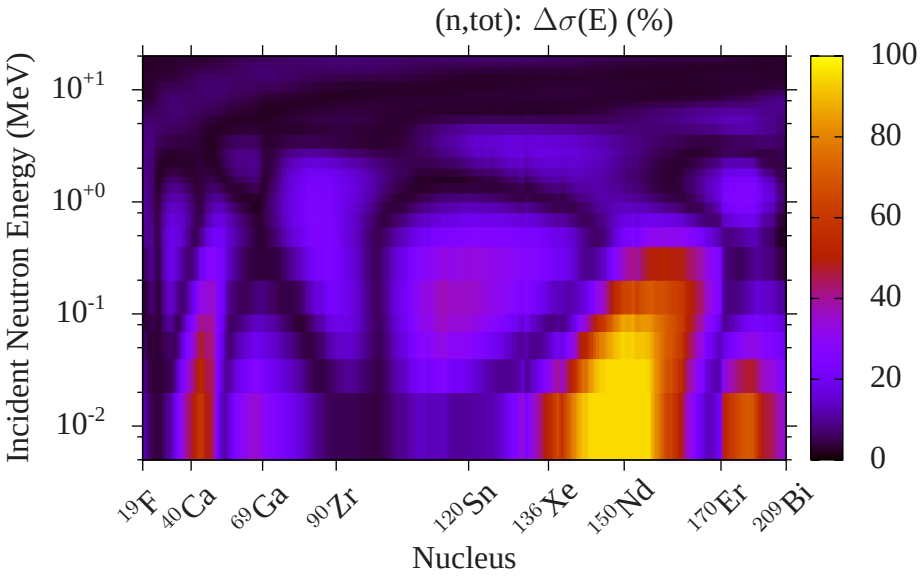

Figure 16. Relative uncertainties for the total cross sections on 307 materials obtained with the EMPIRE-KALMAN method in the fast neutron energy region.

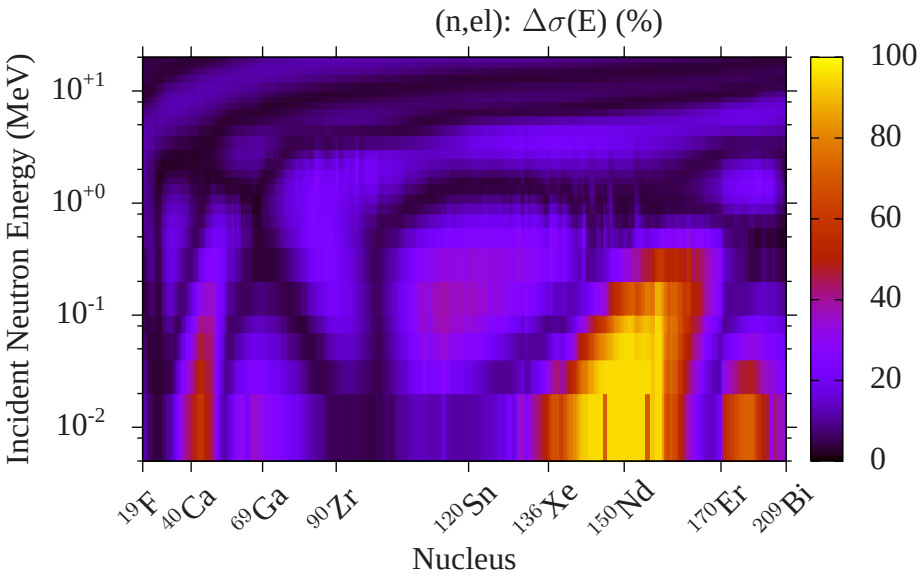

Figure 17. Relative uncertainties for the elastic cross sections on 307 materials obtained with the EMPIRE-KALMAN method in the fast neutron energy region.

The present results confirm previous notions about the structure of the uncertainties plotted as a function of incident energy and mass number (atomic number dependence also might be possible). In particular, we note very similar patterns observed in the total and elastic channels. A reflection of these patterns also is found in the inelastic channel. The (n,2n) and capture channels do not seem to be affected by the structure seen in the total and elastic channels. Instead, they display short-range fluctuations as a function of mass number. High and low uncertainties alternately produce vertical lines on the plots. Since all nuclei were treated on the same footing using the same set of models and default set of parameters, it should be possible to explain the patterns in terms of the physics underlying our calculations. For example, the structure showing up in the total and elastic channels arises from the optical model, and we understand the origin of deep minima in the cross section uncertainties at certain energies. Mass dependence of the energies at which these minima occur is most likely responsible for creating the characteristic patterns in Figs. 16 and 17.

In the future, we intend to address the intriguing structure observed in cross section uncertainties and determine its physical background. Initial results already are available [32].

We consider that our results can be used as a useful starting point for any future work in producing neutron cross section covariances. Such an effort would be a step forward in using more refined modeling, e.g., local parametrization rather than that of a global model, and more explicit use of experimental data.

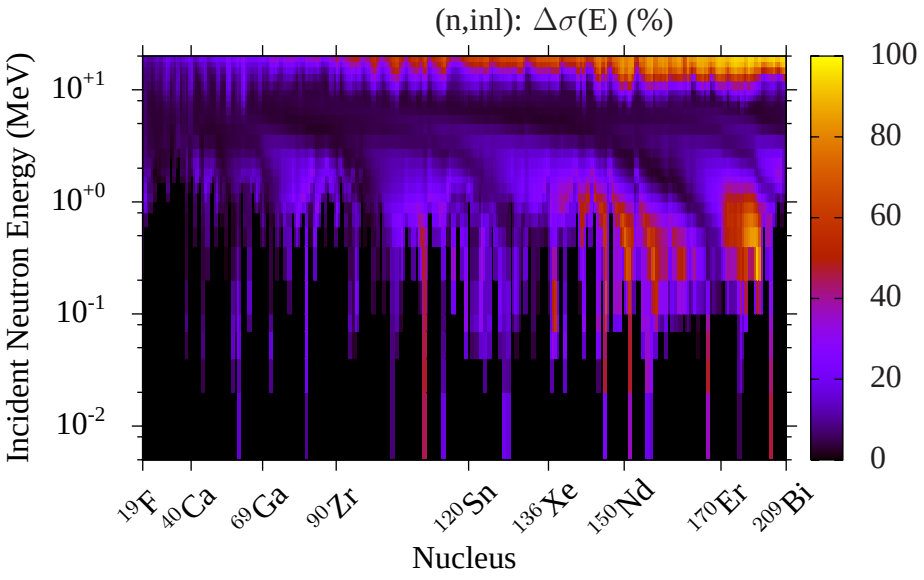

Figure 18. Relative uncertainties for the inelastic cross sections on 307 materials obtained with the EMPIRE-KALMAN method in the fast neutron energy region.

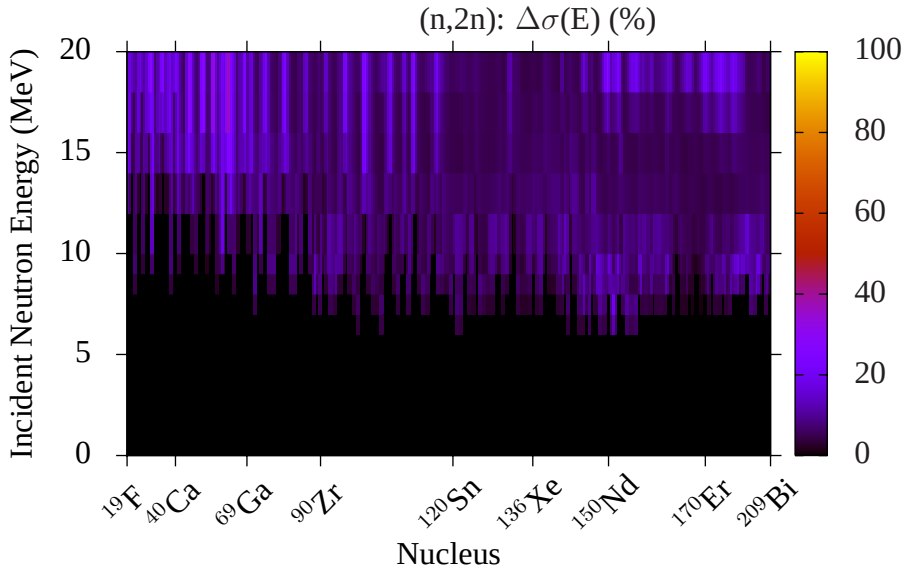

Figure 19. Relative uncertainties for the (n,2n) cross sections on 307 materials obtained with the EMPIRE-KALMAN method in the fast neutron energy region.

Acknowledgments

The authors thank R.C. Little and T. Kawano (LANL), M.E. Dunn and M.L. Williams (ORNL), and R.D. McKnight (ANL) for stimulating discussions and collaboration in this project. We owe special thanks to D.L. Smith (ANL) for his valuable comments. We gratefully acknowledge A. Woodhead, A. Leskovjan, and M. Blennau in reviewing this paper.

The present work was supported by the DOE-NNSA within the Nuclear Criticality Safety Program and this support is gratefully acknowledged. The National Nuclear Data Center is sponsored by the Office of Nuclear Physics, Office of Science of the U.S. Department of Energy under contract No. DE-AC02-98CH10886 with Brookhaven Science Associates, LLC.

References

[1] D. W. MUIR, "Judging the Reliability of Predictions Based on ENDF," *Cross Section Evaluation Working Group (CSEWG)*, Upton, November 4-6, 2007 (available at http://www.nndc.bnl.gov/proceedings/2007csewgusndp/).

[2] M. SALVATORES, G. ALIBERTI, M. DUNN, et al., "Uncertainty and Target Accuracy Assessment for Innovative Systems Using Recent Covariance Data Evaluations," Report NEA/WPEC-26, Nuclear Energy Agency, Paris 2008 (in print).

[3] M. B. CHADWICK, P. OBLOŽINSKÝ, M. HERMAN, et al., "Next Generation Evaluated Nuclear Data Library for Nuclear Science and Technology," *Nuclear Data Sheets*, **107**, 2931 (2006).

[4] M. SALVATORES, et al., Data Adjustment for GNEP, Global Nuclear Energy Partnership, unpublished (2007).

[5] M. HERMAN, R. CAPOTE, B. V. CARLSON, et al., "EMPIRE: Nuclear Reaction Model Code System for Data Evaluation," *Nuclear Data Sheets*, **108**, 2655 (2007).

[6] T. KAWANO AND K. SHIBATA, "Covariance Evaluation System [in

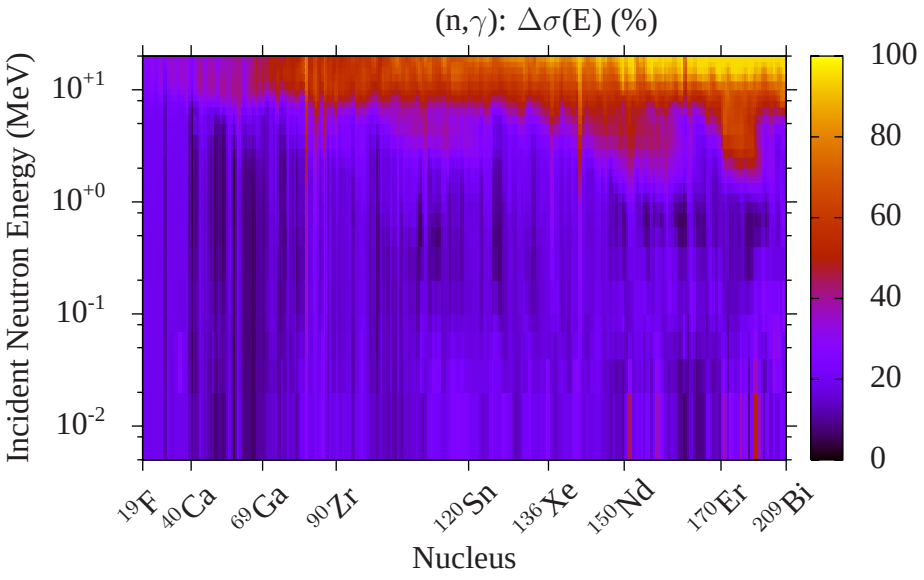

Figure 20. Relative uncertainties for the capture cross sections on 307 materials obtained with EMPIRE-KALMAN method in the fast neutron energy region.

Japanese]," Lab. report JAERI-Data/Code 97-037, Japan Atomic Energy Research Institute (1997).

[7] M. T. PIGNI, M. HERMAN, P. OBLOŽINSKÝ, et al., "Low-Fidelity Cross Sections Covariances for 219 Fission Products in the Fast Neutron Region," Lab. report BNL-79261-2007-IR, Brookhaven National Laboratory (2007).

[8] M. T. PIGNI, M. HERMAN, P. OBLOŽINSKÝ, et al., "Extensive Set of Low-Fidelity Covariances in Fast Neutron region," *8th International Meeting on Nuclear Applications of Accelerator Technology*, Pocatello, USA, July 29 - August 2, 2007. Proceedings, American Nuclear Society, LaGrange Park 2007, p. 753 (2007).

[9] M. T. PIGNI, M. HERMAN, P. OBLOŽINSKÝ, "Low-Fidelity Covariances for Neutron Cross Sections on 57 Structural and 31 Heavy Nuclei in Fast Region," Lab. report BNL-79985-2007-IR, Brookhaven National Laboratory (2008).

[10] M. L. WILLIAMS, B. L. BROADHEAD, M. E. DUNN, et al., "Approximate Techniques for Representing Nuclear Data Uncertainties," *8th International Meeting on Nuclear Applications of Accelerator Technology*, Pocatello, USA, July 29 - August 2, 2007. Proceedings, American Nuclear Society, LaGrange Park 2007, p. 744 (2007).

[11] M. T. PIGNI, M. HERMAN, P. OBLOŽINSKÝ, et al., "The Nuclear Criticality Safety Program "Low-Fidelity" Covariance Project," *Workshop on Neutron Cross Section Covariances*, Port Jefferson, USA, June 24-27, 2008 (to be published in Nuclear Data Sheets).

[12] T. BELGYA, O. BERSILLON, R. CAPOTE, et al., "Handbook for Calculations of Nuclear Reaction Data, Reference Input Parameter Library-2," Technical report IAEA-TECDOC-1506, International Atomic Energy Agency (2006).

[13] A. J. KONING AND J. P. DELAROCHE, "Local and Global Nucleon Optical Model from 1 keV to 200 MeV," *Nucl. Phys. A*, **713**, 231 (2003).

[14] A. FESSLER AND D. L. SMITH, "Parameter Sensitivities in Nuclear Reaction Cross-Section Calculations," *Ann. Nucl. Energy*, **29**, 363 (2002).

[15] A. J. PLOMPLEN et al., Neutron Activation Cross-Section Measurements from Threshold to 20 MeV for the Validation of Nuclear Models and their Parameters, Report NEA/WPEC-19, OECD, Paris (2005).

[16] M. HERMAN et al., Covariance Data in the Fast Neutron Region, Subgroup 24 Report to the WPEC Meeting, Tokai, June 5-6 2008 (unpublished).

[17] C. M. PEREY, F. G. PEREY, J. A. HARVEY, et al., "^{56}Fe and ^{60}Ni Resonance Parameters," *International Conference on Nuclear Data for Science and Technology*, Jülich, Germany, 13-17 May, 1991.

[18] I. A. KORZH, V. A. MISHCHENKO, E. N. MOZHZHUKHIN, et al., "Differential Scattering Cross Sections of 1.5-3.0 MeV Neutrons for Ti, Fe and Bi," *Ukr. Fiz. Zh.*, **22**, 87 (1977).

[19] O. A. SHCHERBAKOV, A. I. STUPAK, A. N. GLUKHOVEC, "Slow Neutron Total and Radiative Capture Cross-Section of ^{56}Fe," *Yadernye Konstanty*, **25**, 51 (1977).

[20] B. JOENSSON, K. NYBERG, I. BERGQVIST, "High Resolution Measurements of Gamma Rays Produced by 15 MeV Neutrons," *Ark. Fys.*, **39**, 295 (1969).

[21] S. P SIMAKOV, A. A ANDROSENKO, P. A. ANDROSENKO, et al., "14-MeV Facility and Research in IPPE," *Vop. At. Nauki i Tekhn., Ser. Yadernye Konstanty*, **4**, 93 (1992).

[22] SHI XIAMIN, SHEN RONGLIN, XING JINJIANG, et al., "Measurements of the Induced Gamma Ray Cross Sections by 14.2 MeV Neutrons with Fe, Ni, Cu," *Chin. J. Nucl. Phys.*, **4**, 120 (1982).

[23] T. W. BARROWS JR, "A Study of the (n,n$'\gamma$) Reactions in ^{51}V and ^{55}Mn and the Reaction ^{19}F(d,n)^{20}Ne," Ph.D. thesis, University of Kentucky (1965).

[24] J. FREHAUT AND G. MOSINSKI, "Measurement of the (n,2n) Cross-Sections for ^{56}Fe, ^{59}Co, ^{89}Y, ^{169}Tm, ^{175}Lu, ^{181}Ta, ^{197}Au, ^{209}Bi, ^{238}U and of the (n,3n) Cross-Section for ^{238}U from Threshold to 15 MeV Incident Neutron Energy," Technical report CEA-R-4627, Commissariat à l'Énergie Atomique (1974).

[25] V. CORCALCIUC, B. HOLMQVIST, A. MARCINKOWSKI, et al.,"A Study of the Neutron Induced Reactions for ^{19}F, ^{56}Fe,^{59}Co in the Energy Interval 16 to 22 MeV," *Nucl. Phys. A*, **307**, 445 (1978).

[26] S. M. QAIM, N. I. MOLLA, "A Systematic Study of (n,p) Reactions at 14.7 MeV," *Nucl. Phys. A*, **283**, 269 (1977).

[27] R. L. MACKLIN, P. J. PASMA, AND J.H. GIBBONS, "Resonance Neutron Capture and Transmission in Sulfur, Iron, and Lead," *Phys. Rev.*, **136**(3B) B695 (1964).

[28] A. ERNST, F. H. FRÖHNER, AND D. KOMPE, "High Resolution Measurements of Radiative Neutron Capture in ^{47}Ti, ^{56}Fe, ^{58}Ni, ^{60}Ni and ^{61}Ni between 7 and 200 keV," *2nd International Conference on Nuclear Data for Reactors*, Helsinki, Finland, June 1970.

[29] HUANG ZHENG-DE, CAO ZHONG, WANG HUI-ZHU, et al., "Radiative Capture of 14.2 MeV Neutron by ^{56}Fe and ^{238}U," Conference report LBL-11118, Lawrence Berkeley Laboratory (1980).

[30] "SCALE: a Modular Code System for Performing Standardized Computer Analysis for Licensing Evaluation," Report NUREG/CR-0200, Rev. 6 (ORNL/NUREG/CSD-2/R6), Vols. I, II, and III, May 2000.

[31] M. WILLIAMS AND B. REARDEN, "SCALE-6 Sensitivity/Uncertainty Methods and Covariance Data," *Workshop on Neutron Cross Section Covariances*, Port Jefferson, USA, June 24-27, 2008 (to be published in Nuclear Data Sheets).

[32] M. T. PIGNI, F. S. DIETRICH, M. HERMAN, et al., “Can Cross Sections be Accurately Known a Priori?,” *Workshop on Neutron Cross Section Covariances*, Port Jefferson, USA, June 24-27, 2008 (to be published in Nuclear Data Sheets).

Appendix F

Processing Covariances

Processing Neutron Cross Section Covariances using NJOY-99 and PUFF-IV

R. Arcilla,[1*] A.C. Kahler,[2] P. Obložinský[1], M. Herman[1]
[1] *National Nuclear Data Center, Brookhaven National Laboratory, Upton, NY 11973-5000 and*
[2] *Nuclear Physics Group (T-16), Theoretical Division,*
Los Alamos National Laboratory, Los Alamos, NM 87545
(Dated: September 26, 2008)

With the growing demand for multigroup covariances, the National Nuclear Data Center (NNDC) has been experiencing an upsurge in its covariance data processing activities using the two US codes NJOY-99 (LANL) and PUFF-IV (ORNL). The code NJOY-99 was upgraded by incorporating the new module ERRORJ-2.3, while the NNDC served as the active user and provided feedback. The NNDC has been primarily processing neutron cross section covariances on its 64-bit Linux cluster in support of two DOE programs, the Global Nuclear Energy Partnership (GNEP) and the Nuclear Criticality Safety Program (NCSP). For GNEP, the NNDC used NJOY-99.259 to generate multigroup covariance matrices of ^{56}Fe, ^{23}Na, ^{239}Pu, ^{235}U and ^{238}U from the JENDL-3.3 library using the 15-, 33-, and 230-energy group structures. These covariance matrices will be used to test a new collapsing algorithm which will subsequently be employed to calculate uncertainties on integral parameters in different fast neutron-based systems. For NCSP, we used PUFF-IV 1.0.4 to verify the processability of new evaluated covariance data of ^{55}Mn, ^{239}Pu, ^{233}U, ^{235}U and ^{238}U generated by a collaboration of ORNL and LANL. For the data end-users at large, the NNDC has made available a Web site which provides a static visualization interface for all materials with covariance data in the four major data libraries: ENDF/B-VI.8 (47 materials), ENDF/B-VII.0 (26 materials), JEFF-3.1 (37 materials) and JENDL-3.3 (20 materials).

I. INTRODUCTION

The nuclear data community has seen renewed interest in neutron cross section covariances in recent years. This has been largely driven by DOE-initiated programs such as the Nuclear Criticality Safety Program (NCSP), Global Nuclear Energy Partnership (GNEP), Generation IV (Gen-IV) reactor systems studies and the Advanced Fuel Cycle Initiative (AFCI). In these programs, the urgent and compelling need to reduce uncertainties in the nuclear data being used to meet target accuracies cannot be overemphasized. This revival already resulted in improved methodology for the generation of covariance data, mostly as a consequence of the utilization of advanced nuclear modeling and information merging techniques, followed by sample covariance evaluations for the new US library ENDF/B-VII.0 [1].

In the GNEP initiative, availability of covariances is crucial to the generation of a multigroup adjusted library, using a statistical adjustment method, to be used in advanced fast reactor design calculations. Emphasis is on fast, metal-cooled actinide burner reactors which would address GNEP non-proliferation objectives and also produce energy from recycled nuclear fuel.

In the NCSP, computational tools are being developed and tested, requiring an extensive amount of covariance data for all materials in the evaluated data libraries. BNL through NNDC is a member of a network of national laboratories mandated to produce nuclear data covariances which will meet the needs of criticality safety applications. In addition, NNDC serves as the linchpin for the NCSP nuclear data efforts at the other three national laboratories: LANL, ORNL and ANL.

The ENDF covariance files contain covariances of energy-dependent cross sections, as well as the covariances of resolved resonance parameters. On the other hand, end-users working in neutron-based applications usually require the covariances of multigroup-averaged cross sections, as input, for example, to sensitivity and uncertainty calculations. It is the job of processing codes to generate the required multigroup information from the energy-dependent data in the ENDF files. Advances in the processing codes and computer technology have placed in the hands of nuclear data centers, evaluators and end-users alike the unprecedented capability to generate multigroup-averaged covariances for use in neutron-based applications. This combination of factors has contributed to the upsurge in covariance processing activities in recent years.

In the succeeding sections, we will first describe the advances in the two US covariance processing codes, NJOY-99 and PUFF-IV. Then, we will discuss our results and experience in using these codes. We note that the NNDC is probably the only laboratory actively using both codes for covariance processing and thus in the best position to provide considerable feedback to code developers.

II. ADVANCES IN THE PROCESSING CODES

A. LANL code NJOY-99

For many years, the LANL code NJOY-99 [2] has had the capability to process ENDF covariance data from File

*Electronic address: arcilla@bnl.gov

31 (nubars) and File 33 (cross sections) with the ERRORR module, including limited capabilities to process File 32 (resonance parameters). Recently this module was extracted from NJOY, and an improved version, ERRORJ, was created by Go Chiba, JAEA [3]. ERRORJ expanded upon ERRORR to include processing of resolved resonance parameters in the Reich-Moore formalism (File 32), angular distribution (File 34) and energy spectra (File 35) covariance data.

A preliminary merge of ERRORJ-2.3 into NJOY-99 was performed in 2006 prior to the release of ENDF/B-VII.0. More recently, NJOY-99.259 with fully incorporated ERRORJ-2.3 was officially released to the user community.

A suite of five test problems were executed to verify that ERRORJ was correctly merged into NJOY-99. Two of these problems are from the historical NJOY test suite available at http://t2.lanl.gov/codes/NJOY-99/index.html. The first of these test problems processes ENDF/B-V ^{235}U File 31 and File 33 data. The second problem processes ENDF/B-V ^{nat}C File 33 data, including execution of the COVR and VIEWR modules to produce covariance plots. The output files generated by NJOY-99.259 were identical to those produced by earlier NJOY-99 versions that contain the original ERRORR module.

In addition, three new test problems were developed by Go Chiba. These require processing of various JENDL-3.3 neutron files. The first problem processes covariance data from ^{238}U Files 31, 33, 34 and 35. This job follows the usual sequence of producing Doppler broadened pointwise data with the RECONR and BROADR modules. These data are then group averaged with GROUPR prior to executing the ERRORJ module. The second new test problem only uses RECONR and BROADR before executing ERRORJ, thereby testing the capability to produce the necessary group average data to then process Files 31 and 33. Again, the JENDL-3.3 ^{238}U file provides the basic nuclear data input. The final new test job processes the three major actinides, ^{235,238}U and ^{239}Pu. Pointwise, room temperature data are created using the RECONR and BROADR modules which is subsequently group-averaged with GROUPR. The three GROUPR output files are merged onto a single tape with MODER and ERRORJ is executed to process file ^{238}U including cross material covariances for MT18 (the fission cross section) with ^{235}U and ^{239}Pu. The output files created by NJOY-99.259 agreed well with those provided by Go Chiba with only occasional differences observed in the least significant digit of various output quantities.

Additional visualization capability for covariance matrix data is still required. Covariance matrices developed from Files 31 and 33 only may be visualized using the COVR and VIEWR modules; a limitation consistent with the processing capability of the original ERRORR module. Visualization of File 34 and File 35 derived matrices remains a future option.

B. ORNL code PUFF-IV

In early 2006, PUFF-III had only limited capabilities to process the resonance parameter covariance data (File 32) of the new ENDF/B-VII.0 library. To address this deficiency, ORNL completely rewrote PUFF-III in Fortran 90 and released PUFF-IV which has the built-in capability to fully process ENDF/B-VII.0 File 32 data in the resonance region. This made PUFF-IV the only code at the time which could handle both the Reich-Moore ENDF-6 format for resolved resonance parameters and the new ENDF-6 "compact" covariance format.

An important new feature in PUFF-IV is the capability to process ENDF data files which do not contain File 33. PUFF-IV will automatically recognize which covariance data (File 31, 32, and/or 33) are present and process them according to user input specifications.

We note that while NJOY-99 uses numerical methods for calculating resonance sensitivities, the PUFF-IV code uses analytical methods. These sensitivities are needed to determine cross section uncertainties and correlations.

In early 2007, ORNL released an upgrade for PUFF-IV from 1.0.3 to 1.0.4. Among the many improvements was the resolution of the "step-size underflow" problem which would lead to the generation of "0.0" cross sections in cases wherein the user supplied an energy group structure having boundaries not monotonically increasing.

In April 2007, new ORNL-LANL covariance evaluations of ^{233,235,238}U and ^{239}Pu were released to the nuclear data community for testing. These evaluations were stored in huge data files due to their large resonance parameter covariance matrices which required unprecedented amount of PUFF-IV processing time. To address this issue, ORNL overhauled PUFF-IV's matrix multiplication modules to take advantage of the efficiencies in the Basic Linear Algebra Subprograms (BLAS) routines when available on a computing system. As a result, significant reduction in processing time was achieved as reported by D. Wiarda [4]. However, the latest version has not yet been released for distribution through RSICC.

To date, PUFF-IV still cannot process the covariances of angular and energy distributions of secondary neutrons (File 34 and File 35) as well as covariance data for the production of radioactive nuclei (File 40) [5].

III. PROCESSING COVARIANCES FOR GNEP

As part of the data adjustment project, the GNEP core group headquartered in Idaho National Laboratory has been conducting rigorous testing on the validity of a new algorithm which allows collapsing an integral parameter's fine-group (reference) covariance data to a coarse group while preserving the uncertainty calculated in the fine group structure. For the integral parameters to be used in the investigation, they used: 1) the neutron multiplication factor (k_{eff}) in different fast neutron systems with different fuels, coolants and reactivity coefficients,

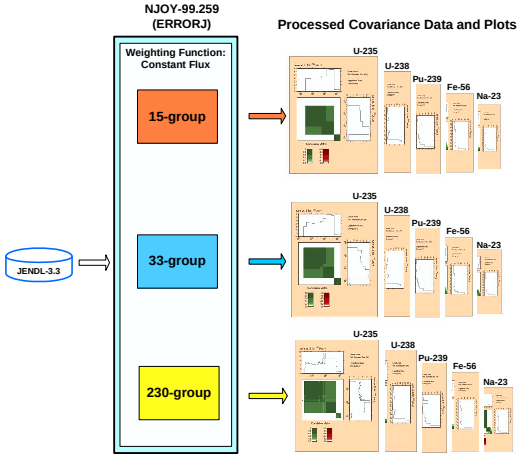

FIG. 1: Generation of multigroup covariance matrices for ^{56}Fe, ^{23}Na, ^{239}Pu, ^{235}U and ^{238}U using NJOY-99.259 and 15-, 33-, and the 230-energy group structures. Evaluations were taken from JENDL-3.3.

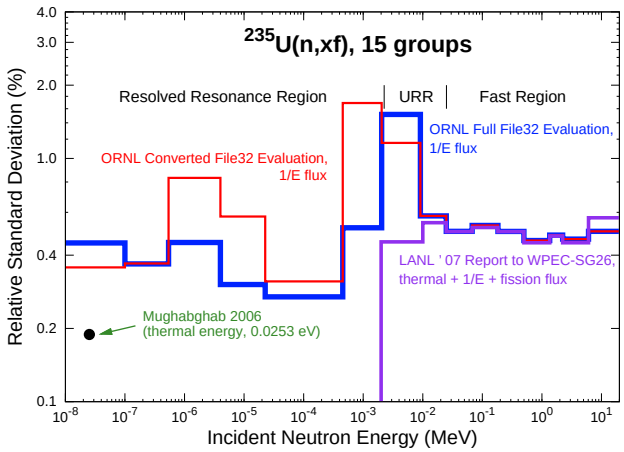

FIG. 2: Relative uncertainties in ^{235}U fission cross section processed by PUFF-IV in the 15-energy group structure. ORNL supplied resolved resonance and URR data, while LANL covered fast region. Shown are various stages of the evaluation process, the final result being in red. Also shown is the thermal pointwise value [7].

and 2) reactivity coefficients [6]. These tests will help INL to asses whether the use of the collapsed matrices will have an impact on the statistical adjustment procedure.

To enable the GNEP core group to conduct the tests, NNDC provided them with multigroup covariance matrices of ^{56}Fe, ^{23}Na, ^{239}Pu, ^{235}U and ^{238}U generated by NJOY-99.259 from the JENDL-3.3 library using the 15-, 33-, and 230-energy group structures and the constant weighting function. Fig. 1 shows a general schematic diagram on the flow of processing. The 230-energy group structure served as the reference group representation in the study. Furthermore, the processed covariance matrices covered the five reaction channels of interest: elastic, inelastic, (n,2n), fission, capture, and total for redundancy.

The processed covariance matrix files are by default voluminous because of the generation of cross correlation matrices for every combination of reaction types available for an isotope. To address this issue, the COVR module in NJOY-99.259 was used to confine the generation of plots and numeric data files to include only the five reaction types of interest to GNEP.

IV. PROCESSING COVARIANCES FOR NCSP

NNDC provides technical support to the Criticality Safety Support Group. As the U.S. clearinghouse for nuclear data we are tasked to check the processability and completeness of covariance data files before they are stored in the ENDF/A repository, see *http://www.nndc.bnl.gov/exfor/4web/ENDF-A/complete -evaluations/*.

In late 2007, NNDC began processing new ORNL-LANL evaluations of ^{233,235,238}U and ^{239}Pu with NJOY-99 and PUFF-IV. The new evaluated data files were the largest ever received by the NNDC because they contained huge covariance matrices of resonance parameters (File 32). For instance, the ^{235}U File 32 contained more than 21 million lines resulting in a file size of 1.7 GB. As a consequence, NNDC had to modify the ERRRORJ module in NJOY-99.259 to successfully process ^{233,238}U and ^{239}Pu but failed with ^{235}U. On the other hand, PUFF-IV 1.0.4 was able to successfully process all of these materials but required an enormous amount of computer time. For instance, it took our Linux cluster (3.2-GHz Intel Xeon, 4-GB RAM per CPU) 29 hours to process ^{235}U using the 44-energy group structure and the 1/E weighting function.

In March 2008, NNDC received from ORNL updated covariance evaluations of ^{233,235,238}U and ^{239}Pu with File 32 data converted into File 33 using a method developed at ORNL. As a result of the conversion, the data files were significantly smaller than the immediate preceding evaluations and thus were more manageable and much faster to process with PUFF-IV.

To roughly assess the impact of the conversion, we compared the uncertainties of the File 32 with that of the original (unconverted) data file. Figs. 2 and 3 show the comparison plots for ^{235}U and ^{239}Pu fission cross sections. Observed discrepancies should be attributed to changes in the evaluations rather than conversion. The processing washed out fine details, requiring some caution when comparing group-wise uncertainties with the pointwise values at the thermal energy taken from S. Mughabghab 2006 [7] .

In Fig. 2, the purple curve represents the LANL evaluation of ^{235}U fission cross section uncertainties in the fast energy region. This was integrated with the ORNL covariance evaluation in the resolved and unresolved resonance regions as shown by the blue curve. To address

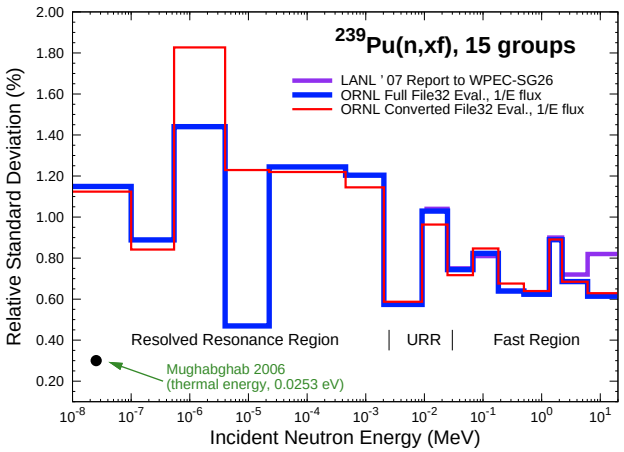

FIG. 3: Relative uncertainties in ^{239}Pu fission cross section calculated by PUFF-IV using the 15-energy group structure. See also the text in Fig. 2.

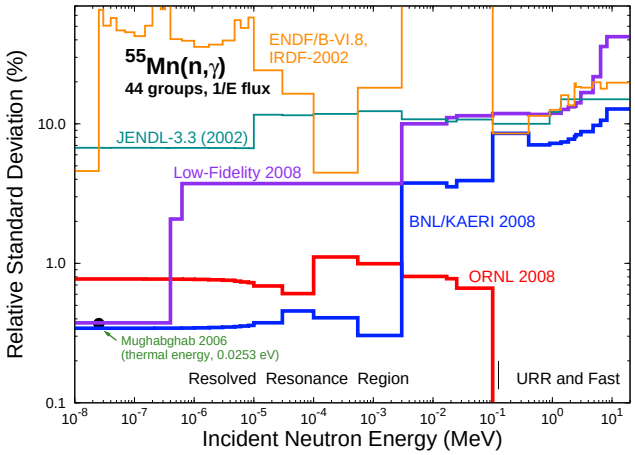

FIG. 4: Relative uncertainties in ^{55}Mn capture cross section processed by PUFF-IV using the 44-energy group structure and 1/E flux. Recent evaluations are marked as Low-Fidelity 2008, followed by the intermediate quality BNL/KAERI 2008, and the new high-fidelity ORNL 2008. Shown for comparison are legacy evaluations in ENDF/B-VI.8, adopted by IRDF-2002, and JENDL-3.3.

the file size issue, ORNL converted the File 32 covariances, after some improvements in the evaluation, into the File 33 shown by the red curve. The final covariance data file was verified by the NNDC for and included in the ENDF/A library.

As shown in Fig. 3, the evaluation of ^{239}Pu fission cross section uncertainties underwent the same series of stages. LANL performed the evaluation for the fast energy region (purple curve), ORNL handled the evaluation for the resolved and unresolved regions and then integrated the LANL and ORNL evaluations (blue curve), and ORNL converted File 32 data into the File 33 representation (red curve) to reduce the file size. The final covariance data file was verified by the NNDC and included in the ENDF/A library.

Wiarda and Leal [4] emphasized that great care must be taken in selecting the energy group structure to use in the conversion process in order to achieve good agreement. For a detailed description of the impact of the conversion process on multigroup covariances, see Ref. [8].

NNDC also processed with PUFF-IV 1.0.4 a new evaluation of ^{55}Mn from ORNL in March 2008. ^{55}Mn is an important material from the point of view of the criticality safety of reactor fuel stored in thick stainless steel (constituents Fe, Ni, Cr, Mn) cans or inserts. Covariances for this material were subject to past and also recent interest, providing a rare possibility to compare a rich variety of existing covariance results.

Shown in Fig. 4 are plots of the relative uncertainties of ^{55}Mn neutron capture cross sections. In the processing, we used the 44-energy group structure and the 1/E flux. Presently, the new high-fidelity evaluation contains covariance data in the resolved resonance region (ORNL 2008), while the evaluation by BNL/KAERI represents an intermediate quality result in the entire energy region. To determine the significance of these new results, we compared them with the recent low-fidelity estimate by ORNL-BNL. Legacy evaluations from ENDF/B-VI.8, IRDF-2002 and JENDL-3.3 are also shown to illustrate the impact of new data and new evaluation techniques and methods on uncertainty estimation and analyses.

V. COVARIANCES WEB PAGE

For the last few years, there has been a frequent request from the data end-users at large for a capability to enable a quick glance of available covariances in the nuclear data libraries. In response to such a request, the NNDC developed a Web page which provides a static covariance data visualization interface for the four major evaluated nuclear data libraries: ENDF/B-VI.8 (47 materials), ENDF/B-VII.0 (26 materials), JEFF-3.1 (37 materials) and JENDL-3.3 (20 materials).

To build this Web page, NNDC processed with NJOY-99.259 all materials which have covariance information using constant flux in the 44- and 187-energy group structures. Fig. 5 depicts the flow of the processing. Plots of relative uncertainty (%) versus incident neutron energy (eV) and their associated correlation and cross correlation matrices were generated and posted on the Web page.

The above covariance Web page should be viewed only as a stop-gap solution. It is intended as a precursor to the dynamic visualization capabilities to be provided by the Sigma ENDF Retrieval and Plotting System. This new Web interface will provide powerful but easy-to-use viewing functionalities such as the ability to view uncertainties and covariance matrices directly from any text file [9]. In the near future, data end-users will be able to view unprocessed File 33 (cross sections) covariances

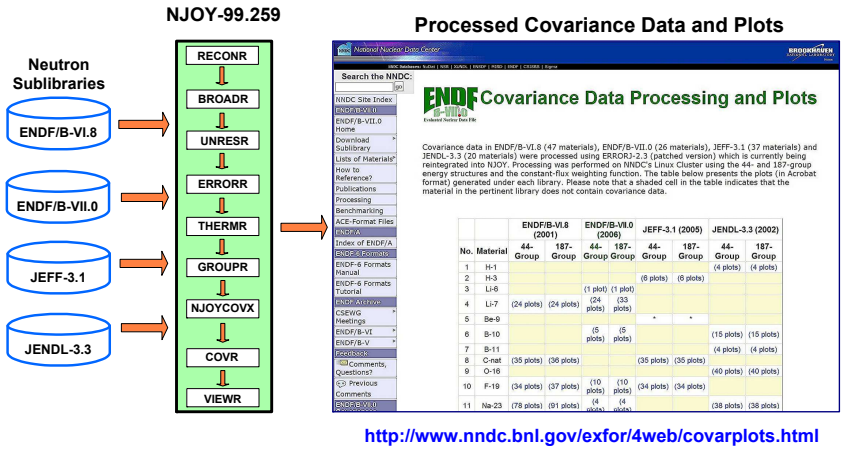

FIG. 5: Processing of covariance data from the four major evaluated nuclear data libraries using NJOY-99.259. The constant flux and the 44- and 187-energy group structures were used. For each reaction channel, plots of relative uncertainty versus incident neutron energy and their associated correlation and cross correlation matrices can be accessed.

and later also File 32 (resonance parameters) covariances where pre-processing would be necessary.

VI. CONCLUSION

With the recent advances in the processing codes, NJOY-99 and PUFF-IV have proven to be invaluable tools in generating multigroup uncertainties and correlation matrices for use in DOE-initiated programs such as GNEP and criticality safety. In the development of the first extensive covariance Web page, NJOY-99 provided the processing and plotting capabilities to build a static covariance data visualization interface for the major evaluated data libraries.

Active use of these two US codes by the NNDC appeared to be crucial in checking and verifying new covariance evaluations. In this process we also provided considerable feedback to code developers. Close collaboration between the NNDC and the processing code developers will remain to be an important element in the current US effort to develop new covariances, with the ultimate goal being their inclusion into the future ENDF/B-VII.1 library.

Acknowledgments

We would like to acknowledge the kind assistance provided by Dr. Go Chiba in the use of ERRORJ-2.3. Great appreciation should also be accorded to Dr. Dorothea Wiarda for her invaluable assistance in running and modifying PUFF-IV.

The work at BNL has been performed with support from the Office of Nuclear Physics, Office of Science of the U.S. Department of Energy under Contract No. DE-AC02-98CH10886 with Brookhaven Science Associates, LLC.

[1] M.B. Chadwick *et al.*, "ENDF/B-VII.0: Next Generation Evaluated Nuclear Data Library for Nuclear Science and Technology," *Nucl. Data Sheets vol. 107*, p. 2931, 2006.

[2] R.E. MacFarlane and D.W. Muir, *The NJOY Nuclear Data Processing System, Version 91*, Report LA-12740-M, October 1994.

[3] Go Chiba, *ERRORJ: A Code to Process Neutron-nuclide Reaction Cross Section Covariance, Version 2.3*, Report JAEA-Data/Code 2007-007, March 2007.

[4] D. Wiarda, G. Arbanas, L. Leal, and M. Dunn, "*Recent Advances with the AMPX Covariance Processing Capabilities in PUFF-IV*," see this issue of Nuclear Data Sheets.

[5] D. Wiarda, M. Dunn, "*PUFF-IV: A Code for Processing ENDF Uncertainty Data into Multi-Group Covariance Matrices*," Report ORNL/TM-2006/147, October 2006.

[6] H. Hiruta *et al.*, "*Few Group Collapsing of Covariance Matrix Data Based on a Conservation Principle*," see this issue of Nuclear Data Sheets.

[7] S.F. Mughabghab, *Atlas of Neutron Resonances: Resonance Parameters and Thermal Values Z=1-100*, Elsevier, Amsterdam, 2006.

[8] L.C. Leal, G. Arbanas, D. Wiarda, and H. Derrien, "*Resonance Region Covariance Analysis Method and New Covariance Data for ^{232}Th, ^{233}U, ^{235}U, ^{238}U, and ^{239}Pu*," see this issue of Nuclear Data Sheets.

[9] B. Pritychenko and A. Sonzogni, "*Sigma: Web Retrieval Interface for Nuclear Reaction Data*," see this issue of Nuclear Data Sheets.

Appendix G

Covariance Retrieval and Visualization

Sigma: Web Retrieval Interface for Nuclear Reaction Data

B. Pritychenko,* A.A. Sonzogni
National Nuclear Data Center, Brookhaven National Laboratory, Upton, NY 11973-5000
(Dated: September 22, 2008)

We present Sigma, a Web-rich application which provides user-friendly access in processing and plotting of the evaluated and experimental nuclear reaction data stored in the ENDF-6 and EXFOR formats. The main interface includes browsing using a periodic table and a directory tree, basic and advanced search capabilities, interactive plots of cross sections, angular distributions and spectra, comparisons between evaluated and experimental data, computations between different cross section sets. Interactive energy-angle, neutron cross section uncertainties plots and visualization of covariance matrices are under development. Sigma is publicly available at the National Nuclear Data Center website at *www.nndc.bnl.gov/sigma*.

I. INTRODUCTION

Motivated by the recent release of the ENDF/B-VII.0 evaluated nuclear reaction data library by CSEWG [1], the NNDC embarked on a project to develop an advanced Web interface for data dissemination, analysis and online processing of ENDF-6 formatted libraries. The resulting product, called Sigma would address the growing needs of traditional ENDF users as well as novel applications such as neutron cross section covariances. Sigma was designed focusing on achieving ease of use as well as taking advantage of the many software and hardware advances that took place in the last few years.

II. WEB INTERFACE

Sigma's web interface makes profuse use of modern HTML design, such as JavaScripts and CSS, as well as Java and relational database technologies. Sigma's primary goal is to provide search and browsing capabilities in a transparent way for four major evaluated libraries: ENDF/B-VII.0, JEFF-3.1, JENDL-3.3 and ENDF/B-VI.8. Sigma should offer the raw ENDF-6 data as well as processed versions and plots. Additionally, Sigma should allow the comparison between evaluated data and experimental data from the EXFOR/CSISRS database, and basic mathematical operations between evaluated data.

The ENDF utility codes ENDF2HTML (ENDF Interpreted), X4toC4, ENDVER [2–4] and PREPRO [5], are used to process the raw ENDF data. PREPRO, in particular, is used to produce a point-wise version of the libraries for plotting and further computation. Plotting is performed by using the Java plotting package jplots [6].

Requests from users are processed by the 'Java Search & Navigation Engine' that creates SQL queries. The results of the queries are stored in Java data structures and passed back to the user, or further processed with jplots, ENDF2HTML, X4toC4 or ENDVER packages before making them available. Dedicated Java wrapping classes run FORTRAN utility codes for data processing and pass results to NNDC graphic package [6] for plotting. Final results are available in text, plot (in Portable Network Graphics format PNG) and zip formats. The Sigma schematical design diagram is shown in Fig. 1.

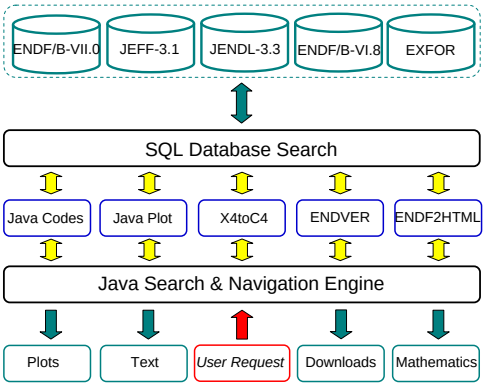

FIG. 1: Sigma Web Interface schematical design diagram.

The Sybase ASE 15 relational database software is used in Sigma; a separate EXFOR database is available if necessary [7]. Relational design allows fast and flexible retrievals of evaluated and associated experimental nuclear reaction data; the main part of Sigma's database schema is shown in Fig. 2, it consists of four major tables: Evals, PlotTable, DataTable and X4toC4, as well as five additional tables. The original evaluated nuclear reaction data are stored in the Evals and DataTable, PlotTable contains pre-processed point-wise data and X4toC4 contains pre-processed CSISRS/EXFOR data.

Sigma 1.0 was first made available to the public in April 2007, featuring browsing, searching and cross sections plots. Version 2.0 made its debut in January 2008, which incorporated angular distribution plots and mathematical operations of cross section data. Future work includes spectra plots, covariance visualization and vectorial graphics. Brief reviews of some of its most salient features are given in the following sections.

*Electronic address: pritychenko@bnl.gov

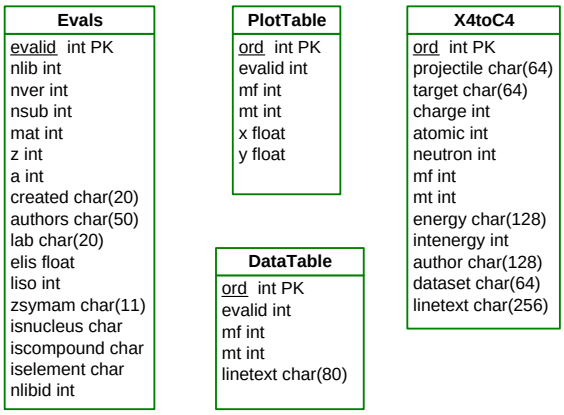

FIG. 2: Simplified Sigma relational database schema.

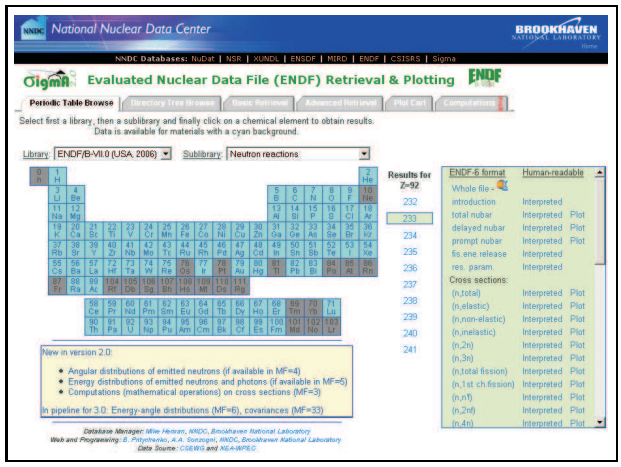

FIG. 3: Example of Sigma front page navigation capabilities (*www.nndc.bnl.gov/sigma*) for ^{233}U.

A. Browsing and Searching

Sigma's front page has a 'Periodic Table' and 'Directory Tree' options for graphical navigation; on top of the 'Periodic Table' tab, there are pull-down menus to select library and sub-library. Fig. 3 shows an example of what the front page would look like after clicking on Uranium (U, Z=92) and then clicking on A=233. The scrollable table on the right of Fig. 3 with a light green background shows all the data available for this material, which can be retrieved in the ENDF-6 format, and some of them processed in an interpreted form or in a plot. Two search capabilities have been implemented, a basic one and a more advanced one. We have tried to shield the user from having to know the intricacies of the ENDF-6 format when using Sigma. However, the advanced search feature, would require some knowledge in order to make full use of it.

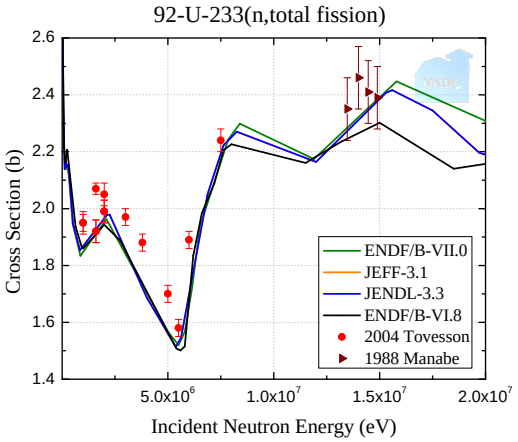

FIG. 4: Comparison between ENDF/B-VII.0, JEFF-3.1, JENDL-3.3 and ENDF/B-VI.8 libraries and selected experimental cross sections [8, 9] for ^{233}U(n,fission) reaction in the 0.1 - 20 MeV neutron energy range.

B. Connection to CSISRS/EXFOR

A key feature in Sigma, and perhaps the most rewarding from the user's standpoint, is the possibility to also query the CSISRS/EXFOR database, which contains a wealth of experimental data that has been carefully added to the database over several decades. The connection is made possible by the fact that both Sigma and CSISRS/EXFOR use the same relational database software and by the work performed by V. Zerkin *et al.* [7] to facilitate this interconnection. The code X4toC4 [3] is used in Sigma to present data from CSISRS/EXFOR. As an example, cross sections for ^{233}U(n,fission) from different evaluated libraries together with selected experimental data sets [8, 9] in the 0.1 - 20 MeV neutron energy range are shown in Fig. 4. The energy scale has been zoomed to show extra detail in the MeV region and only a few of the many experimental datasets are shown.

C. Angular Distributions and Energy Spectra

Neutron angular distributions, $d\sigma/d\omega$, are reconstructed from the MF=4 file using the MF=3 cross section data at T=300° K. Absolute differential cross sections for emitted neutrons are defined as follows [10]:

$$\sigma(\mu, E) = \sigma_s(E) f(\mu, E)/2\pi, \quad (1)$$

where σ_s is the scattering cross section given in MF=3, μ is cosine of the angle for scattered neutrons, E is the incident energy and $f(\mu, E)$ is the normalized probability as given in the MF=4 file.

Evaluated neutron angular distributions can be accessed and compared with the experimental nuclear reaction data stored in Sigma. As an example, ENDF/B-VII.0 ^{233}U(n,elastic) neutron angular distributions nor-

malized to unity are shown in Fig. 5. One can see that the shape, as a function of the incident neutron energy evolves from the isotropic distribution at low energies into forward peaking distributions at higher energies. The cumulative plot of all angular distributions of neutron elastic scattering provides a useful tool for a quick assessment of the quality of evaluation.

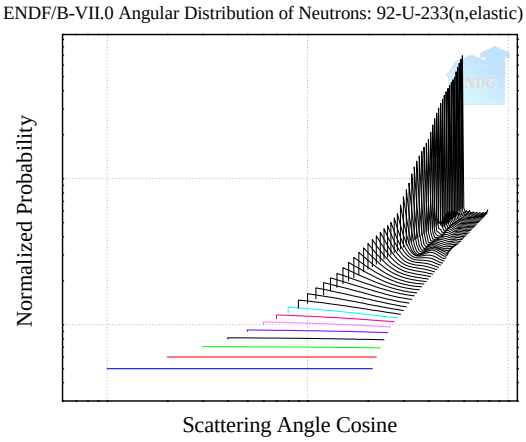

FIG. 5: ENDF/B-VII.0 ^{233}U(n,elastic) angular distributions normalized to unity for all incident neutron energies. A gradual shape evolution is indicative of a good evaluation quality.

Energy distribution, dσ/dE, plots are reconstructed from the MF=5 file using the cross section data from MF=3 at T=300° K [10]:

$$d\sigma(E \rightarrow E')/dE' = m\sigma(E)p(E \rightarrow E'), \quad (2)$$

where $\sigma(E)$ is the cross section as given in MF=3, m is the neutron multiplicity and $p(E \rightarrow E')$ is the energy distribution from the MF=5 file.

The plotting of energy-angle spectra (d$^2\sigma$/dωdE) is currently being tested. Reaction product (emitted neutrons, photons or residual nuclei) cross sections are calculated as [10]

$$\sigma_i(\mu, E, E') = \sigma(E)y_i(E)f_i(\mu, E, E')/2\pi, \quad (3)$$

where i denotes one particular product, E is the incident energy, E' is the energy of the product emitted with cosine μ, σ(E) is the interaction cross section (MF=3), y_i is the product yield or multiplicity and $f_i(\mu$,E,E$')$ is the normalized distribution from the MF=6 file. Neutron energy spectra from the ^{233}U(n,2n) reaction retrieved from the ENDF/B-VII.0 library are shown in Fig. 6.

ENDF evaluations contain angular distributions of emitted neutrons, photons and residual nuclei for a particular reaction channel. In general, many reaction channels are open and combined spectra are observed in experiments, creating a challenge when comparison between evaluation and experimental results need to be done. This was solved by the ENDVER code [4] that is integrated in Sigma as 'Full Spectra'.

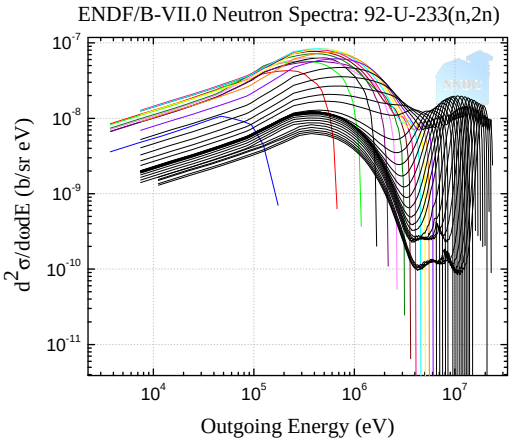

FIG. 6: Energy spectra of neutrons emitted from the ^{233}U(n,2n) reaction at a 30° scattering angle. The spectra for all neutron incident energies up to 30 MeV, contained in the ENDF/B-VII.0 file, are shown.

D. Computations

The possibility to perform mathematical operations with evaluated cross section data has been recently implemented. Sigma stores cross section data from MF=3 together with cross sections derived from the resonance parameters in MF=2 that have been Doppler broadened to 300° K and linearized using PREPRO [5]. These data can be plotted simultaneously in Sigma for a variety of different reactions (MT values) using the *Plot Cart* feature. The *Plot Cart* is made up of different sets of (x,y) data points. Almost any mathematical equation can be easily typed in and a new set of (x,y) points resulting from such mathematical operation can be added to the *Plot Cart* and visualized.

As an example, the ENDF/B-VII.0 neutron capture cross section for the *s*-process nuclide ^{100}Ru is shown in Fig. 7, together with the same cross section multiplied by a factor of *E×exp(-E/30000)*, a term proportional to a Maxwellian neutron flux distribution with kT=30 keV. By examining the integrals of each curve, one can deduce that for this nuclide, the cross sections from the resonance region contribute the most of the Maxwellian-weighted cross section at kT=30 keV. We note that a recently released web application [11], offering Maxwellian-averaged cross sections and astrophysical reaction rates derived from ENDF-6 formatted evaluations, is a direct spin-off from Sigma.

Another example of mathematical operations would be the ratio of the ^{237}Np(n,fission) from JENDL-3.3 and ENDF/B-VI.8, shown in Fig. 8. The disagreement between these two data sets of evaluated data in the fast region has triggered a recent experimental effort to accurately measure it [12]. These types of comparisons between data can be easily accomplished in Sigma.

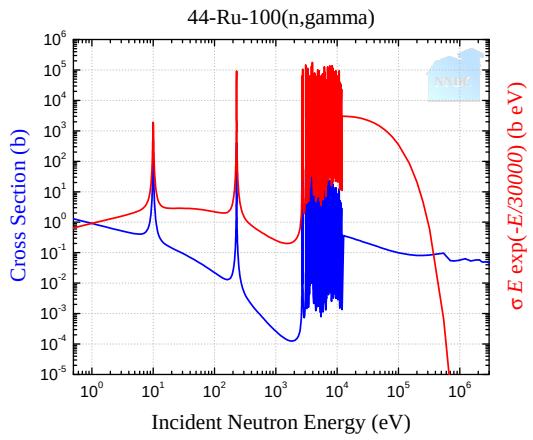

FIG. 7: Neutron capture cross sections for the *s*-process nuclide ^{100}Ru retrieved from ENDF/B-VII.0 (blue curve) and computed Maxwellian-weighted values for kT=30 keV (red).

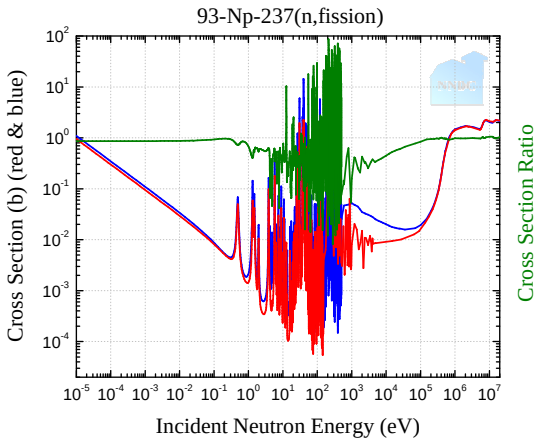

FIG. 8: Mathematical ratio of ^{237}Np(n,fission) cross sections between ENDF/B-VI.8 and JENDL-3.3 libraries, green, red and blue curves, respectively.

E. Cross Section Covariance Data

The strong interest in the production and use of covariance data is evidenced by several recent sub-groups organized under the auspices of OECD-NEA as well as the current workshop. In response to this demand we are developing Sigma covariance capabilities. We have in mind a tool that would allow direct retrieval of covariance data and their visualization, which is important for both covariance producers and users. In this way we would avoid the use of complex processing codes, such as NJOY [13], where complete ENDF-6 files are needed and multigroup data must be produced before plot of uncertainties and correlations can be obtained.

In the ENDF-6 format cross section covariance matrices are stored in file MF=33 and the resonance parameter covariance matrices in MF=32. Retrieval of MF=33 is straightforward, while MF=32 would need pre-

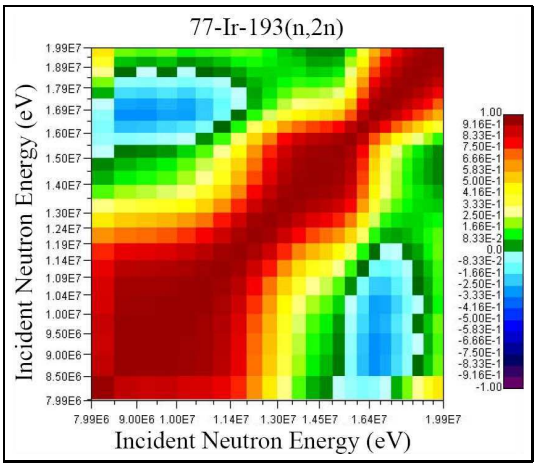

FIG. 9: ENDF/B-VII.0 correlation matrix for ^{193}Ir(n,2n) reaction.

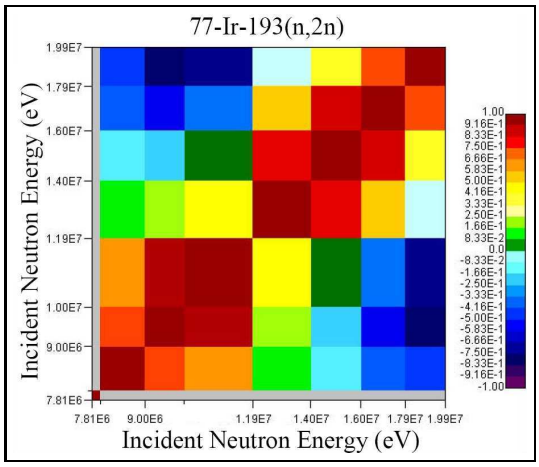

FIG. 10: The correlation matrix for ^{193}Ir(n,2n) reaction from the low-fidelity project [14].

processing. In Fig. 9 we show an example of a correlation matrix directly retrieved from the ENDF/B-VII.0 library for the ^{193}Ir(n,2n) reaction, which has a threshold of 7812 keV.

Direct plotting of covariance matrices shows the data exactly as given in MF=33, the disadvantage being that the covariance patterns are somewhat difficult to analyze and compare. Often, a more suitable approach is to visualize the same data as uncertainties and correlation matrices that are obtained after simple renormalization:

$$corr(i,j) = \frac{cov(i,j)}{\sqrt{cov(i,i) * cov(j,j)}} \quad (4)$$

In Fig. 10 we show the correlation matrix for ^{193}Ir(n,2n) reaction produced by the Low-fidelity Project [14]. One can see a pattern with clearly visible strong positive correlations centered around the diagonal.

Sigma offers retrieval of covariances from the preloaded libraries, such as ENDF/B-VII.0 or Low-fidelity, but a

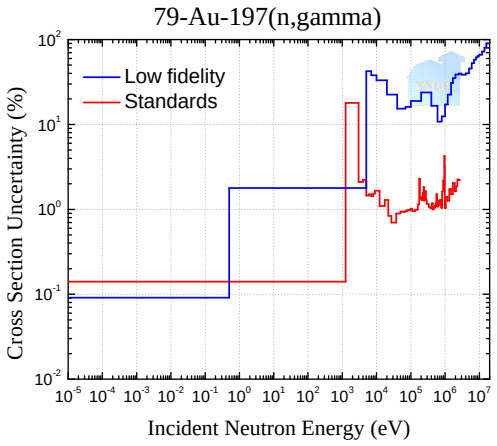

FIG. 11: Neutron cross section uncertainties for ^{197}Au(n,γ) taken from the ENDF/B-VII.0 Standards sub-library are compared with the Low-fidelity data [14] .

user can also input a MF=33 file and plot covariances. This would facilitate comparison of data, such as cross section uncertainties for ^{197}Au(n,γ), where two extremes can be compared, the ENDF/B-VII.0 Standards sub-library and the Low-fidelity Project [14], which are shown in Fig. 11.

III. SUMMARY & OUTLOOK

Sigma Web interface, *www.nndc.bnl.gov/sigma*, provides a transparent and easy to use retrieval and visualization tool for the evaluated and experimental nuclear reaction data. Recent additions include energy spectra and angular distributions of emitted particles as well as mathematical operations of cross sections.

Sigma's covariance capabilities are currently being tested and will allow visualization of cross section covariance matrices directly retrieved from MF=33 and, in the near future, also from MF=32. Visualization of uncertainties and correlation matrices is straightforward and avoids the use of complex processing codes. Users will be able to retrieve and view covariance data from several preloaded libraries, including the Low-fidelity covariances, with a couple of clicks. In addition, users can input to Sigma their own data and view them as well. These new capabilities should not only facilitate covariance development, but should be appreciated also by covariance users.

Web access to evaluated and experimental nuclear reaction data continues to grow exponentially [15]. Continuing effort is needed to satisfy current needs and future demands.

Acknowledgments

We are grateful to M. Herman and A. Trkov for their help with ENDF utility codes, to P. Obložinský and M.T. Pigni for useful suggestions, and to M. Blennau and S.F. Mughabghab for a careful reading of the manuscript. This work was sponsored by the Office of Nuclear Physics, Office of Science of the U.S. Department of Energy under Contract No. DE-AC02-98CH10886 with Brookhaven Science Associates, LLC.

[1] M.B. Chadwick, P. Obložinský, M. Herman *et al.*, *Next Generation Evaluated Nuclear Data Library for Nuclear Science and Technology*, Nucl. Data Sheets **107** (2006) 2931.
[2] R.E. MacFarlane, *ENDF Interpreted (ENDF2HTML)*, Available from ⟨http://t2.lanl.gov/⟩.
[3] D.E. Cullen, *Program X4toC4: converts nuclear data from EXFOR format to a computational format*, IAEA-NDS-80, September 1986.
[4] A. Trkov, *ENDVER: ENDF file verification support package*, Available from ⟨http://www-nds.iaea.org/ndspub/endf/endver/⟩.
[5] D.E. Cullen, *The ENDF/B Pre-processing codes (PREPRO)*, Available from ⟨http://www-nds.iaea.org/ndspub/endf/prepro/⟩.
[6] A.A. Sonzogni, private communication.
[7] V.V. Zerkin *et al.*, *EXFOR-CINDA-ENDF: Migration of Databases to Give Higher-Quality Nuclear Data Services*, Inter. Conf. on Nucl. Data for Sci. and Tech., AIP **769** (2005) 586.
[8] F. Tovesson *et al.*, *233Pa(n, f) cross section up to En = 8.5 MeV*, Nucl.Phys. **A 733**, 3 (2004).
[9] F. Manabe *et al.*, *Measurements of Neutron Induced Fission Cross Section Ratios of 232Th, 233U, 234U, 236U, 238U, 237Np, 242Pu and 243Am Relative to 235U around 14 MeV*, Tech. Rep. Tohuku University, **52**, No.2.
[10] M. Herman (editor), *ENDF-6 Formats Manual: Data Formats and Procedures for the Evaluated Nuclear Data File ENDF/B-VI and ENDF/B-VII*, Tech. Rep. BNL-NCS-44945-05-Rev, Document ENDF-102, Brookhaven National Lab, June 2005.
[11] B. Pritychenko, A.A. Sonzogni, *Maxwellian-Averaged Cross Sections and Astrophysical Reaction Rates*, Available from ⟨http://www.nndc.bnl.gov/astro/⟩.
[12] F. Tovesson, T.S. Hill, *Neutron-induced fission cross section of 237Np from 100 keV to 200 MeV*, Phys. Rev. **C 75**, 034610 (2007).
[13] R.E. MacFarlane and D.W. Muir, *The NJOY nuclear data processing system, version 91*, Tech. Rep. LA-12740-M, Los Alamos National Lab, NM, 1994.
[14] M.T. Pigni, M.Herman, P. Obložinský *et al.*, *Low-fidelity Covariance Project*, these proceedings.
[15] B. Pritychenko *et al.*, *Nuclear Reaction and Structure Data Services of the National Nuclear Data Center*, Ann. Nucl. Energy **33** (2006) 390.